

AD 668328

1 ~~4~~ (1)

Bulletin 37  
Part 6  
(of 7 Parts)

# THE SHOCK AND VIBRATION BULLETIN

(30)

JANUARY 1968

A Publication of  
**THE SHOCK AND VIBRATION  
INFORMATION CENTER**  
Naval Research Laboratory, Washington, D.C.



Office of  
The Director of Defense  
Research and Engineering

Reproduced by the  
**CLEARINGHOUSE**  
for Federal Scientific & Technical  
Information Springfield Va 22151



This document has been approved for public release and sale; its distribution is unlimited.

86

ACCESSION FOR	
CFSTI	WHITE SECTION <input checked="" type="checkbox"/>
DDC	DIFF SECTION <input type="checkbox"/>
UNANNOUNCED	<input type="checkbox"/>
JUSTIFICATION	
BY	
DISTRIBUTION/AVAILABILITY CODES	
DIST.	AVAIL. and or SPECIAL
↓	

## SYMPOSIUM MANAGEMENT

### THE SHOCK AND VIBRATION INFORMATION CENTER

William W. Mutch, Director  
 Henry C. Pusey, Coordinator  
 Rudolph H. Volin, Coordinator  
 Katherine G. Jahnelt, Administrative Secretary

#### 37th Program Committee

David Askin, U.S. Army Frankford Arsenal  
 Jerry Sullivan, Naval Ship Systems Command Hdq.  
 Robert F. Wilkus, Systems Engineering Group, W-PAFB  
 Dennis J. Martin, NASA Langley Research Center

#### Navy Liaison

Naval Training Device Center

William Powell  
 Allan Collier

#### Bulletin Production

Graphic Arts Branch, Technical Information Division,  
 Naval Research Laboratory

**Bulletin 37**  
**Part 6**  
**(of 7 Parts)**

# **THE SHOCK AND VIBRATION BULLETIN**

**JANUARY 1968**

**A Publication of  
THE SHOCK AND VIBRATION  
INFORMATION CENTER  
Naval Research Laboratory, Washington, D.C.**

The 37th Symposium on Shock and Vibration was held in Orlando, Florida, on 24-26 October 1967. The U.S. Navy was host.

**Office of  
The Director of Defense  
Research and Engineering**

# CONTENTS

## PART 6

### Helicopter Environments

HELICOPTER VIBRATIONS .....	1
C. D. Roach, U. S. Army Aviation Materiel Laboratories, Fort Eustis, Virginia	
HELICOPTER VIBRATION--A MAJOR SOURCE, ITS PREDICTION AND AN APPROACH TO ITS CONTROL .....	5
R. P. White, Jr., and F. A. DuWaldt, Cornell Aeronautical Laboratory, Inc., Buffalo, New York	
*IN-FLIGHT VIBRATION AND ACOUSTIC STUDY ON THE UH-1F HELICOPTER C. E. Thomas and J. T. Ach, Air Force Flight Dynamics Laboratory, Wright-Patterson AFB, Ohio	
HELICOPTER FUSELAGE VIBRATION PREDICTION BY STIFFNESS MOBILITY METHODS ..	19
J. J. Sciarra, The Boeing Company, Morton, Pennsylvania	
ISOLATION OF HELICOPTER ROTOR-INDUCED VIBRATIONS USING ACTIVE ELEMENTS ..	29
P. C. Calcaterra and D. W. Schubert, Barry Research & Development, Watertown, Massachusetts	
HYBRID VIBRATION-ISOLATION SYSTEM FOR HELICOPTERS .....	39
D. A. Bies and T. M. Yang, Bolt Beranek and Newman Inc., Los Angeles, California	
RECENT ADVANCES IN THE STUDY OF SYNCHRONOUS VIBRATION ABSORBERS .....	49
A. V. Srinivasan, Kaman Corporation, Bloomfield, Connecticut	
OPTIMIZING THE DYNAMIC ABSORBER TO INCREASE SYSTEM DAMPING .....	57
G. K. Jones, NASA Goddard Space Flight Center, Greenbelt, Maryland	
APPLICATION OF THE DYNAMIC ANTIRESONANT VIBRATION ISOLATOR TO HELICOPTER VIBRATION CONTROL .....	63
R. Jones and W. G. Flannelly, Kaman Corporation, Bloomfield, Connecticut	

### PAPERS APPEARING IN PART 1

Part 1 - Classified  
(Titles Unclassified)

RECENT WORK ON SHOCK AT N. C. R. E. A. M. MacIntosh, Naval Construction Research Establishment, Dunfermline, Fife, Scotland	
STATE OF SHOCK IN THE NAVY, 1967 H. L. Rich, Naval Ship Research and Development Center, Washington, D. C.	
NAVY DYNAMIC DESIGN ANALYSIS METHOD - PANEL SESSION	
SHOCK HARDENING RIVERINE WARFARE CRAFT FOR VIETNAM O. H. Porter and F. Weinberger, Naval Ship Research and Development Center, Washington, D. C.	
SHOCK TESTING OF SONAR TRANSDUCERS -- A STATUS REPORT G. M. Mayer and C. D. Johnson, Navy Underwater Sound Laboratory, New London, Connecticut	
AN EXPLOSION SHOCK-TESTING METHOD FOR SHIPBOARD EQUIPMENT R. R. Higginbotham, Naval Ship Research and Development Center, Portsmouth, Virginia	

\*This paper appears in Shock and Vibration Bulletin 37, Supplement.

RIGID BODY RESPONSE OF NAVAL SURFACE VESSELS TO AIR BLAST  
J. T. Irick, AVCO Corporation, Lowell, Massachusetts, S. Silverman and W. E. Baker, Southwest Research Institute, San Antonio, Texas

REACTION OF MILD STEEL TARGETS TO EXPLODING MUNITIONS  
J. W. Apgar, Ballistic Research Laboratories, Aberdeen Proving Ground, Maryland

RESPONSE OF A MISSILE STRUCTURE UNDER HIGH VELOCITY IMPACT  
C. Riparbelli, General Dynamics/Pomona, Pomona, California

AIM4D/F4 CAPTIVE-FLIGHT VIBRATION LOADS AND ENVIRONMENTAL MEASUREMENTS PROGRAM  
C. D. Knauer, Jr. and P. E. McHorney, Hughes Aircraft Company, El Segundo, California

#### PAPERS APPEARING IN PART 2

##### Instrumentation and Analysis

PORTABLE LASER INSTRUMENT FOR VIBRATION ANALYSIS AND TRANSDUCER CALIBRATION  
G. A. Massey and R. R. Carter, Sylvania Electronic Systems, Mountain View, California

HIGH-FREQUENCY MICROPHONE CALIBRATION USING A SUPERSONIC FREE-FLIGHT RANGE  
C. D. Hayes, Jet Propulsion Laboratory, Pasadena, California, and R. C. Binder, University of Southern California, Los Angeles, California

METHOD OF MEASURING VIBRATORY DISPLACEMENTS IN TERMS OF A LIGHT WAVELENGTH  
J. L. Goldberg, National Standards Laboratory, Sydney, Australia

CALIBRATION OF ACCELEROMETERS BY IMPULSE EXCITATION AND FOURIER INTEGRAL TRANSFORM TECHNIQUES  
J. D. Favour, The Boeing Company, Seattle, Washington

BIDIRECTIONAL SHOCK AND HIGH-IMPACT EFFECTS ON SHOCK TRANSDUCERS  
V. F. DeVost and P. S. Hughes, Naval Ordnance Laboratory, Silver Spring, Maryland

INFLUENCE OF FIXTURE STRESS CONCENTRATIONS ON RING ACCELEROMETERS  
J. A. Nagy and C. E. Henley, Jr., NASA Goddard Space Flight Center, Greenbelt, Maryland

SONAR TRANSDUCER VIBRATION REQUIREMENTS AND MEASUREMENT TECHNIQUES  
G. M. Mayer and E. G. Marsh, Navy Underwater Sound Laboratory, New London, Connecticut

AUTOMATED VIBRATION ANALYSIS  
R. J. Pabich and W. H. Sellers, Raytheon Company, Bedford, Massachusetts

A COMPACT, LOW-COST SHOCK-SPECTRUM ANALYZER  
W. W. Mebane, Naval Ordnance Laboratory, Silver Spring, Maryland

DYNAMIC PHASE PLOTTING  
T. E. Smart, Sandia Corporation, Albuquerque, New Mexico

RANDOM-VIBRATION-INDUCED ERRORS IN A MISSILE CAUSED BY NONLINEAR INERTIAL ACCELEROMETERS  
N. A. Leifer, Bell Telephone Laboratories, Inc., Whippany, New Jersey

VIBRATION DISTRIBUTIONS IN MULTIPANEL STRUCTURES: COMPARISON OF MEASUREMENTS WITH STATISTICAL ENERGY PREDICTIONS  
E. E. Ungar and N. Koronaios, Bolt Beranek and Newman Inc., Cambridge, Massachusetts

CONSTANT BANDWIDTH FM DATA SYSTEM DESIGNED FOR SATURN S-IVB/V VIBRATION TESTS  
D. F. Redford, Thiokol Chemical Corporation, Brigham City, Utah

DYNAMICS PORTION OF GEMINI AGENA TARGET VEHICLE ENGINE MODIFICATION AND TEST PROGRAM (PROJECT SURE FIRE)  
N. Angelopoulos, Lockheed Missiles & Space Company, Sunnyvale, California

DYNAMIC ANALYSIS OF COMPLEX STRUCTURES  
M. D. Benton, G. K. Hobbs, Hughes Aircraft Company, El Segundo, California, and J. R. Dickerson, University of Texas, Austin, Texas

PAPERS APPEARING IN PART 3

Vibration Testing

ADVANCES IN NUMEROLOGY

J. P. Salter, Royal Armaments Research and Development Establishment, Fort Halstead, Sevenoaks, Kent, England

INTERNAL VIBRATION OF ELECTRONIC EQUIPMENT RESULTING FROM ACOUSTIC AND SHAKER INDUCED EXCITATION

A. D. Houston, Lockheed Missiles & Space Company, Sunnyvale, California

RANDOM-VIBRATION RESPONSE DATA FOR ORBITING GEOPHYSICAL OBSERVATORY: FLIGHT, ACOUSTIC, AND VIBRATION TEST

W. C. Elsen, NASA Goddard Space Flight Center, Greenbelt, Maryland

RANDOM-VIBRATION TEST LEVEL CONTROL USING INPUT AND TEST ITEM RESPONSE SPECTRA

A. J. Curtis and J. G. Herrera, Hughes Aircraft Company, Culver City, California

RANDOM-FORCE VIBRATION TESTING

J. V. Otts and N. F. Hunter, Jr., Sandia Corporation, Albuquerque, New Mexico

CONTROL POINT AVERAGING FOR LARGE SPECIMEN VIBRATION TESTS

H. R. Berkman, Litton Systems, Inc., Van Nuys, California

VIBRATION METHODS FOR MULTIPLE RANDOM EXCITATION

W. E. Noonan, McDonnell Company, St. Louis, Missouri

DYNAMIC TESTING OF FULL-SCALE SATURN LAUNCH VEHICLES

B. R. Jacobs, Northrop Nortronics, Huntsville, Alabama

BUFFET RESPONSE MEASUREMENTS OF A SEVEN PERCENT AEROELASTICALLY SCALED MODEL OF VARIOUS TITAN III CONFIGURATIONS

J. T. Uchiyama and F. W. Peters, Martin-Marietta Corporation, Denver, Colorado

HIGH-FORCE VIBRATION TESTING OF THE SATURN S-IVB STAGE

L. G. Smith, McDonnell Douglas Corporation, Huntington Beach, California

SIMPLIFIED METHOD OF CONDUCTING A DUAL RANDOM-VIBRATION INTEGRATED SYSTEM TEST

J. G. Colt, Radio Corporation of America, Burlington, Massachusetts

CONTROL STABILIZATION FOR MULTIPLE SHAKER TESTS

N. F. Hunter, Jr., Sandia Corporation, Albuquerque, New Mexico, and J. G. Helmuth, Chadwick-Helmuth Company, Inc., Monrovia, California

THE SHIM SPRING ISOLATOR

L. Wallerstein, Jr., Lord Manufacturing Company, Erie, Pennsylvania

Test Facilities

ADVANCED COMBINED ENVIRONMENTAL TEST FACILITY

E. J. Kirchman and C. J. Arcilesi, NASA Goddard Space Flight Center, Greenbelt, Maryland

DEVELOPMENT OF SIMULATED AIRCRAFT DELIVERY USING A ROCKET SLED

W. R. Kampfe and K. M. Timmerman, Sandia Corporation, Albuquerque, New Mexico

AERODYNAMIC NOISE INVESTIGATION IN A SHORT-DURATION SHOCK TUNNEL

D. H. Ross, Aerospace Corporation, El Segundo, California

IMPACT TESTING WITH A FOUR-INCH AIR GUN AND LEAD TARGETS

H. J. Davis, Harry Diamond Laboratories, Washington, D. C.

PAPERS APPEARING IN PART 4

Shock Analysis and Simulation

MEASUREMENT AND ANALYSIS OF SPACECRAFT SEPARATION TRANSIENT RESPONSE FOR MARINER-TYPE SPACECRAFT

P. Barnett, Jet Propulsion Laboratory, Pasadena, California

MECHANICAL SHOCK OF HONEYCOMB STRUCTURE FROM PYROTECHNIC SEPARATION

J. R. Olsen, J. R. West, Jr., H. Himelblau, North American Rockwell Corporation, Los Angeles, California, C. D. Knauer, Jr., and P. E. McHorney, Jr., Hughes Aircraft Company, El Segundo, California

A SIMPLE STRENGTH CONCEPT FOR DEFINING PRACTICAL HIGH-FREQUENCY LIMITS OF SHOCK SPECTRUM ANALYSIS

M. Gertel and R. Holland, Allied Research Associates, Concord, Massachusetts

TRANSIENT VIBRATION SIMULATION

T. E. Fitzgerald and L. C. Kula, The Boeing Company, New Orleans, Louisiana

PREDICTING MECHANICAL SHOCK TRANSMISSION

J. E. Manning and K. Lee, Bolt Beranek and Newman Inc., Cambridge, Massachusetts

SHOCK DAMAGE MECHANISM OF A SIMPLE STRUCTURE

L. T. Butt, Naval Ship Research and Development Center, Portsmouth, Virginia

GENERAL MOTORS ENERGY-ABSORBING STEERING COLUMN AS A COMPONENT OF SHIP-BOARD PERSONNEL PROTECTION

J. T. Hawkins and A. E. Hirsch, Naval Ship Research and Development Center, Washington, D. C.

HEAVY WEIGHT SHOCK TEST FIXTURES: DESIGN AND RESULTS

C. G. Schrader, San Francisco Bay Naval Shipyard, San Francisco, California

DERIVATION AND IMPLICATIONS OF THE NAVY SHOCK ANALYSIS METHOD

F. J. Heymann, Westinghouse Electric Corporation, Lester, Pennsylvania

DYNAMIC ANALYSIS OF A TYPICAL ELECTRONIC EQUIPMENT CABINET SUBJECTED TO NUCLEAR-WEAPON-INDUCED SHOCK

J. H. Putukian, Kaman Avidyne, Burlington, Massachusetts

DEVELOPMENT OF A ZERO-G COAST PHASE AIR GUN

S. Rodkin, General Electric Company, Philadelphia, Pennsylvania

DEVELOPMENT OF A MISSILE LAUNCH SHOCK TEST FACILITY FOR SHILLELAGH

R. W. Stevens, Martin-Marietta Corporation, Orlando, Florida

USE OF EXPLODING WIRE APPARATUS FOR LABORATORY SIMULATION OF SHOCK WAVES

F. B. Safford, Mechanics Research Inc., El Segundo, California, and R. C. Binder, University of Southern California, Los Angeles, California

NIKE-X SHOCK TUBE FACILITY

R. G. Donaghy and J. J. Healy, Office of the Chief of Engineers, Department of the Army, Washington, D. C.

DESIGN AND PERFORMANCE OF DUAL MODE SHOCK MACHINE

W. D. Everett, Naval Missile Center, Point Mugu, California

Air Blast and Ground Shock

INFLUENCE OF SHIP MOBILITY ON INTERNAL FORCES PRODUCED BY BLAST

A. Chajes, F. J. Dzialo, and M. P. White, Department of Civil Engineering, University of Massachusetts, Amherst, Massachusetts

DYNAMIC BEHAVIOR OF SHIPBOARD ANTENNA MASTS SUBJECTED TO BLAST-GENERATED OVERPRESSURES

F. A. Britt and R. H. Anderson, Mechanics Research, Inc., El Segundo, California

**\*HARDENED ANTENNA TECHNOLOGY**

D. A. Benson, A. F. Gurdo, R. W. Mair and D. J. Waters, Rome Air Development Center, Griffiss AFB, New York

**ABSOLUTE UPPER AND LOWER BOUNDS FOR THE CRITICAL BLAST LOADING ENVIRONMENT OF TARGET ELEMENTS AND SYSTEMS**

E. Sevin and W. D. Pilkey, IIT Research Institute, Chicago, Illinois

**ELASTIC-PLASTIC COLLAPSE OF STRUCTURES SUBJECTED TO A BLAST PULSE**

W. B. Murfin, Sandia Corporation, Albuquerque, New Mexico

**INTERNAL LOADING OF STRUCTURES BY BLAST WAVES**

J. F. Melichar, Ballistic Research Laboratories, Aberdeen Proving Ground, Maryland

**EFFECTS OF SLIDING ON BLAST LOADS REQUIRED TO OVERTURN STRUCTURES**

C. E. Gebhart, IIT Research Institute, Chicago, Illinois

**USE OF DETONABLE GAS EXPLOSIONS FOR BLAST AND SHOCK STUDIES**

M. R. Johnson and M. J. Balcerzak, General American Research Division, Niles, Illinois

**INCORPORATION OF SHOCK PROTECTION IN EXISTING ABOVEGROUND CYLINDRICAL STRUCTURES SUBJECTED TO NUCLEAR BLAST**

E. Cohen, S. Weissman and L. Sanchez, Ammann and Whitney, New York, New York

**PAPERS APPEARING IN PART 5**

Large Vibro-Acoustic Test Facilities

**VIBROACOUSTIC ENVIRONMENTAL SIMULATION FOR AEROSPACE VEHICLES**

K. McK. Eldred, Wyle Laboratories, El Segundo, California

**\*RTD SONIC FATIGUE FACILITY, DESIGN AND PERFORMANCE CHARACTERISTICS**

A. W. Kolb and H. A. Magrath, Air Force Flight Dynamics Laboratory, Wright-Patterson AFB, Ohio

**OPERATIONAL CHARACTERISTICS OF A 100,000 CUBIC FOOT ACOUSTIC REVERBERATION CHAMBER**

F. M. Murray, Wyle Laboratories, Huntsville, Alabama

**CONCEPT, DESIGN, AND PERFORMANCE OF THE SPACECRAFT ACOUSTIC LABORATORY**

R. J. Wren, W. D. Dorland, J. D. Johnston, Jr., NASA Manned Spacecraft Center, Houston, Texas, and K. McK. Eldred, Wyle Laboratories, El Segundo, California

**THEORETICAL STUDY OF ACOUSTIC SIMULATION OF IN-FLIGHT ENVIRONMENTS**

R. W. White, Wyle Laboratories, Huntsville, Alabama

**DATA HANDLING METHODS FOR LARGE VEHICLE TESTING**

D. J. Bozich, Wyle Laboratories, Huntsville, Alabama

**DEVELOPMENT AND VERIFICATION OF THE VIBRATION TEST REQUIREMENTS FOR THE APOLLO COMMAND AND SERVICE MODULES**

D. E. Newbrough, General Electric Company, Houston, Texas, R. A. Colonna, NASA Manned Spacecraft Center, Houston, Texas, and J. R. West, North American Rockwell Corporation, Downey, California

**DEVELOPMENT AND VERIFICATION OF THE APOLLO LUNAR MODULE VIBRATION TEST REQUIREMENTS**

D. E. Newbrough, General Electric Company, Houston, Texas, M. Bernstein and E. F. Baird, Grumman Aircraft Engineering Company, Bethpage, New York

**SATURN S-II, S-IVB, AND INSTRUMENT UNIT SUBASSEMBLY AND ASSEMBLY VIBRATION AND ACOUSTIC EVALUATION PROGRAMS, PARTS 1 AND 2**

R. W. Schock, J. M. Everitt, NASA Marshall Space Flight Center, Huntsville, Alabama, and J. R. Seat, Brown Engineering Company, Huntsville, Alabama

\*This paper appears in Shock and Vibration Bulletin 37, Supplement.



**DEVELOPMENT OF ACOUSTIC TEST CONDITIONS FOR APOLLO LUNAR MODULE  
FLIGHT CERTIFICATION**

W. D. Dorland, R. J. Wren, NASA Manned Spacecraft Center, Houston, Texas, and K. McK.  
Eldred, Wyle Laboratories, El Segundo, California

**\*FACILITY SONIC FATIGUE PROOF TESTING**

O. F. Maurer, Air Force Flight Dynamics Laboratory, Wright-Patterson AFB, Ohio

**VIBROACOUSTIC TEST METHODS FOR VIBRATION QUALIFICATION OF APOLLO  
FLIGHT HARDWARE**

R. W. Peverley, General Electric Company, Houston, Texas

**ACOUSTICAL QUALIFICATION OF S-1C FIN STRUCTURES**

C. J. Beck, Jr., The Boeing Company, Huntsville, Alabama, and D. R. Kennedy, Brown Engi-  
neering Company, Huntsville, Alabama

**\*SIMULATION OF ACOUSTIC FATIGUE FAILURE IN THE WIDEBAND NOISE TEST FACILITY  
OF THE AIR FORCE FLIGHT DYNAMICS LABORATORY**

R. C. W. van der Heyde, Air Force Flight Dynamics Laboratory, Wright-Patterson AFB, Ohio

**REAL-TIME COMBINED ACOUSTIC-VACUUM TESTING OF SPACECRAFT**

L. J. Demas, NASA Goddard Space Flight Center, Greenbelt, Maryland

**PAPERS APPEARING IN PART 7**

Environmental Data

**SURVEY OF THE CARGO-HANDLING SHOCK AND VIBRATION ENVIRONMENT**

F. E. Ostrem, General American Research Division, Niles, Illinois

**A NEW LOOK AT TRANSPORTATION VIBRATION STATISTICS**

J. W. Schlue and W. D. Phelps, Jet Propulsion Laboratory, Pasadena, California

**RECENT SHOCK AND VIBRATION MEASUREMENTS ON THE M-151 (JEEP) VEHICLE**

R. D. Brunnemer and G. M. Pomonik, Hughes Aircraft Company, Canoga Park, California

**LATERAL IMPACT SHOCK DURING SHIP LOADING OF THE A3 POLARIS MISSILE**

E. G. Fischer, C. R. Brown, and A. J. Molnar, Westinghouse Electric Corporation, Pittsburgh,  
Pennsylvania

**\*RF-4C VIBRATION AND ACOUSTIC ENVIRONMENT STUDY**

J. F. Dreher, Air Force Flight Dynamics Laboratory, and W. D. Hinegardner, Systems Engi-  
neering Group, Wright-Patterson AFB, Ohio

**EMPIRICAL CORRELATION OF FLIGHT VEHICLE VIBRATION RESPONSE**

W. H. Roberts, Martin-Marietta Corporation, Orlando, Florida

**VIBRATION DATA SUMMARY OF MINUTEMAN WING VI FLIGHT TEST MISSILES**

R. R. Burnett and R. E. Morse, TRW Systems, Redondo Beach, California

**SPACECRAFT VIBRATION: COMPARISON OF FLIGHT DATA AND GROUND TEST DATA**

G. Kachadourian, General Electric Company, Philadelphia, Pennsylvania

**MEASUREMENT AND ANALYSIS OF GUN FIRING AND VIBRATION ENVIRONMENTS OF THE  
RIVER PATROL BOAT**

R. S. Reed, Naval Ordnance Laboratory, Silver Spring, Maryland

**\*RESPONSE OF THE AIM-9D (SIDEWINDER) MISSILE TO CAPTIVE-FLIGHT VIBRATION**

W. W. Parmenter, Naval Weapons Center, China Lake, California

**SCALE-MODEL WIND-TUNNEL ACOUSTIC DATA**

J. R. Baratono and F. A. Smith, Martin-Marietta Corporation, Denver, Colorado

<sup>a</sup>This paper appears in Shock and Vibration Bulletin 37, Supplement.

# HELICOPTER ENVIRONMENTS

## HELICOPTER VIBRATIONS

Charles D. Roach  
U. S. Army Aviation Materiel Laboratories  
Fort Eustis, Virginia

Of all mechanical contrivances, the helicopter probably experiences the greatest variety of unpredictable loads. The problems presented by the full range of mechanical vibrations to which the helicopter is subjected are eclipsed by the almost overwhelming complexity of the aerodynamically induced vibrations. While computers have eased the profound problem of delineating the aerodynamic forces and moments on a rotating blade translating through the air at a small obliquity, theories of general applicability, or known limitations, have yet to be devised. Much of the difficulty derives from the inability to handle either incompressible or compressible fluid flow. A summary is given of the multitude of vibration problems despite which the helicopter continues to be accepted. Current studies may enable much better definition of the aerodynamics of the rotor throughout the operating range. Flow control, better management of pitch variations, better airfoil designs, and boundary-layer control may be possible. Vibration isolation will still be required.

Perhaps no mechanical contrivance is subjected to so great a variety of unpredictable loads as the helicopter. Were it not for the important functions of vertical takeoff and landing made possible with these aircraft, I feel sure that vibrations and their concomitant effect on fatigue life would soon relegate the helicopter to an interesting but inconsequential niche in the history of technology. Yet the capability of vertical takeoff and landing is so necessary in military operations and in countless civil operations that we find the helicopter increasing in numbers. Expanded helicopter capabilities and performance are opening up markets unanticipated even a few years ago. So, if we are committed to the instrument, we are obliged to try to understand its peculiarities.

Helicopters are subjected to the full range of mechanical vibrations resulting from mass unbalance, dynamic runout of rotors, torsional vibrations of branched systems, whirl vibrations, and critical shaft conditions, not to mention the vibrational problems of the fuselage controls and appendages. All of these, abhorrent as they are, can be dealt with by well known and understood analysis and corrected by acceptably adequate devices or principles. This is not to say that improvements both in

analysis and in correctional devices are not necessary and encouraged; it is only that the almost overwhelming complexity of the aerodynamically induced vibrations eclipses the more tractable problems.

Early in the development of helicopters, investigators recognized the profound problem of delineating the aerodynamic forces and moments on a rotating blade translating through the air at a small obliquity. So formidable were the analytics that gross simplifications proved to be necessary to achieve even partial understanding. The deficit in analysis was made up to a large degree by trial and error; thus, a body of empirical guidance was formulated which contributed little to the science and which could be used for prediction only with the utmost caution. Fortunately, computers have made commonplace the evaluation of analytical methods previously thought to be completely intractable. We must not assume, however, that all of the problems have been solved. We have not yet devised theories which possess the virtue of general applicability or whose limitations are known for a certainty. Much of the difficulty derives from a frustrating inability to handle either incompressible or compressible fluid flow; indeed, hydrodynamics has lagged

all other fields. Nonetheless, we must deal with the problems even though closed solutions do not yet exist.

Unsteady flow characterizes the rotor difficulties. During flight, the inflow, the wake, and the flow near the blade skin are complex and interrelated. The flow varies from the sum of the instantaneous velocity resulting from the rotation and the forward velocity of the helicopter to the difference between these values. In practice, the velocity varies from about Mach 0.7 (with local Mach numbers approaching 1.0) to sectors where reverse flow exists, that is, flow from the trailing edge toward the leading edge. Lift and drag, varying as the square of the velocity, range over large values. In regions where compressibility effects are experienced, large drag increases appear rather suddenly and disappear almost as quickly, giving rise to sharp-edged loadings. Because the retreating blade moves at a low velocity, the lift must be improved by increasing the angle of attack of the blade, that is, by increasing the pitch. Near the hub, the velocity is not great enough to sustain flow; thus, stalling occurs, with a very sharp rise in drag.

Both the tips and the roots of the blades shed vortices which possess considerable energy. Depending upon the advance ratio, the rotor tilt, and other factors, subsequent blades may intersect a number of these tip vortices shed from the passing of earlier blades. Each intersection causes a momentary change in the blade loading. Since these loads occur in relatively small segments of the blade and at various locations depending upon the speed of the helicopter and the rotational velocity, several bending modes may be excited.

During horizontal flight, the cyclic variations in the pitch of the rotor cause continuously varying changes in circulation, each change giving rise to a shed starting vortex. The shed vortices positioned in the helix of the rotor wake strongly affect the circulation at the blade and the aerodynamic damping at the affected area. While one might expect strong positive aerodynamic damping in a helicopter rotor, the distortion of the flow field can in fact change the damping from strongly positive to strongly negative, depending upon the relative positions of the blades and the elements of the helical vortex sheet. Thus, whether one experiences positive or negative damping depends upon the sector of blade passage under consideration and the advance ratio of the rotor.

The entire rotor is somewhat analogous to a circular wing. There is, correspondingly, a

roll-up of the wake into two strong tip vortices shed from the port and starboard edges of the disk. The individual vortices from each blade wind up on the stronger vortex much as strands of a rope wrap around a common center.

If the roll-up were to occur far downstream, it would be of interest but perhaps have negligible effect on the aircraft. However, the roll-up seems to begin immediately, and the vortex core is inside the periphery of the disk. Thus, each blade passing through the roll-up is subjected to an exciting force of some magnitude.

I will only mention a few of the additional exciting forces that may exist in a rotor system, such as periodic boundary-layer separation and reattachment, large periodic variations in Reynolds numbers which affect both the lift and the drag forces, interference and blockage effects of wings and fuselage, pylon and mast turbulence, inequitable lift distribution throughout the operating range, and many other causes, some of which may be large in magnitude.

With an antitorque rotor, tandem rotors, and a number of compound helicopter configurations, the wake of one rotor becomes the inflow field of the next rotor. All of the difficulties that have been mentioned previously are now compounded.

It is apparent that the vibration problems of helicopters derive from a multitude of sources, most of which are aerodynamic in nature and for which we do not yet have the mathematics to handle. Thus, I have summarized and to a measure explained why in this technical age we still accept aircraft which, in vibrational characteristics, bear a close relationship to a hay baler.

What of the future? We speculate that studies now being conducted will define much better the aerodynamics of the rotor throughout the operating range. Flow control may be possible to reduce the tip vortex strength or to fill the vortex core, diffusing the vortex more rapidly. Better management of pitch variations should enable us to reduce somewhat the variations in loadings occasioned by cyclic control. Better airfoil designs tailored both to transition Mach number velocities and to unsteady flow should allow us to increase the rotational velocity and the advance ratio of the rotor by delaying compressibility effects. As a consequence, retreating blade stall may be minimized. Boundary-layer control may be possible to prevent separation and to reduce undesirable components of periodic spanwise flow.

When all these are done, we will no doubt find that helicopters still need methods of vibration isolation. The future probably will see increasing emphasis on broad-band isolation and damping. Active systems certainly seem

to be indicated for many applications. In the final analysis, however, the solution will be the result of the best efforts of both the aerodynamicist and the mechanical vibrations expert.

\* \* \*

**BLANK PAGE**

# HELICOPTER VIBRATION—A MAJOR SOURCE, ITS PREDICTION, AND AN APPROACH TO ITS CONTROL

Richard P. White, Jr., and Frank A. DuWaldt  
Cornell Aeronautical Laboratory, Inc.  
Buffalo, New York

Techniques for predicting blade loads, developed by Cornell Aeronautical Laboratory, Inc., for the U. S. Army Aviation Materiel Laboratories, are reviewed with the intent of illustrating the importance of nonuniform downwash and the blade vibratory characteristics in the production of vibratory loads transmitted to the helicopter fuselage.

One possible method of controlling the transmitted vibration is through the application of harmonic pitch control to the rotor system. The benefits that can be theoretically gained through the use of various orders of harmonic pitch control are illustrated by results obtained from a research program performed by Cornell. The reliability of present analysis techniques in predicting the transmitted shear will be evaluated in terms of the state of the art in predicting (a) the nonuniform downwash field in which the rotor operates and (b) the vibratory characteristics of the rotor system.

## INTRODUCTION

Since the beginning of powered flight, the propulsive device has been a source of vibration and noise. As the design of reciprocating engines evolved over the years, however, the transmitted vibration from the powerplant was reduced to very comfortable levels through the use of isolation systems and, with the introduction of turbojet aircraft, vibratory excitation of the primary structure of the aircraft from the propulsive device was effectively eliminated. Regarding the helicopter, however, the introduction of the free turbine at first reduced the vibration levels in the fuselage by eliminating the engine-order-induced excitation of the primary structure. The increased power available to the designer, however, soon advanced the forward speed of rotor-propelled aircraft and, since the rotor is a very efficient shaker system, the helicopter was soon speed limited because of the vibratory loads developed by the rotor system. As soon as the vibration was again brought within acceptable limits through design changes, more power was installed and the flight speed was again increased until the rotor-induced vibration was again unacceptable—and the cycle of design, more power, increased speed, etc., was repeated. There are very few ships flying today that have not been limited, are not now limited, or will not be limited in

performing according to the installed power because of rotor-induced vibration.

It might be thought that, since vibration isolation systems were successfully used with propeller installations, such systems would be applicable to helicopter rotor systems. In a very direct way, they are, but not in the simplified manner in which they were used for the propeller-engine installations of fixed-wing aircraft. In fact, the helicopter rotor system has successfully defied the use of this simple solution to eliminate the rotor-generated vibration transmitted to the fuselage since its inception many years ago. The reasons for this are fairly clear when the operating conditions of the conventional propeller and the helicopter rotor are compared. The conventional propeller generally operates with its propeller plane normal to the direction of flight, and each section of the blade is subjected to a more or less constant velocity with respect to the air as it rotates. The helicopter rotor, on the other hand, experiences this type of velocity field only when it is in hover—as, during translational flight, the rotor plane is nearly parallel to the free-stream velocity. Because of this orientation with respect to the free stream, each section of the rotor experiences a cyclic velocity variation once per shaft revolution and, thus, the dynamic pressure on a given blade section cycles at twice per revolution.

When cyclic control (or a freedom to flap) is also applied to the rotor blade during translational flight, cyclic variation of the sectional lift will occur also at a frequency of three per revolution. In addition, because of the orientation of the rotor with respect to the airstream, its wake, unlike the propeller wake, does not immediately leave the vicinity of the actuator plane, and higher-order variations of the induced velocity (and lift) are developed. Since the cyclic control inputs and the wake location of the rotor change with forward velocity and thus the magnitude and frequency of the primary exciting forces also vary, it is not hard to see why a simple passive isolation system has not been successful for the helicopter application. Possibly, active vibration absorbers could be used successfully with helicopters; but when it is realized that the response at a number of frequencies (which change with flight speed) must be controlled, it can be seen that such a system would, indeed, be a very complicated one.

If the shaft-transmitted rotor-developed vibratory forces cannot be eliminated through the use of an isolation system, is it possible to eliminate the transmitted rotor-induced shaking force and thus stop the annoying fuselage vibration? It can be reasoned that, since it is the oscillatory aerodynamic forces on the rotor blades that are responsible for the transmitted shaking force, it should be possible to eliminate these oscillatory forces through the use of blade angle-of-attack control. Attempts have been made to use this approach to eliminate the major transmitted oscillatory forces by introducing blade angle-of-attack control at higher frequencies than the normal cyclic input used to fly the helicopter. It is noted, however, that these attempts (1) did not meet with the success that was expected. It is believed that, while the approach of using blade angle-of-attack control to eliminate or reduce shaft-transmitted oscillatory forces is a valid one, past attempts have not been successful because they were based on too simplified a representation of the rotor wake and blade dynamics. The analyses did not retain the problem complexity required for quantitative judgments. Since the initial unsuccessful attempts at controlling the oscillatory force inputs to the fuselage were made, the theoretical representation of the helicopter blade dynamic and aerodynamic characteristics has advanced greatly. Today, a relatively realistic representation of these characteristics can be formulated, and it is believed that an analytical investigation of the possibility of using blade pitch control to eliminate the harmonic aerodynamic excitation can be undertaken with confidence.

While the rotor develops oscillatory forces and moments in all planes, this paper deals only with those forces that are developed and transmitted to the fuselage in the vertical direction parallel to the rotor transmission shaft. Benefits that might be obtained in the reduction of the harmonics of transmitted shears through the use of harmonic pitch control of the blades are presented. An evaluation of the validity of the computed results is given through an evaluation of the modeling and analysis technique used in the theory on which the results were based.

## BACKGROUND OF APPROACH

It has been known for some time (2) that if helicopter periodic airloads and blade bending moments are to be predicted accurately, then the gross simplifying assumptions associated with uniform inflow to the rotor disk have to be rejected. A realistic representation of the effects of the rotor wake at the plane of the rotor is required.

The Cornell Aeronautical Laboratory, Inc. (CAL) has been developing practical analysis techniques for predicting the periodic airloads and dynamic response of rotor blades for single- and tandem-rotor helicopters (based on work done for the U.S. Army Aviation Materiel Laboratories). The main feature of these developments has been the inclusion of a realistic rotor wake in the analysis techniques so that the wake-induced effects on the rotor blade can be properly accounted for in the determination of the aerodynamic loads. References (3) through (7) present the details of the analysis techniques that have been developed and the results that have been obtained for both single- and tandem-rotor configurations.

As noted, a principal feature of the analysis techniques that have been developed is the consideration of the rotor wake which leads to a nonuniform induced velocity distribution at the rotor plane. Since this is a very important feature of the analysis techniques, it is worth considering in a little more detail. The induced velocity distribution at the helicopter rotor is not uniform because the vorticity, originating as trailing and shed components at the blades, remains in the vicinity of the rotor plane. This is seen most easily in the limiting case of hovering, where the vertical displacement of the tip vortex from a blade may be only a few chord lengths from the rotor while the blade travels one revolution. In the forward flight case, of course, the wake vorticity array is not

symmetrical with respect to the rotor because of the translational velocity, and thus gradients of induced velocity occur in the rotor plane. These gradients of induced velocity developed in translational flight are illustrated in Fig. 1 for the UH-1A at an advance ratio of 0.26. It is noted for comparison purposes that the value of the uniform induced velocity based on momentum considerations is about 5 fps and the total mean inflow is about 24 fps. As can be seen, the range of the induced velocities indicated on Fig. 1 is +10 fps (i.e., velocity up through the rotor plane) to -60 fps. Some significant conclusions can be drawn from Fig. 1 for the single-rotor helicopter in translational flight. First, the distribution is certainly nonuniform. Second, the large downwash velocities near the tip when the blade is in the retreating semicircle should delay blade stall. Third, the downwash velocity gradients in the spanwise direction appear to be appreciably smaller on the advancing side than on the retreating side of the disk, while the azimuthal gradients are almost non-existent on the retreating side but significant on the advancing side.

Figures 2a and 2b present the induced velocity distributions computed for the CH-47A at

its cruise speed. As might be expected, the induced velocity distribution for the tandem overlapped rotor is much more complicated than it is for the single rotor and, in fact, most of the conclusions regarding the downwash distribution of the single rotor do not apply for the tandem. One interesting feature of the induced velocities computed for the tandem rotors is that the minimum spanwise or azimuthal gradients for both rotors occur in the regions in which the rotor disks are overlapped.

Since the induced velocities are significant in the determination of the effective aerodynamic angle of attack to which each blade section is subjected, it is not surprising that appreciable oscillatory airloads are developed by the blades of the helicopter rotor as it rotates. Similarly, the nonuniform induced velocity distribution should be considered in any theory used to determine blade pitch controls necessary for attenuating oscillatory loads.

#### APPROACH USED TO CALCULATE REQUIRED CONTROL INPUTS

In the theory just discussed to determine the periodic blade loadings and the resulting

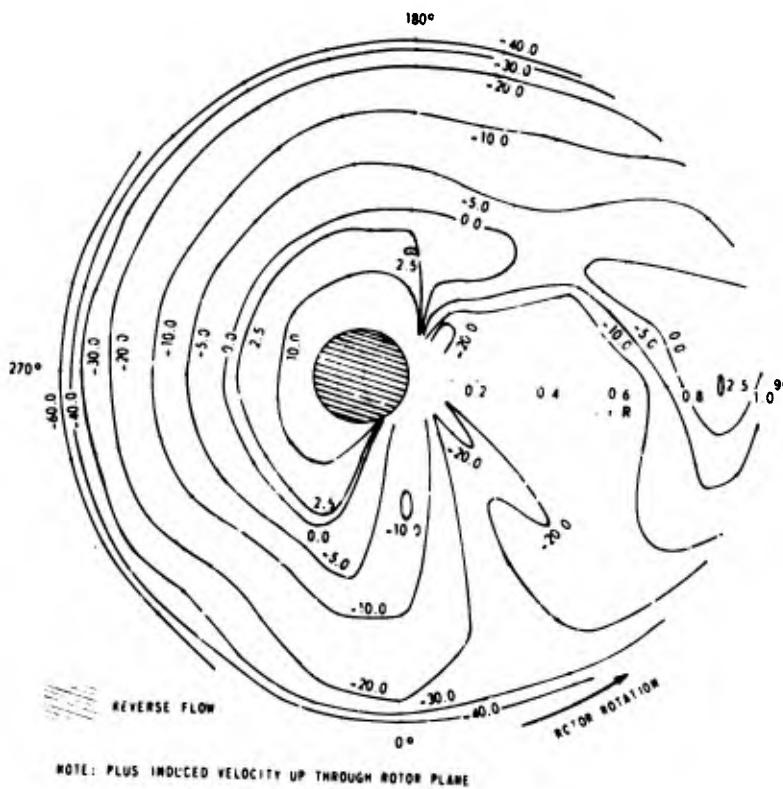


Fig. 1. Induced velocity distribution: ft/sec; UH-1A;  $\mu = 0.26$



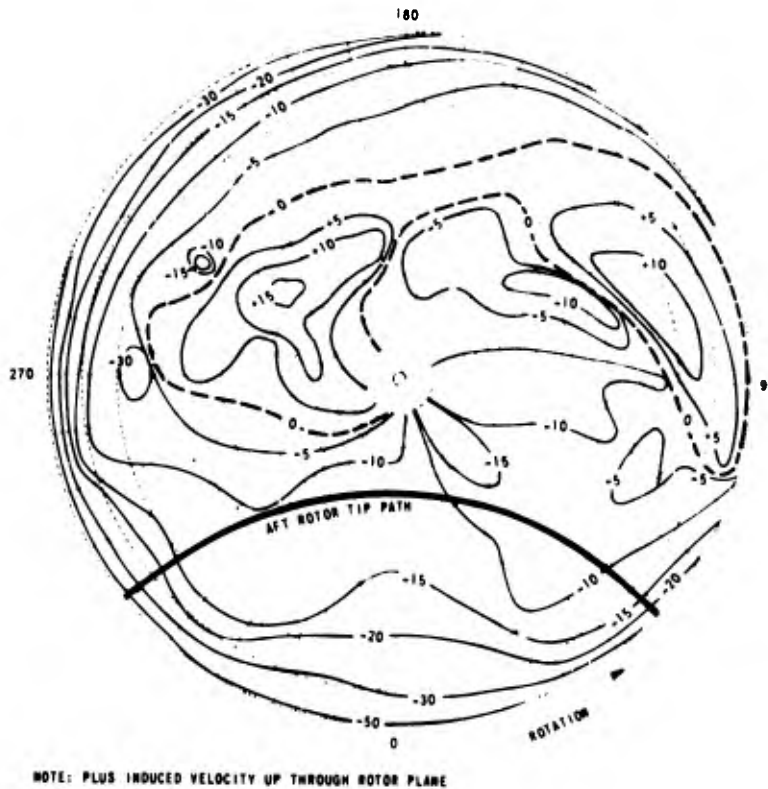


Fig. 2a. Induced velocity distribution: ft/sec; CH-47A;  
 $\mu = 0.29$  (forward rotor)

dynamic response of the rotor, the rotor control settings (both collective and cyclic), forward speed, shaft angle, etc., are inputs to the computing program. In the program reviewed here, the inverse problem was solved: that is, for a given set of trimmed flight conditions and blade parameters, what is the blade pitch control required to obtain a specified aerodynamic loading? Specifically, the theory was used to determine the required control inputs to create load distributions producing the following specified characteristics during translational flight of the helicopter:

1. Constant azimuthal loading at each radial station;
2. Zero values of the noncreating vertical root shears.

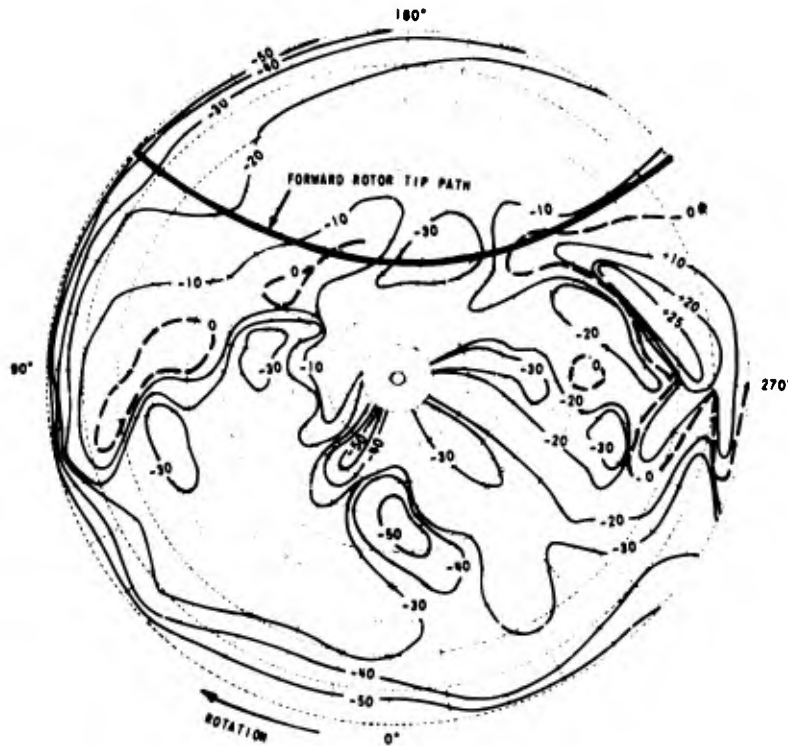
The first loading condition is the same as is obtained in pure hovering flight and, since there are no azimuthal variations of the air loads, no periodic loads are developed. The second loading condition specifies that the spanwise integral of the aerodynamic and inertial

loadings is zero for the noncanceling periodic vertical shears (those at frequencies which are multiples of the number of blades).

The theory for transmitted shear control was developed (8) and calculations were carried out for a two-bladed teetering-rotor system having physical characteristics very similar to those of the UH-1A. Some of the results obtained for this rotor system for both of the specified loading conditions are presented.

The results presented in Fig. 3 show the radial variation of the blade pitch angles, at three azimuth stations and two flight speeds, required to develop the first loading condition. Inspection of the results for this case of no azimuthal variation of load indicate that:

1. There is a significant radial variation of angle of attack;
2. The radial distribution of angle of attack changes with azimuth angle and with forward velocity;



NOTE: PLUS INDUCED VELOCITY UP THROUGH ROTOR PLANE

Fig. 2b. Induced velocity distribution: ft/sec; CH-47A;  
 .. = 0.29 (aft rotor)

3. The mean spanwise gradient of angle of attack is opposite to that generally built into rotor blades (washout).

These facts make it evident that an extremely complicated control system would be required to develop the desired uniform loading distribution; therefore, obtaining this type of loading is probably impractical.

In the calculations conducted to determine the blade pitch control required to make the vertical noncanceling root shears become zero, it was assumed that the only control that would be used was the collective control applied at the blade root. The results of the calculations that were performed are summarized in Fig. 4. It can be seen that the oscillatory vertical root shear is approximately  $\pm 200$  lb per blade and occurs at twice per revolution during flight under normal blade pitch control. When collective blade pitch control is applied only at the second and fourth harmonics of the rotor rpm, the oscillatory root shears are reduced to approximately  $\pm 15$  lb—which is better than a 90

percent reduction. If all the noncanceling vertical root shears were eliminated, a straight horizontal line would emanate from the 3200-lb point (about half of the gross weight of the helicopter). The collective pitch controls required for these three conditions are presented in Fig. 5. The conventional flight control collective pitch is, of course, independent of azimuthal position and appears as a horizontal line at about 18 deg. Elimination of the second and fourth harmonics requires the azimuthal time history shown by the dotted line. Note that the double amplitude is about 3 deg. The elimination of all noncanceling vertical root shears (up through the twelfth harmonic) is indicated by the solid line. In this latter case, a double amplitude excursion of about 6 deg is required and fairly rapid control motions are indicated.

Based on the results presented in Figs. 4 and 5, over 90 percent of the oscillatory root shears might be eliminated through the use of only second and fourth harmonic control. Roughly 20 times the control force would be

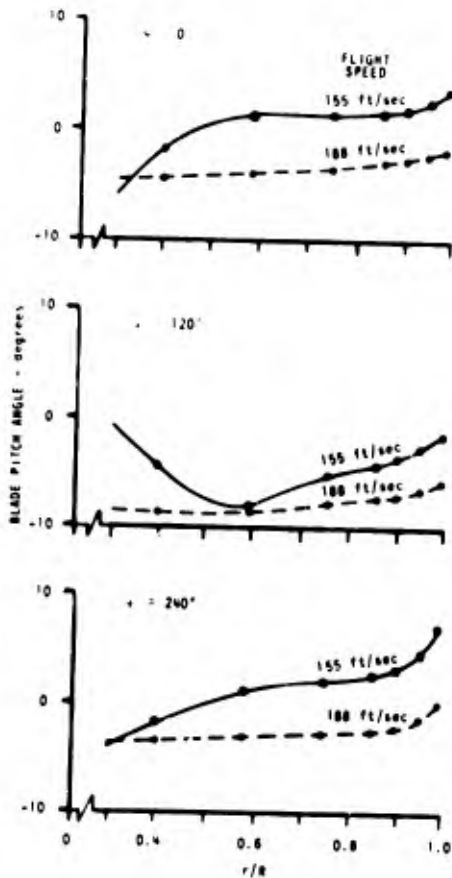


Fig. 3. Radial variation of blade pitch angles required to eliminate all harmonic airloads (two-bladed rotor)

required to eliminate the last 10 percent of the transmitted shears.

It is not unreasonable to expect that the use of harmonics of blade collective pitch control to

modify the transmitted vertical root shear characteristics might adversely affect the time histories of the aerodynamic loadings and thus the blade strains. Figure 6 compares the azimuthal variation of the lift loading at three radial stations when harmonic collective pitch control is used with that obtained when only normal collective control is present. The results on the left of Fig. 6 indicate that the use of control up through the twelfth harmonic does, in fact, adversely affect the blade loading. The large components of higher-harmonic lift load could adversely affect the blade life. On the other hand, the use of just the second and fourth harmonics (right-hand side of Fig. 6) does not alter the azimuthal variation of the lift a great deal, and thus the blade life probably would not be significantly affected by these control inputs. Use of just the second and fourth harmonics of blade collective pitch control, then, provides practical reduction of oscillatory vertical root shears for a two-bladed rotor system without attendant fatigue problems.

While not shown here, the results of calculations at other translational velocities indicate the same trends, and the same conclusions can be drawn. However, the magnitudes and phasings of the harmonic control inputs change with flight speed, and some type of servo-feedback system would probably be required for the reduction of oscillatory vertical shears throughout the flight region.

The requirements of such a control system, as well as the control inputs required to eliminate the inplane shears and torques, are the subject of the continuing investigation being conducted by CAL under U. S. Army sponsorship.

Since only computed results have been presented, one might ask what confidence can be placed in them—particularly after it has been stated that previous theoretical results did not

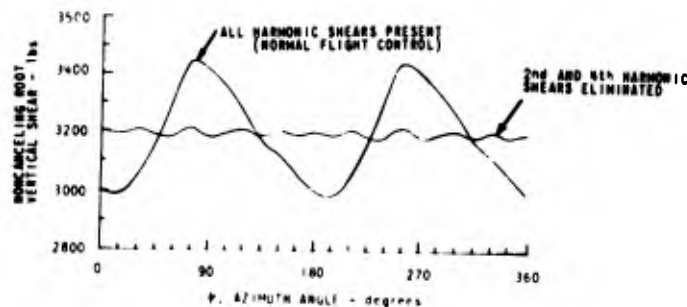


Fig. 4. Azimuth variation of noncanceling vertical root shears per blade (two-bladed rotor; 188 ft/sec)

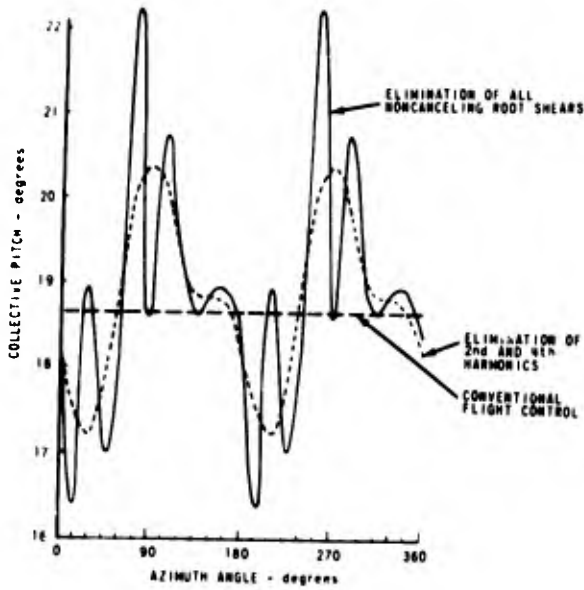


Fig. 5. Comparison of pitch control schedules for eliminating noncanceling harmonic root shears (two-bladed rotor; 188 ft/sec)

prove out in practice because of limitations imposed by the assumptions in the analysis techniques. It is reasonable, therefore, to examine the assumptions upon which the analysis has been based to determine if all the important basic features of the environment have been satisfactorily considered.

Analyses of the transmitted shears and, in fact, of the helicopter blade loading in general depend upon two interconnected aspects: (a) prediction of the blade aerodynamic loadings, and (b) the dynamic response of the elastic structure. The aerodynamic and structural aspects of the response problem are, in fact, interconnected because the blade loading acts as a forcing function of the structure, and the resulting structural dynamic response creates a velocity change which, in turn, affects the angle-of-attack distribution and hence the aerodynamic loading. For purposes of discussion, however, these are treated separately in the subsequent remarks.

Blade aerodynamic lift depends upon the local effective angle of attack, and a significant

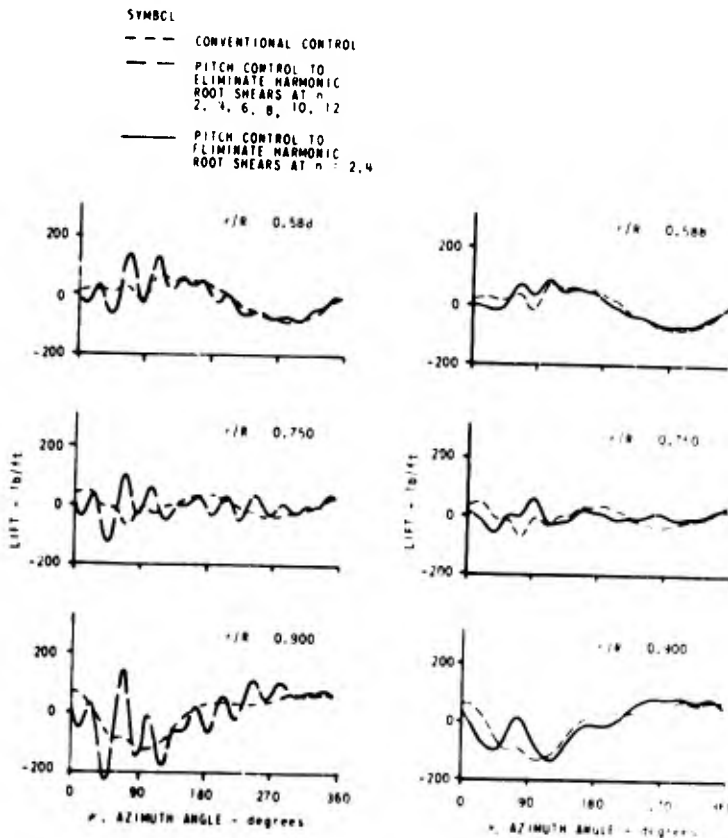


Fig. 6. Effect of higher harmonic pitch control on oscillatory lift loadings (two-bladed rotor)

part of this angle may arise from the induced velocity field. Measurements of rotor velocity fields, such as those previously presented in Figs. 1 and 2, are difficult if not impossible to make. As far as is known, no one has ever been sufficiently motivated, dedicated, and ingenious to undertake measuring the time histories of the three velocity components in a helicopter tip path plane. Fortunately, however, local aerodynamic pressures are easier to measure and have been obtained for a few well-controlled flight conditions on three well-known helicopters—the UH-1A, UH-34, and CH-47A. These measurements therefore must be, for the time being, the interface at which theoretical and experimental results can be compared. Figure 7 shows a comparison of the predicted and measured oscillatory lift (the mean values have been extracted) for three radial stations of an H-34 helicopter. It can be seen from the results presented that the theoretically predicted values taken from Ref. (5) are in generally good

agreement with the experimental values extracted from Ref. (9).

Similar results for both rotors of the CH-47A tandem-rotor helicopter are shown in Fig. 8. The theoretical curves are taken from Ref. (7) and the experimental from Ref. (10). As might be expected for this overlapped rotor configuration, the azimuthal variation of the aerodynamic loads is more extensive for both the forward and aft rotors than for the single-rotor configuration. This is particularly true for the aft rotor, as might be expected after inspecting the induced-velocity distributions shown in Figs. 2a and 2b. It is noted that while the agreement between the analysis and the measurement is reasonably good, the success in predicting the azimuthal variation of the aerodynamic loadings for the tandem configuration is less than that for the single rotor. For both configurations, however, the major peaks and valleys in the aerodynamic loading that

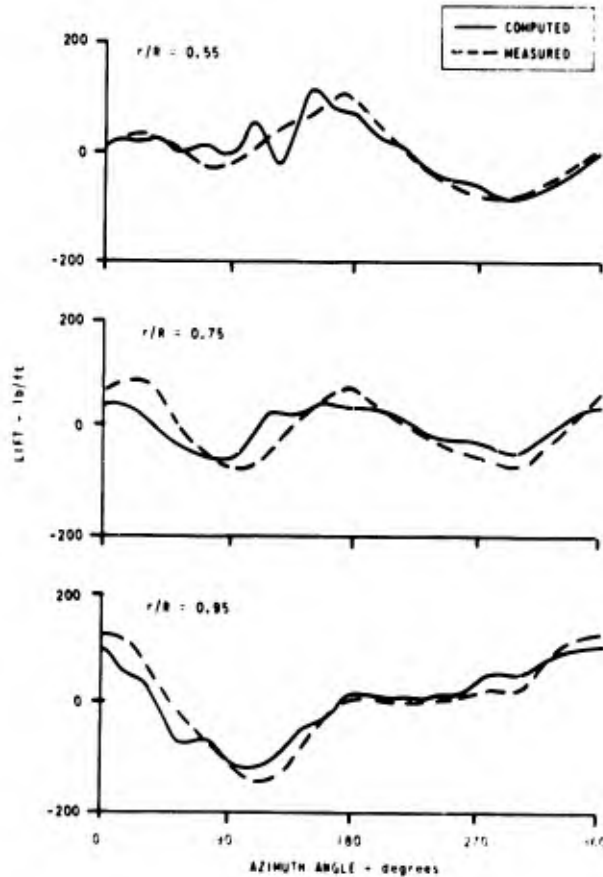


Fig. 7. Measured and computed oscillatory lift of three spanwise stations of the H-34 at  $\mu = 0.29$

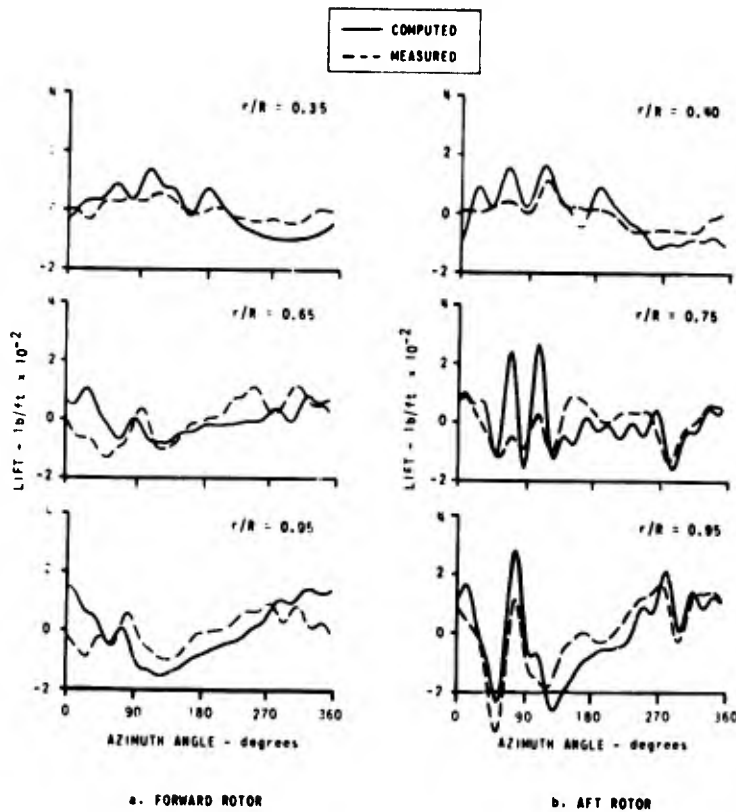


Fig. 8. Azimuthal variation of measured and computed oscillatory lift of the CH-47A at  $\mu = 0.24$

result from blade proximity to vortex elements introduced by previous blade passages are reasonably well predicted. There seems to be a tendency for the theory to indicate greater load excursions than are experienced. The important aspect of the predicted results is, however, that the peaks and values of the measured results were in fact reasonably well calculated.

Overall agreement between theoretical and experimental oscillatory lift distributions is displayed in Figs. 7 and 8. It is also apparent from the data that improvements remain to be made. It might be well, therefore, to review some of the idealizations introduced in the theoretical method.

One of the approximations introduced in the aerodynamic model was the location of the wake. For the cases shown, the wake was fixed as a skewed helical sheet of vorticity with the helix angle fixed on the basis of momentum considerations. However, it is known (for example, Ref. 5) that wake distortions can have a very significant effect on the blade loadings. The

results presented in Ref. (5), which show this significant effect, were based on a wake location deduced from flow-visualization studies. For prediction purposes, however, it is desirable to avoid this empiricism and to have a means of calculating the spatial array of the wake vorticity. Efforts to develop a method of predicting the location of the free wake trailed by the blades of a rotor system have been undertaken by CAL, and some of the more recent efforts have been reported in Ref. (11). In the analysis reported there, the rotor tip vortex was allowed to distort under the influence of the blade-bound vortex and, of course, under the influence of the induced velocities of the previously trailed vortices.

Figure 9, extracted from Ref. (11), compares the paths of the trailed tip vortices for a momentum-specified fixed skewed helix (that which is used in all the blade-loads analyses previously discussed here) with those obtained by letting the wake convect under its own influence. As can be seen, the distortions of the path from a helix are very significant. The

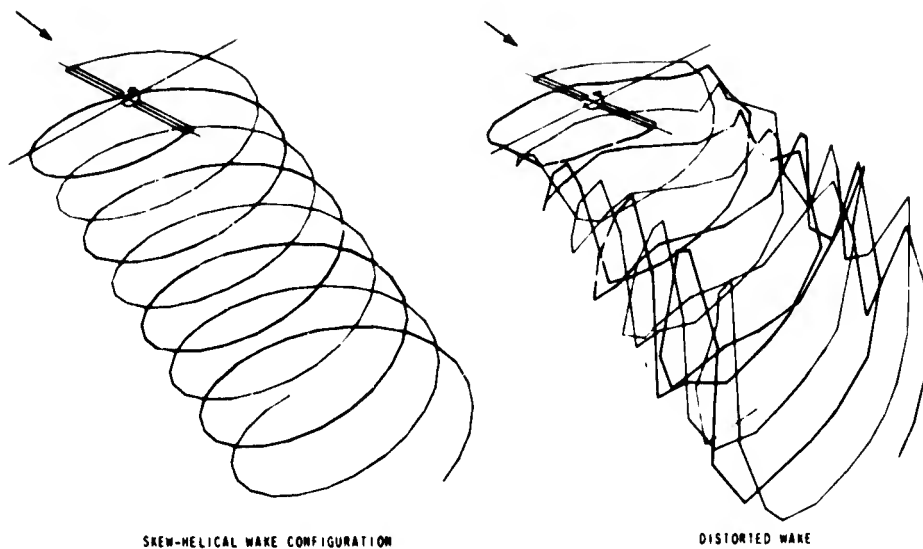


Fig. 9. Comparison of fixed and free wake geometries for a two-bladed rotor at  $\mu = 0.14$

wake trajectory shows a tendency to roll up at the extremities in a manner reminiscent of wing wakes. The "rolled-up vortex" is not circular in this case, of course, and it is not difficult to see that the local vorticity vector has an alignment quite different from the wing case. Further, spatial truncation of the wake and the neglect of diffusion and dissipation processes probably invalidate the rotor-tip vortex path depicted downstream—but the distortions near the blade should have meaning. Comparison of the wake geometries presented in Fig. 9 indicates that there are significant differences near the plane of the rotor, and, thus, the oscillatory aerodynamic loading developed by the blades would be expected to reflect the same significant changes.

It would be expected that the wake for the tandem helicopter would have a more confused shape than that for the single rotor and a more significant effect on the airloads. The comparison of theoretical and experimental data of Fig. 8 appears to bear out this heuristic view.

It might be concluded on the basis of the foregoing discussions that the aerodynamic modeling of the rotor and its wake for both single- and tandem-rotor helicopters is reasonably good in that the azimuthal variations are reasonably well predicted. However, the detailed harmonic content is needed for structural response analyses; it is believed that an improvement in this respect can be realized if the free vortical wake is treated more realistically.

As previously stated, there are two aspects of the modeling that must be examined, the aerodynamic and the dynamic, since both must be represented if the shears transmitted to the fuselage through the rotor shaft are to be accurately predicted. It has been shown that the aerodynamic modeling contains all the features required for predicting the oscillatory aerodynamic forces developed by the blade, although refinements in the wake model must be considered. Now the adequacy of the structural modeling will be considered.

In all the blade-loads prediction methods previously discussed and in the analysis of the transmitted shears, the structural dynamic characteristics of the blades were represented by modal functions. That is, the natural rotating flapwise-bending modes of the rotor were used to describe the dynamic characteristics of the rotor system. The response of these modes to the oscillatory aerodynamic forces was used to compute the oscillatory bending-moment distributions of the rotor blades. The azimuthal variation of the measured and predicted flapwise-bending moments for three radial stations of the H-34 are presented in Fig. 10 for the same flight condition for which the aerodynamic loads were presented in Fig. 7.

If the results presented in Figs. 7 and 10 are compared, it is noted that the airload data contain relatively small amounts of high-frequency components, while the bending-moment data show a significant high-frequency

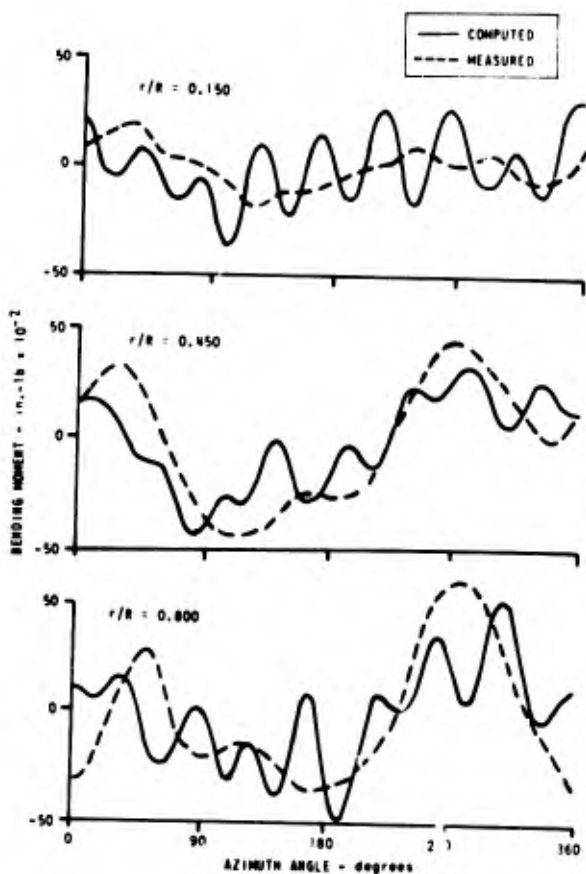


Fig. 10. Measured and computed flapwise bending moments; H-34 at  $\mu = 0.29$

content, at least in the computed values. It is believed that most of the disparity between the predicted and measured bending moments arises from errors in the calculated vibration characteristics of the blading; that is, relatively small errors in natural frequency estimates can cause large errors in the oscillatory bending-moment estimates. This can be seen easily in the resonance diagram presented for the H-34 rotor in Fig. 11 where the flapwise-bending frequency is plotted as a function of the rotor speed and lines of constant harmonic order are superimposed.

At the operating rotor speed of 216 rpm for this flight condition, the third bending mode has a calculated natural frequency very nearly equal to the eighth harmonic of the rotational speed, which is the same harmonic order as the large bending-moment oscillations shown in Fig. 10. It is noted that a 2 percent shift in

computed frequency would place the frequency of the third flapwise-bending mode right at the eighth harmonic of the rotor rpm. Since the structural damping of rotor blades is characteristically low, large changes in blade response can occur if the frequency of the forcing function nearly coincides with a natural frequency. It is believed that if the predicted frequency of the third mode of the H-34 were slightly lower, on the order of 2 or 3 percent, the predicted bending moments shown in Fig. 10 would be in much closer agreement with the measured values. While calculations were not carried out for this flight condition of the H-34 to prove this point, calculations carried out for other flight conditions have verified this hypothesis.

From the results presented, it is obvious that very accurate prediction of the vibratory characteristics of helicopter rotor blades is required if the magnitudes of the oscillatory bending moments and transmitted shears are to be accurately predicted. Unfortunately, the prediction accuracy that is required is not now within the state of the art, and, therefore, improvements must be made. This problem is now under investigation at CAL under U. S. Army sponsorship, and it is hoped that in the foreseeable future it will be possible to demonstrate that an analysis procedure has been developed that will predict the vibratory characteristics of helicopter rotors to the desired accuracy.

#### SUMMARY

An attempt has been made to outline one aspect of the helicopter vibration problem, namely, the excitation of the fuselage by the lift shear forces transmitted at the blade root. Results were presented that indicated harmonic control of the rotor-blade pitch angle could significantly reduce the forces that are transmitted; that is, attention was devoted to modifying the vibratory forcing function. A 90 percent reduction of the transmitted shears (in the lift direction) was calculated for a two-bladed rotor when second and fourth harmonic collective pitch signals were incorporated. Computations also indicated that the control program is a function of flight condition, and hence an adaptive system might be required. The analysis was based upon an aerodynamic and structural dynamic model which appears to give reasonable agreement with measured data; thus, the results presented are believed to be valid, at least on a qualitative basis.



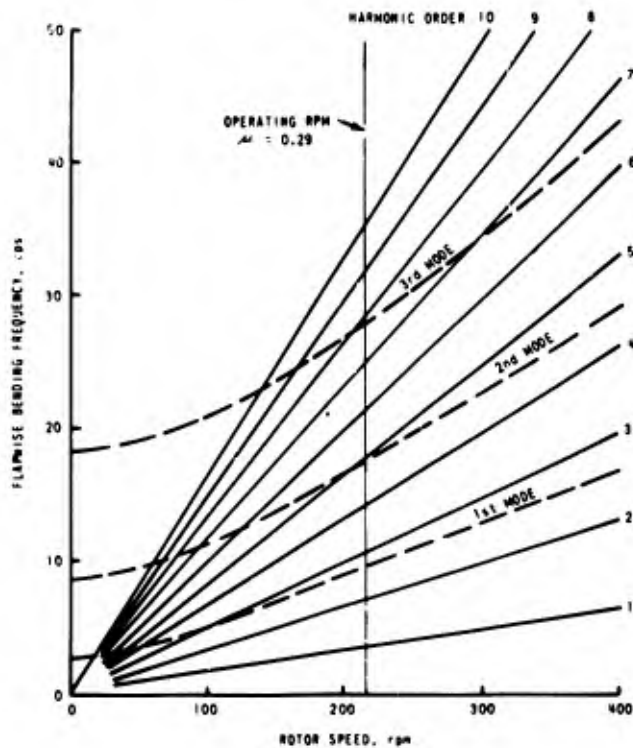


Fig. 11. Rotor blade resonance diagram of flapwise modes of H-34

#### REFERENCES

1. U. S. Army Transportation Research Command, "An Experimental Investigation of a Second Harmonic Feathering Device on the UH-1A Helicopter," TCREC Tech. Rept. 62-109, June 1963
2. H. Daughaday and J. Kline, "An Approach to the Determination of Higher Harmonic Rotor Blade Stresses," Cornell Aeronautical Laboratory Report CAL-52; see also Proceedings of Ninth Annual Forum, American Helicopter Society, Inc., 1953
3. R. A. Piziali and F. A. DuWaldt, "A Method for Computing Rotary Wing Airload Distribution in Forward Flight," U. S. Army Transportation Research Command, TRECOM Tech. Rept. 62-44, Nov. 1962
4. R. A. Piziali and F. A. DuWaldt, "Computation of Rotary Wing Harmonic Air Loads and Comparison With Experimental Results," paper presented at Eighteenth Annual National Forum, American Helicopter Society, Inc., Washington, D. C., May 1962
5. R. A. Piziali, "A Method for Predicting the Aerodynamic Loads and Dynamic Response of Rotor Blades," U. S. Army Aviation Materiel Laboratories, USAAVLABS Tech. Rept. 65-74, Jan. 1966
6. T. T. Chang, "A Method for Predicting the Trim Constants of a Single-Rotor Helicopter and the Rotor-Blade Loadings and Responses," U. S. Army Aviation Materiel Laboratories, USAAVLABS Tech. Rept. (in press)
7. J. C. Balcerak, "A Method for Predicting the Aerodynamic Loads and Dynamic Response of the Rotor Blades of a Tandem-Rotor Helicopter," U. S. Army Aviation Materiel Laboratories, USAAVLABS Tech. Rept. 67-38, June 1967
8. H. Daughaday, "Suppression of Transmitted Harmonic Rotor Loads by Blade Pitch Control," U. S. Army Aviation Materiel Laboratories, USAAVLABS Tech. Rept. 67-14 (in press)

9. J. Scheiman, "A Tabulation of Helicopter Rotor-Blade Differential Pressures, Stresses, and Motions as Measured in Flight," NASA TM X-952, Mar. 1964.
10. R. R. Pruyn, "In-Flight Measurement of Rotor Blade Airloads, Bending Moments, and Motions, Together With Rotor Shaft Loads and Fuselage Vibration, on a Tandem-Rotor Helicopter," Boeing Company, Vertol Division Rept. D8-0382-4 (in press)
11. P. Crimi, "Theoretical Prediction of the Flow in the Wake of a Helicopter Rotor, Part I - Development of Theory and Results of Computations," Cornell Aeronautical Laboratory Rept. BB-1944-S-1, Sept. 1965

#### DISCUSSION

Mr. Rice (Goodyear Aerospace Co.): If you put on such a control would that actually make the rotor blades much quieter? Would it reduce the noise that snaps off the tips if you were trying to build a quiet helicopter?

Mr. White: Not necessarily. For lower harmonic blade pitch control, the loading on the

blade would not appreciably change. If you go to higher harmonic blade pitch control, you will develop much higher loading conditions in the blade, not only transmitted through it, but the blade may develop much higher loading conditions which may increase the noise

\* \* \*

**BLANK PAGE**

# HELICOPTER FUSELAGE VIBRATION PREDICTION BY STIFFNESS MOBILITY METHODS

John J. Sciarra  
The Boeing Company  
Morton, Pennsylvania

Through the use of the direct stiffness and mobility methods, many aspects of a helicopter fuselage's dynamic characteristics may be investigated. The objective of such studies would be to economize on flight tests, and also to yield insight as to inflight vibration response reduction methods. For many years, helicopter fuselages have been idealized and analyzed by use of the stiffness method. The results were natural frequencies, mode shapes, and the forced vibratory response. Correlation was good. It was then observed from this analysis and by test that certain natural frequencies of the fuselage could be altered by structural modification to yield a lower vibratory response. More recently, a crudely idealized model of a helicopter fuselage was dynamically analyzed by using the stiffness method. Results were compared with those obtained for a refined model. Agreement indicated that preliminary vibratory design of fuselages was feasible in the proposal stage. The stiffness method was then extended to allow for the analysis of the effectiveness of antivibration devices by using mobility techniques. It was found that by using the mobility method, the analysis of the effectiveness of antivibration devices at the point of attachment, and at remote points, compared well with testing.

## INTRODUCTION

A helicopter in flight will always generate hub vibratory forces of magnitudes ranging from a few hundred pounds to one or more tons. Similarly, high hub vibratory moments can occur. The frequency of these hub forces and moments is an integral multiple of the number of blades. The forces occur in the vertical, longitudinal, and lateral direction, and the moments occur in the rolling, pitching, and twisting mode. These hub loads are phased, since they have a sine and cosine component, or, in other words, an amplitude and a phase angle. These loads feed into the fuselage structure, and a vibratory response results which will be further intensified if the natural frequencies of the blades or fuselage are close to the frequencies of the exciting loads.

To design a new helicopter properly or modify an existing one, analyses must be available which can predict vibratory hub loads and determine the fuselage forced response. The response solution should include the capability of using phased forcing loads and structural damping. With the availability of these procedures in the form of computer programs, parameters could be varied economically to minimize hub loads and remove blade or fuselage natural frequencies from exciting frequencies.

Recently, good correlation has been obtained in the determination of hub loads. Vibration reduction methods associated with the rotor system have been analyzed mathematically for effectiveness, and correlation has been obtained by physical test. A few of these methods have been by cyclic pitch control, by concentrated weights, and by tapering the outboard portion of the blade (e.g., Ref. 1). The philosophy behind these rotor modifications is that reducing the hub loads will reduce the vibration level in the fuselage. However, the phasing of the input loads may be such that reducing some hub loads may not reduce the fuselage response in all locations.

Also, a tandem rotor helicopter has a second phasing because of loads from two separate rotor systems which excite the airframe simultaneously; for instance, a force from the aft pylon with the correct phasing could cancel the response of a force from the forward rotor system in the crew station.

Structural damping would cause a third type of phasing which could affect the response of the many vibratory loads. It would appear that the mathematical difficulties involved in developing a fuselage analysis technique are considerable. However, the use of matrix methods and high speed computers considerably simplifies the

procedure. In fact, a damped forced response solution utilizing stiffness methods can easily consider load phasing and phasing resulting from structural damping and twin rotors. Such a computer program has been completed, and through its use analytical studies have been performed to determine the effectiveness of structural modifications, size variations, and mass changes in tuning the fuselage away from its many exciting frequencies. The program has also been used to evaluate the effect of load reduction in the rotor system on the airframe, since it is inside the craft that the final evaluation of load reduction must be made.

Nevertheless, in a helicopter, some vibration will remain, even with the reduction in hub loads and the detuning of the airframe. To reduce this remaining response, vibration neutralizers or force generators must be used. In order to obtain mathematically the effectiveness of these antivibration devices, the mobility method (based on displacements) may be used with stiffness analysis results or with shake test results. This combined stiffness-mobility method can yield many studies economically. For example, because of the expense of flight tests and ground shake tests, it may be necessary to determine analytically the location in the fuselage which is most efficient for the placement of the antivibration device. Also, as another example of using this method, the weight penalty of the vibration reducer may be minimized by utilizing computer studies of its components.

#### DIRECT STIFFNESS METHOD

Probably the most promising applications for the direct stiffness method, as applied to the dynamics of semimonocoque structures, exist in the helicopter. The method is well documented in the literature, and is given specifically for helicopters in Ref. (2), which covers the analytical and computer aspects.

A structure to be analyzed dynamically is first idealized into an assemblage of a large number of smaller components such as beams, skins, and stringers. The elements meet at node points or junctions. All these node points can have six degrees of freedom, and boundary conditions may be imposed. The stiffness matrix of each structural element is first determined. Then its stiffness contributions to every degree of freedom of all the nodes of the structure are added to contributions from other structural elements. This is done for every degree of freedom, each of which comprises

one row of a large matrix called a stiffness matrix or  $[k]$ .

In general,

$$\{F\} = [k]\{\delta\} \quad (1)$$

where  $\{F\}$  is the column matrix of forces or moments at all the degrees of freedom of the nodes, and  $\{\delta\}$  is the matrix of deflections or rotations.

Equation (1) may be partitioned to give:

$$\begin{Bmatrix} F_1 \\ F_2 \end{Bmatrix} = \begin{bmatrix} k_{11} & k_{12} \\ k_{21} & k_{22} \end{bmatrix} \begin{Bmatrix} \delta_1 \\ \delta_2 \end{Bmatrix} \quad (2)$$

If all  $F_2$ 's are zero, then a lumping of the masses has been assumed, and Eq. (2) may be solved:

$$\begin{aligned} \{F_1\} &= [k_{11} - k_{12}k_{22}^{-1}k_{21}]\{\delta_1\} \\ &= [k_{eff}]\{\delta_1\} \end{aligned} \quad (3)$$

Equation (3) is a matrix operation called reduction, which immediately illustrates an analytical method for determining the effective spring constant of a complex structure; if necessary, this spring constant could be used in a simplified analysis.

Utilizing the mass matrix  $[M]$ , Eq. (3) gives a dynamic solution:

$$[M]^{-1}[k_{eff} - \lambda]\{\delta\} = 0 \quad (4)$$

where  $\lambda$  is an eigenvalue, and  $\{\delta\}$  is the matrix of modal displacements or rotations. These values correspond to the structure's natural frequencies and mode shapes, respectively. Contrary to many vibrating systems, some of the eigenvalues of simple symmetric structures, or even of complicated ones, may be equal. If this occurs, the mode shapes may have to be determined using special techniques; fortunately, however, this is not usually the case.

Although the matrices in the stiffness method are large, numerical correctness can be ensured if care is taken. The accuracy of this method may best be illustrated by comparing results in Fig. 1 for a medium transport helicopter; a lumped-mass analysis, a stiffness method computation, and shake test results are compared. The mode shape of each natural frequency is both described and pictured.

The lumped-mass results are derived from a Myklestad-type analysis wherein the fuselage

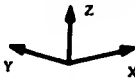





NATURAL FREQUENCY CPS			DESCRIPTION OF MODE SHAPE	MODE SHAPE 
LUMPED MASS ANALYSIS	STIFFNESS ANALYSIS	SHAKE TEST		
	7.1	7.0	PREDOMINANT MOTION OF AFT PYLON LATERALLY	
7.35	7.7	8.0	VERTICAL LONGITUDINAL MOTION OF STRUCTURE. FORWARD AND AFT PYLONS MOVING IN OPPOSITE DIRECTIONS	
	10.7	10.5	FUSELAGE TORSION. FORWARD AND AFT PYLONS MOVING LATERALLY IN OPPOSITE DIRECTIONS	
11.15	11.7	11.4	VERTICAL LONGITUDINAL MOTION OF STRUCTURE. FORWARD AND AFT PYLONS MOVING IN SAME DIRECTION	
15.53	15.6	14.3	PREDOMINANT MOTION OF FORWARD PYLON LONGITUDINALLY	

Fig. 1. Comparison of test and analytical results

is assumed to be a beam capable of executing uncoupled vertical bending or coupled lateral torsion bending. Note that the lumped-mass analysis skips some frequencies.

Once the natural frequencies and mode shapes have been obtained, the damped forced response of the fuselage may be determined. In Ref. (3), this matrix method for a phased external exciting force or moment is derived. The basic matrix equation is:

$$[A^T M A] \{\ddot{\delta}\} + [A^T C A] \{\dot{\delta}\} + [A^T k A] \{\delta\} = \{A^T F\} \quad (5)$$

where  $A$  is the modal matrix composed of the mode shapes,  $M$  is the mass matrix,  $C$  is a damping matrix obtained by assuming modal damping, and  $F$  is the external exciting loads column matrix. Equation (5) is completely general in that it includes a form of structural damping, has the capability of using an external loading with sine and cosine components, and can accommodate twin rotors.

The system for the direct stiffness analysis as it is now used at The Boeing Company is shown in block diagram form in Fig. 2.

#### Applications

When a fuselage has been idealized into an assemblage of longitudinal stringers

circumferential frames, skins, and pylon support structure, the natural frequencies and mode shapes are determined and a modal matrix is generated. The applications of the forced response solution listed below are then available and are explained in the succeeding paragraphs:

1. Simulate shake tests;
2. Determine in-flight fuselage response;
3. Calculate the effectiveness of force generators;
4. Calculate the effectiveness of simple vibration neutralizers (mass-spring-damper systems);
5. Calculate the effective mass in any direction of any point;
6. Calculate the effectiveness of force nullifiers situated at the hubs.

**Application 1** — To simulate a shake test, forces or moments are applied to a hub one at a time; then the response of all degrees of freedom of the fuselage may be determined by using Eq. (5). Associated with each of the responses will be a structural damping phase lag. The responses and phase lags are the direct or transfer displacement mobilities. In other

STRUCTURAL DYNAMICS ANALYSIS COMPUTER SYSTEM

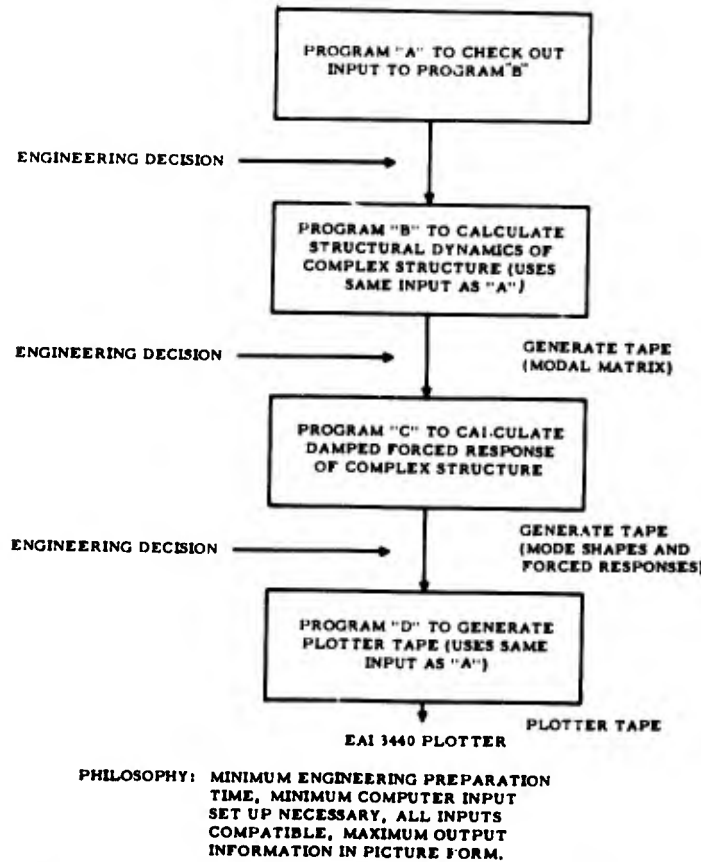


Fig. 2. Computer flow diagram for stiffness analysis

words, they are the response (with phase lag) due to a unit force or moment. They may be represented as complex numbers. Reference (4) develops the theory of their use. The frequency of the exciting load may be varied to give a sweep, which would again indicate the natural frequencies.

**Application 2** – The in-flight fuselage response may be determined first by using a rotor system analysis wherein the hub loads are determined for any flight condition. For a tandem rotor helicopter, there will be 12 each of sine and cosine components, whose lowest exciting frequency will usually be the rotor angular velocity times the number of blades. The response for any degree of freedom of the fuselage may then be determined, along with its phase lag, by using these loads in Eq. (5).

In some helicopters the vibration in the cargo section of the fuselage is higher on one

side than on the other. In fact, the vibration level at the pilot's feet could be higher than at his seat. This difference has been theoretically predicted using the stiffness method. The response differential would be difficult to determine using a lumped-mass representation and analysis.

**Application 3** – If an antivibration device is employed within the airframe, which will actively (in contrast to passively) generate forces that cancel the effects of hub loads on the response at certain fuselage locations, its effectiveness on all the degrees of freedom may be predicted. This is done by allowing its sine and cosine output force components to excite the point of attachment within the fuselage in the proper directions. More than one force generator, each at a different location, may be used at one time. These forces plus the hub loads for any flight condition are then combined in Eq. (5), and the response is determined for

all degrees of freedom. This vibratory response is then compared with results that are obtained for the in-flight condition without the force producers.

**Application 4** — When the structure is initially analyzed as to natural frequencies and mode shapes, mass-spring systems which act as vibration neutralizers may be added to the basic framework by representing them as stringers of stiffness  $AE/L$  (area (A), modulus (E), and length (L)). The damped forced response may now be obtained for any flight condition to determine the effectiveness on all the degrees of freedom. Since vibration neutralizers are tuned to an exciting frequency, their critical damping controls the amplitude of the local response and should be determined accurately by bench test. A value of critical damping ( $C/2m\omega$ ) here might be 0.017, compared to a typical assumed modal critical damping coefficient of 0.03 for the framework.

**Application 5** — In a simplified La Grangian analysis of an advanced type of linear antivibration device, such as given in Ref. (5), or of an isolation study, such as rotor isolation, the items in a schematic diagram of the system react mathematically with an effective mass at their point of attachment in the fuselage. The purpose of the analysis might be to determine the device's capabilities, or to optimize its effectiveness without an excessive weight penalty. This effective mass should be as accurate as possible in the calculations, if the final response, or degree of isolation desired, is to be specified beforehand. However, the value of the effective mass varies considerably from point to point in the structure. It is also impossible to measure this value experimentally because of the difficulty in pinpointing a shaker in some inaccessible locations in the craft. However, by using the forced response of the solution stiffness method, any degree of freedom may be excited theoretically, and the response at the point of excitation determined, to find the effective mass there. For example, Fig. 3 might be used in a simplified analysis to determine the effectiveness of the antivibration device at the point of attachment. For a fuselage, this point could be the cockpit area. In a hypothetical case, by using Eq. (5), the maximum vertical vibratory response at this point was determined to be  $x = 0.0212$  in. for a vertical 1000-lb force  $F$  there. The external exciting force operated at the frequency of  $\Omega = 72$  rad/sec. The natural frequency of the fuselage was 70.94 rad/sec.

The effective mass was then:

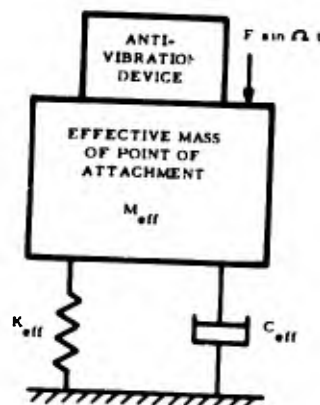


Fig. 3. Antivibration device attached to reduce linear response

$$M_{eff} = \frac{\mu F}{x \omega^2} = \frac{(14.3)(1000)}{(0.0212)(70.94)^2} = 134 \text{ chugs.}$$

or a weight of about 52,000 lb. The amplification factor  $\mu$  was determined by using a critical damping ratio of 0.03 and a forcing frequency ratio of 1.015 ( $\Omega/\omega$ ).

**Application 6** — Another promising type of antivibration device is located at the hubs; it prevents displacement in two directions in the same plane simultaneously. Its effectiveness may be determined using the forced response solution, by deleting the forces which correspond to the displacements nullified; the remaining forces and moments still remain as the exciting loads for a given flight condition, and their effect on all degrees of freedom may be determined.

Figure 4 presents the automatically plotted absolute values of the analytical responses of a helicopter fuselage for a high-speed level flight condition. Then an antivibration device, which nullifies the vertical exciting force only, at both hubs, is attached; Fig. 5 shows the absolute values of the responses. These, in general, are less; however, at some degrees of freedom, particularly in the crew station (nodes 29 and 39), the response is increased with the device attached. This local increase in response could lead to the erroneous conclusion that the device was ineffective.

#### Application to Fuselage Tuning

The rotor-blade lower rotating flap-bending natural frequencies occur among the exciting



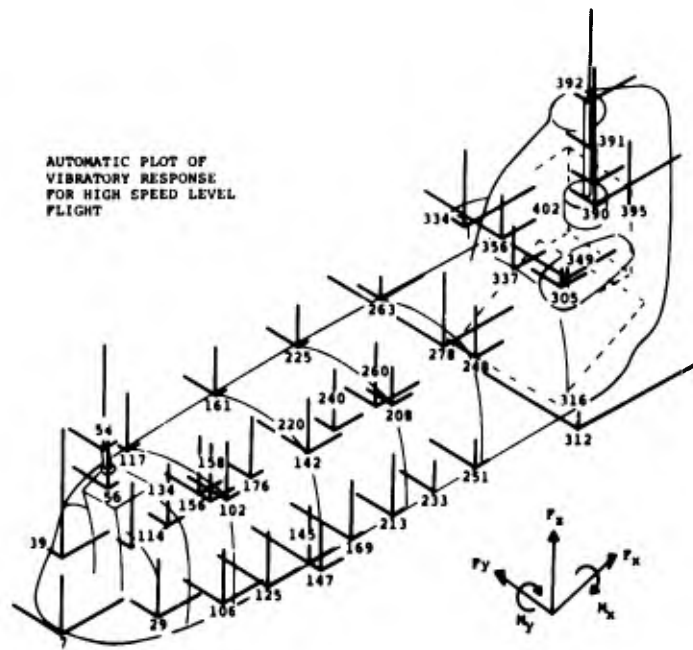


Fig. 4. Vibratory forced response for high-speed level flight

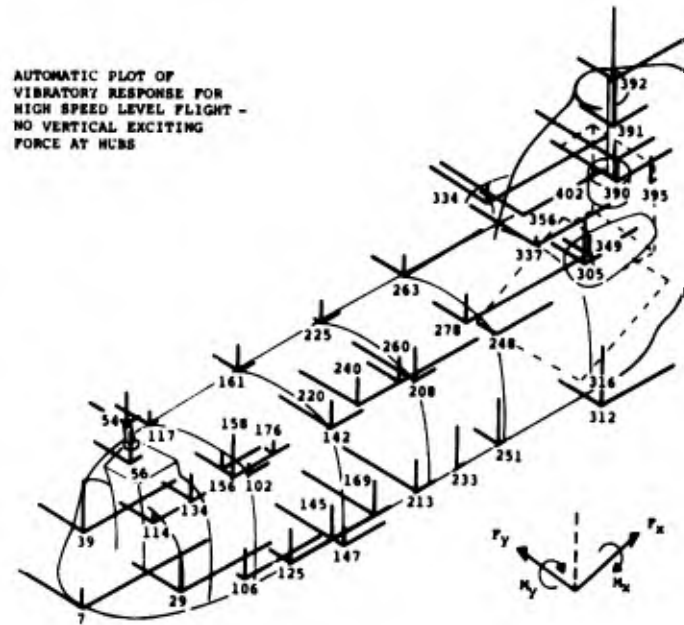


Fig. 5. Vibratory forced response for high-speed level flight with antivibration device

frequencies and, by tuning, they may be placed away from these harmonics of the rotor angular velocity. This tuning reduces vibratory stresses along the blade, and also reduces hub loads that feed into the airframe. In a similar way, the fuselage natural frequencies of any helicopter occur in the vicinity of some harmonics of the rotor angular velocity. By using the stiffness method, the fuselage may be tuned by a study of structural modifications of the mathematical idealized model of the airframe. This detuning will cause a reduction in the fuselage dynamic response. The limiting criteria in any structure change would be weight, space limitation, and expense.

In general, it is difficult to alter the fundamental lower natural frequencies of the fuselage. However, the pylons (shaft, transmission, and support) may be modified to produce a desirable frequency shift, for instance in the second vertical fuselage bending mode. Skin thickening, lateral and vertical stiffening of beams, and floor isolation may also be used for detuning. Without a preliminary mathematical model to study, it would be expensive to attempt each of these by test.

In addition, fuel burnoff can cause a change in one of the higher natural frequencies. This mass change could be large enough to cause a natural frequency to coincide momentarily with an exciting frequency. The direct stiffness method would indicate means for isolation, such as decoupling the fuel tanks from the main structure by adding soft springs in the vertical supports. As an alternate, the tank supports could be stiffened to allow them to couple more heavily with the fuselage. This could change the troublesome natural frequency.

A complete study for fuselage vibration reduction using stiffness methods was presented in Ref. (6). Figure 6, which is taken from that study, indicates analytically some effects of fuselage structural modifications and fuel mass change.

Another new area of application for fuselage tuning is in evaluating the effects of high-stiffness, low-weight boron composites in the fuselage by the stiffness method. The variation with direction of the modulus of elasticity could be considered.

#### Preliminary Design of Fuselages

One of the more important recently investigated uses of the stiffness method has been for the preliminary design of a helicopter

fuselage by using an extremely simplified mathematical model. If this were possible, the dynamic characteristics of the fuselage could be ascertained in the proposal stage and corrective action then taken.


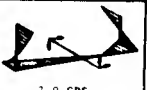
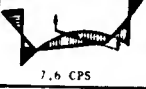
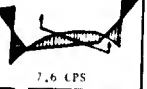
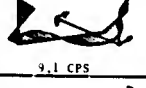
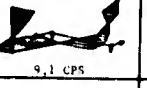
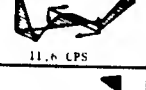
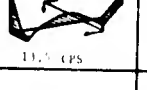
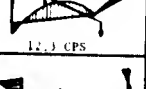
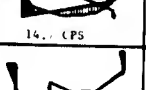
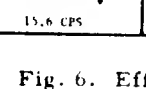
BASIC 100% FUEL	BASIC 25% FUEL	130% TORSIONAL STIFFENING	260% LATERAL STIFFENING	200% LOWER KING STRINGERS
 7.0 CPS	 7.0 CPS	7.2 CPS	7.2 CPS	7.0 CPS
 7.6 CPS	 7.6 CPS	8.0 CPS	8.0 CPS	7.8 CPS
 9.1 CPS	 9.1 CPS	9.6 CPS	9.8 CPS	9.2 CPS
 11.6 CPS	 11.5 CPS	12.3 CPS	13.2 CPS	12.0 CPS
 12.3 CPS		12.8 CPS	13.7 CPS	12.6 CPS
 14.7 CPS		15.3 CPS	15.8 CPS	14.7 CPS
 15.6 CPS		16.1 CPS	16.1 CPS	15.7 CPS

Fig. 6. Effects on natural frequencies and mode shapes with structural modification and mass change

Such a study has been undertaken with initial results indicating the feasibility of this approach. In fact, with an extremely crude structural idealization, the natural frequencies for a medium transport helicopter were obtained and compared with those natural frequencies derived from a very complex idealization. The results were:

Simple Model (cps)	Exact Model (cps)
7.4	7.2
8.5	8.8
10.4	9.23
11.3	11.2
13.0	14.00

It had been found from prior studies that the dynamic analysis of a complex structure was sensitive to the boundary conditions, the dimensions of the fuselage, and the masses; however, the analysis was relatively insensitive to individual stiffness changes. In fact, the elimination of cutouts and skin buckling from one detailed idealization indicated no noticeable change in the lower frequencies and mode shapes. This meant that a crude structural assemblage could possibly lead to reasonable results.

This conception is interesting in that it is somewhat opposed to the present industry trend to go to larger matrices and more sophisticated idealizations. In fact, if this simple approach yields good results, it would be more economical

always to use the simple model for analysis rather than the more expensive and complicated one.

Figure 7 is the exact original idealization, while Fig. 8 is the so-called simplified match-box version. The statistics are:

	Original	Matchbox
Nodes	241	97
Structural elements	1241	362
Initial matrix order	921	369
Computer running time (hr)	2.8	0.4

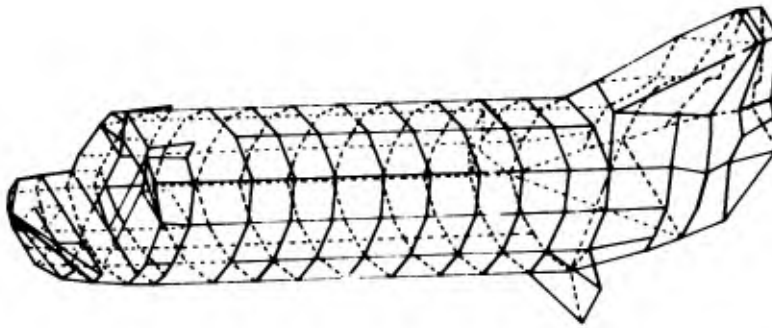


Fig. 7. Refined fuselage idealization

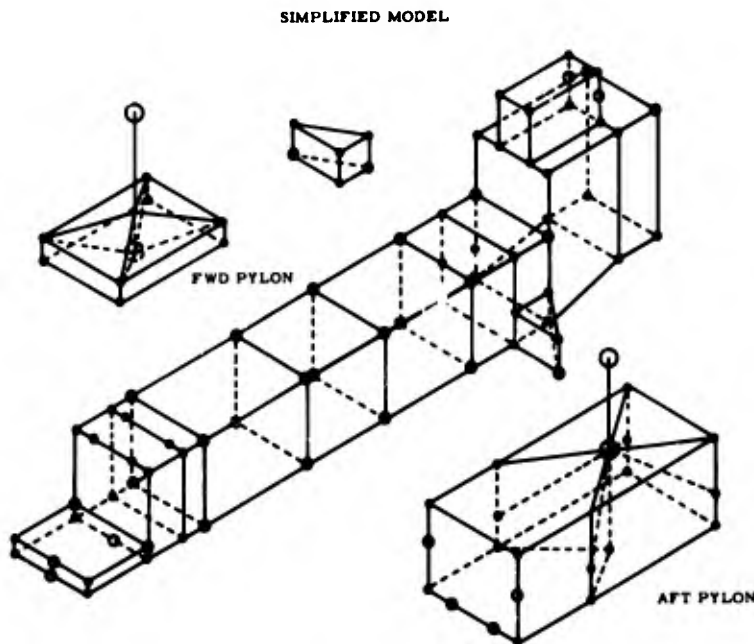


Fig. 8. Simplified fuselage idealization

However, it is presently necessary to establish ground rules for the structural idealization of the simplified model. Some of these rules are needed for the definition of the hub-supporting structure, the longitudinal stringers, and fuel tank representation.

A computer program has also been written which produces a detailed breakdown of all the contributors to each stiffness at every degree of freedom. This project was referred to as a structural idealization study. Early results have indicated that the skins, particularly in the cargo area, are the main contributors.

The combination of the matchbox conception and the structural idealization study lends itself readily to fuselage design through a computer-linked graphic display unit. The flow of this procedure is given in Fig. 9.

In this method an isometric of the idealization of the fuselage is displayed on the scope. Its natural frequencies and mode shapes and its forced response are determined by the computer and are displayed. At a console, the stiffness matrix can be modified using information from a structural idealization study to produce a new display for comparison. This cycle can be repeated to produce an optimum dynamic fuselage.

#### Applications of Mobility Techniques

**Application 1** — Reference (3) presents the application of the mobility method to helicopter vibration prediction where it was shown that if "n" mass-spring-damper systems are attached to different locations in a complex vibrating structure, the response  $X_k$  can be determined by the solution of the n complex simultaneous equations:

$$\sum_{k=1}^n (\delta_{ik} + M_{ik} \bar{M}_{kk}) X_k = M_{iA} F_A \quad (i = 1, 2, \dots, n) \quad (6)$$

where  $\delta_{ik} = 1$ , if  $i = k$ , and  $\delta_{ik} = 0$ , if  $i \neq k$ . Also,  $M_{ik}$  is the phased displacement at point i caused by a unit load at point k, and  $M_{iA}$  is the phased displacement at point i caused by the unit load  $F_A$ . The mobility of one device at its point of attachment is:

$$\bar{M}_{kk} = a + ib \quad (7)$$

with:

$$a = \frac{[\omega^2 - (\omega_n^2 + 4\zeta^2 \omega^2)]}{[m\omega^2 (\omega_n^2 + 4\zeta^2 \omega^2)]} \quad (8)$$

and

$$b = \frac{[-2\zeta\omega]}{[m\omega(\omega_n^2 + 4\zeta^2 \omega^2)]} \quad (9)$$

#### FUSELAGE PRELIMINARY DESIGN

##### DYNAMICS GRAPHICS DISPLAY METHOD

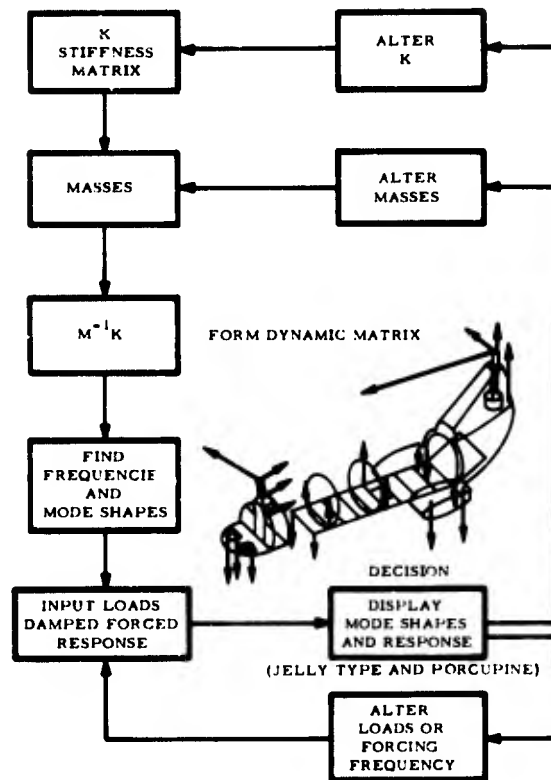


Fig. 9. Flow diagram for design using graphic display unit

where  $\omega$  is the exciting frequency,  $\omega_n$  is the natural frequency of the neutralizer,  $m$  is its mass, and  $\zeta$  is its critical damping ratio.

The mobilities and vibratory loads are complex numbers, so that phasing in the calculation is automatically considered. By using Eq. (6), one can find the effect on vibration reduction by attaching vibration neutralizers. Since a study to vary parameters in Eqs. (8), (9), and then (6) to minimize weight and maximize effectiveness would involve many computer runs, this analytical method is preferred over application 4 above (i.e., using stringers as springs) because it is faster to calculate. The mobilities in Eq. (6) may be obtained from Eq. (5) using the stiffness method (simulating a shake test), or they may be obtained from physical test.

Once the displacements are obtained for the points of attachment, they may be determined for a remote point  $X_p$  from

$$X_p = M_{pA} F_A + \sum_{k=1}^n (M_{pk} M_{kk}) X_k \quad (10)$$

**Application 2** – To determine the amount of force needed from  $n$  force-generating devices attached to the fuselage for the reduction of the responses  $X_i$  at the  $n$  points of attachment, the methods of Ref. (3) yield:

$$X_i = M_{iA} F_A + \sum_{k=1}^n M_{ik} F_k \quad (i = 1, 2, \dots, n) \quad (11)$$

where the  $F_k$ 's are the phased forces generated by the antivibration devices, and the  $X_i$ 's are zero or specified. Equation (11) represents, once again,  $n$  complex simultaneous equations. The displacement at a remote point  $X_p$  can then be found from:

$$X_p = M_{pA} F_A + \sum_{k=1}^n M_{pk} F_k \quad (12)$$

Actually, any combination of  $n$   $X_p$ 's or  $X_i$ 's may be specified for a solution. The output forces which are determined from Eq. (11) or (12) can then be input into Eq. (5), along with the hub loads for the given flight condition, to find the resulting response of all the degrees of freedom of the fuselage.

**Application 3** – In general, for a tandem helicopter the response at a point may be written, assuming superposition, as:

$$X_i = \sum_{k=1}^{12} M_{ik} F_k \quad (i = 1, 2, \dots, 12) \quad (13)$$

where the  $F_k$ 's are the 12 hub loads, and it is assumed that the mobilities,  $M_{ik}$ , are known. If 12 point responses ( $X_i$ 's) are available within the fuselage from a flight test, Eq. (13) may be

solved for the vibratory hub loads. When these hub loads are determined, Eq. (13) may be employed again to yield the response at other points by using the resulting  $F_k$ 's. This has been done with good correlation.

**Application 4** – As a final application of the mobility method, consider Eq. (13). The response at a point  $X_p$  is composed of the various responses to each of the 12 loads, namely each  $M_{pk} F_k$ . If the vibratory loads and the mobilities are known, the response at  $X_p$  may be decomposed into each of its contributors. This is referred to as a vibration synthesis. Each contribution will be a vector quantity with phase and amplitude (since all quantities are complex numbers). A diagram of these vectors would indicate the major loads causing the response at a point. For example, the aft pylon vibratory vertical force and pitching moment may be the main factors which cause the vertical response in the cargo area.

## CONCLUSIONS

Stiffness and mobility methods are excellent analytical tools for the prediction of helicopter fuselage dynamics, including the evaluation of the effects of antivibration devices.

In addition, it may be seen that some, but not all, of the fuselage natural frequencies may be altered without a severe weight penalty by certain structural modifications, and that these may be evaluated by the stiffness method.

Finally, for a dynamic analysis, a crude representation of the fuselage may give good results; hence, it could be used for preliminary design or proposal preparation. This simplified model would be desirable both from an engineering and an economical point of view, since it eliminates the problems and cost of a complex idealization.

## REFERENCES

1. P. F. Leone, "A Method for Reducing Helicopter Vibrations," *J. Amer. Helicopter Soc.*: 12 (1957)
2. J. J. Sciarra, "Dynamic Unified Structural Analysis Method Using Stiffness Matrices," Paper presented at the AIAA/ASME 7th Structures and Materials Conference, Apr. 1966
3. J. J. Sciarra, "Application of a Combined Direct Stiffness and Mobility Method to Vibration Absorber Studies," *ASME/MDD Vibrations Conference*, Paper 67-VIBR-65, Mar. 1967.
4. Austin H. Church, *Mechanical Vibration* (Wiley, New York), 1964, pp. 187-219
5. F. E. Reed, "The Use of the Centrifugal Pendulum Absorber for the Reduction of Linear Vibration," *J. Appl. Mech.*: 190-194 (1949)
6. R. Gabel, *AVID Program, Advanced Vibration Development*, Boeing Rept. 107M-D-09, Vertol Division, Morton, Pa., Apr. 1965

# ISOLATION OF HELICOPTER ROTOR-INDUCED VIBRATIONS USING ACTIVE ELEMENTS\*

Peter C. Calcaterra and Dale W. Schubert  
Barry Research and Development  
Watertown, Massachusetts

Vibratory helicopter rotor-induced forces contain energy at frequencies which are harmonics of the blade passage frequency and typically occur in the range of 10 to 30 Hz. Isolation of these low-frequency vibratory excitations by conventional passive isolators results in large relative deflections between rotor and fuselage, particularly under the transient accelerations experienced during flight maneuvers and landing. Helicopter control requirements prohibit any excessive relative deflections between rotor and fuselage.

Results of an investigation are presented which demonstrate the feasibility of providing virtually 100 percent isolation of rotor-induced vibratory forces at the blade passage frequency,  $b$  rev, and its second and third harmonics, while limiting the relative deflection between rotor and fuselage during normally encountered maneuver loads (1.5 to 2 g) and landings (2 to 3 fps) to less than 1/8 in. The analysis considered helicopter gross weights ranging from 2000 to 80,000 lb with blade passage frequencies ranging from 13 to 26 Hz. Vibration isolation is provided in all cases by electrohydraulic isolators (consisting of a hydraulic cylinder, acceleration and displacement feedback sensors, and servo amplifier) designed to be compliant only at the  $b$  rev and second and third harmonics. Displacement control is achieved by the system because of its noncompliance at all other frequencies.

## INTRODUCTION

The aerodynamic characteristics of a helicopter rotor in forward flight give rise to shear forces at the hub which are transmitted through the rotor shaft into the fuselage. The magnitude of these forces is a function of the rotor blade angle of attack and the velocity of the airstream into the rotor plane. The frequency of the forces is a direct function of the rotor speed and number of blades, and generally coincides with frequencies which are critical to the comfort and/or task performance capabilities of passengers and crew, respectively. As a result, helicopters are frequently operated at speeds reduced 20 percent below those they might otherwise achieve, because of the extreme vibration environments.

Considerable strides are being made to understand better the basic mechanism and the nature of rotor-induced forces in an attempt to minimize input excitations. Research in the area of vibration control, such as utilizing

phase relationships between the various sources of rotor loads and introducing higher harmonic pitch control to reduce shaft loads [1], appears to hold promise in reducing the level of force transmitted to the fuselage. However, immediate requirements exist to improve the vibration characteristics of helicopters.

Forces acting on the rotor from blade dynamics are numerous and occur in the in-plane and torsional modes as well as in the vertical modes [2]. However, the level of excitation at the hub perpendicular to the plane of the rotor is generally an order of magnitude greater than that occurring along the plane of the rotor. Reduction of the former to acceptable levels would represent a significant step forward in the solution of helicopter vibration problems.

## COMPARISON OF ISOLATION SYSTEM CHARACTERISTICS

Isolation of vertical excitations is extremely difficult because of the conflicting

\*The results presented herein were obtained in part during an investigation conducted for the U.S. Army Aviation Materiel Laboratories, Fort Eustis, Virginia, under contract DA 44-177 AMC-472(1).

requirements of small deflections across the isolation system under imposed thrust loads, and the stiffness values required for effective isolation of low-frequency excitations. The vibratory rotor force contains energy at the rotor shaft speed ( $1 \text{ rev}$ ) and at fundamental and harmonics of the blade passage frequency ( $b \text{ rev}$ ,  $2b \text{ rev}$ , ...) where  $b$  is the number of blades. Figure 1 represents the relationship between levels of rotor-induced vibrations at the rotor frequency and blade passage frequency and its harmonics. The  $1 \text{ rev}$  vibration is induced by rotor unbalance and may be virtually eliminated by proper tracking of the blades. The  $b \text{ rev}$  excitation and its harmonics result from the aerodynamics of existing rotary-wing

aircraft design and cannot be eliminated. A study of existing helicopters indicates that values of  $b/\text{rev}$  range from 10 to 30 Hz [3]. Table 1 shows values of  $b \text{ rev}$  as a function of helicopter gross weight for typical nominal rotor speeds and number of blades of helicopters in each weight range.

A conventional passive isolator placed between the rotor and the fuselage would reduce the vibratory force transmitted to the fuselage. However, because of both the dynamics of the rotor-isolator-fuselage system and the low values of frequency associated with the excitation, effective isolation at  $b \text{ rev}$  would give rise to deflections between the rotor and fuselage

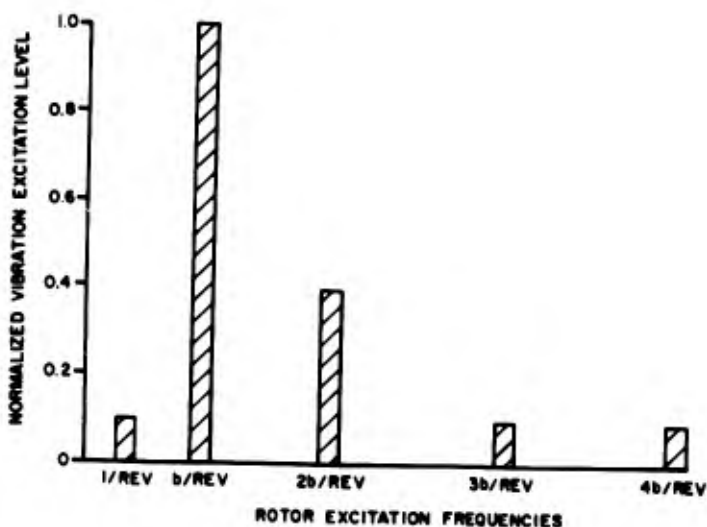


Fig. 1. Relationship between levels of rotor-induced vibrations at the blade passage frequency  $b/\text{rev}$ , and its harmonics, normalized with respect to the level at  $b/\text{rev}$

TABLE 1  
Values of Blade Passage Frequency ( $b/\text{rev}$ ) as a Function of Helicopter Gross Weight for Typical Nominal Rotor Speeds and Number of Blades

Gross Weight (lb)	Rotor Speed (rpm)	Number of Blades	Blade Passage Frequency (Hz)
2,000	400	2	13.3
2,000	400	4	26.6
10,000	260	4	17.7
20,000	214	5	17.9
40,000	194	6	17.5
90,000	145	6	14.5
80,000	145	7	16.8

which would be incompatible with helicopter control requirements, particularly under transient loads associated with maneuvering and landing.

A schematic representation of a rotor and fuselage connected by a conventional isolator is shown in Fig. 2. Expressions for the undamped natural frequency  $\omega_1$ , coupled frequency  $\omega_0$ , and static deflection  $\delta_{\text{STATIC}}$  are also shown. For a given stiffness  $K$ , the degree of isolation provided is controlled primarily by the rotor mass  $M_R$ , since typically  $M_F/M_R \approx 8$  and therefore  $\omega_0^2 \approx K/M_R$ . Relative deflections between the rotor and fuselage, however, are determined by the fuselage mass  $M_F$ . For example, if 70 percent isolation is to be provided at a blade passage frequency of 10 Hz, the coupled frequency  $\omega_0$  should be approximately 2 Hz (47 rad/sec). For typical fuselage-to-rotor weight ratios of 8, the static deflection of a conventional passive isolation system would be in excess of 20 in. Under transient maneuvers, deflections would be multiples of 20 depending on the number of g pulled. It is evident that such values of deflection are unacceptable. Although nonlinearities can be incorporated into the design of passive isolators to limit deflections, snubbing would occur during a large portion of the time, particularly during transition flight and maneuvers when the levels of vibration excitation are most severe and sustained accelerations of several g are experienced.

Several approaches have been studied in the past which incorporate various types of active elements in an attempt to provide vibration isolation of rotor-induced low-frequency excitation, while limiting the relative deflection between the rotor and fuselage. Combinations of a passive stiff spring and force servo in parallel have been investigated [4] where the servo-controlled force would be tuned to negate the vibratory

excitations at the blade passage frequency. A system consisting of a stiff spring, in parallel with a negative spring rate achieved by a special linkage, has been analyzed to obtain a low vertical natural frequency, utilizing a servo-mechanism to position the base of the stiff spring so as to maintain a constant vertical distance between the rotor and fuselage [5]. An electropneumatic servo-controlled system utilizing an air cylinder as both the isolating medium and the energy source was investigated in conjunction with Boeing Vertol 107 helicopter [6]. None of these approaches, however, represents a suitable solution for the isolation of modern high-performance helicopter fuselages from rotor-induced vibrations, primarily because of the high levels of maneuver loads and the resulting deflections associated with transient maneuvers of shorter rise time.

In recent years, techniques have been developed to incorporate electrohydraulic elements in the design of active isolation systems to provide both low-frequency vibration isolation and displacement control [7,8]. As shown in Fig. 3, electrohydraulic isolation systems are servomechanisms comprising excitation and/or response sensors, sensor signal processors, and actuators. The sensors provide signals proportional to dynamic excitation or response quantities. The signal processors modify and combine sensor signals to create a command signal. And, the actuators apply forces or induce motions in accordance with the command signal.

A wide variety of excitation and response sensors can be employed to provide feedback signals to form a closed loop control system. For example, feedback signals can be developed which are a function of jerk, acceleration, velocity, displacement, integral displacement, differential pressure, or force. The signal

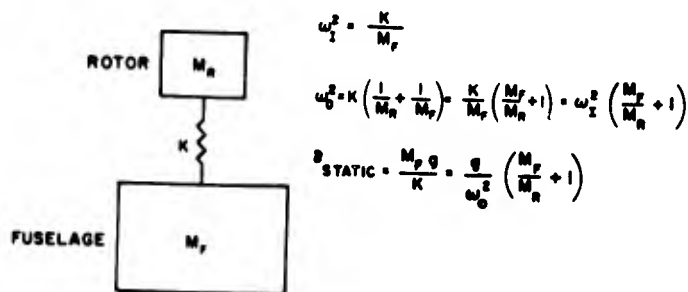


Fig. 2. Relationship between natural frequency  $\omega_1$ , coupled frequency  $\omega_0$ , and static deflection  $\delta_{\text{STATIC}}$  for helicopter rotor and fuselage connected by undamped isolator



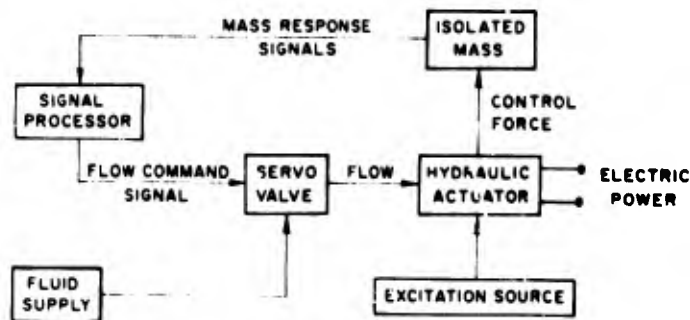


Fig. 3. Block diagram of generalized electrohydraulic isolation system

processor may consist of an active electronic network which performs amplification, attenuation, differentiation, integration, addition, and compensation functions. Because of the wide selection of feedback signals, loop gains, and signal processing networks and the relative incompressibility of the hydraulic fluid, ultra-low-frequency isolation can be provided by the electrohydraulic isolation system even during conditions of sustained acceleration, with zero static deflection, high speed of response, and extreme flexibility in shaping the overall frequency response characteristics [9]. Selection of system design is dictated by the specific requirements of a given application.

One such electrohydraulic isolation system was constructed to evaluate the effect of vibration isolation on pilot performance during simulated low-level high-speed flight conditions [10]. For this application, the system resonant frequency was 0.45 Hz, and better than 80 percent isolation was provided from 5 to 100 Hz. The static deflection of a linear passive system of equivalent isolation performance would be over 4 ft, whereas the static deflection of the electrohydraulic system is zero and, by use of nonlinear feedback, deflected only 2.1 in. under a 3-g acceleration step with a 0.1-sec rise time. Moreover, vibration isolation was provided during conditions of combined vibratory and 3-g sustained accelerations. The broad-band vibration isolation characteristics and displacement control were attained by a combined active-passive isolation system, where active elements provide the desired response at low frequencies and during transient conditions, and the passive elements provide isolation at frequencies beyond the frequency band over which the active elements are operative.

#### SELECTED DESIGN

The components selected for the active isolation system are shown in Fig. 4. The

actuating element is a double acting hydraulic cylinder placed between the rotor and the fuselage. The cylinder is actuated by a flow control servo valve, which in turn is actuated by a servoamplifier. Two feedback signals are sent to the servoamplifier: one is an acceleration signal obtained from an accelerometer attached to the fuselage, and the second is a relative displacement signal obtained from a displacement transducer attached between the fuselage and rotor. The signals from the accelerometer and displacement transducer are fed to the servoamplifier wherein they are first weighted by use of compensation networks, then summed to generate the flow command signal delivered to the servo valve. Hydraulic power is supplied to the servo valve from a hydraulic power source, and electric power is supplied to the servoamplifier.

The flow control servo valve regulates the flow to and from the upper and lower chambers of the hydraulic cylinder in a manner proportional to the flow command signal applied to the valve from the servoamplifier. The flow generated control forces and velocities support the static load of the helicopter fuselage and at the same time provide for the isolation of the sinusoidal rotor-induced forces at the blade passage frequency and its harmonics. The narrow bandwidths of vibration isolation attained at the selected frequencies, called notches, are provided by electrical circuits in the servoamplifier placed in cascade with the acceleration feedback signal. A lead network also placed in cascade with the acceleration signal provides a system having no static deflection and small transient deflections of the fuselage relative to the rotor resulting from maneuver loads and landing excitations.

The basic system transfer functions incorporating a multiplicity of notch circuits are shown below.

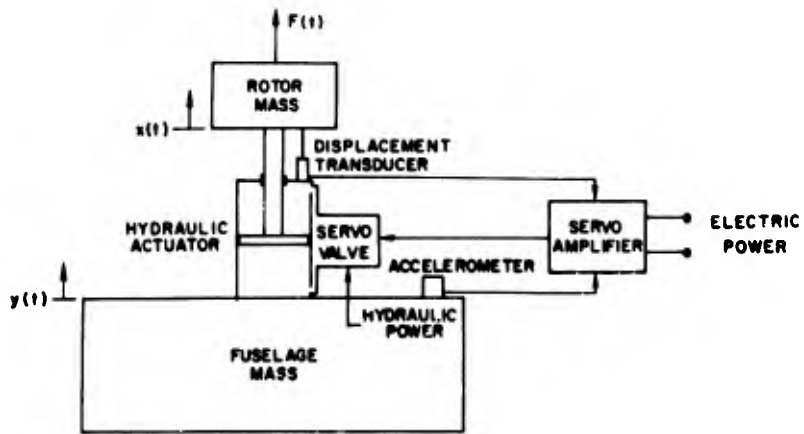


Fig. 4. Schematic diagram of electrohydraulic isolation system for helicopter rotor application

$$s^2 Y(s) = \frac{\left( \frac{C_d}{A} + s \right) (1 + \tau_1 s) \prod_1^N [(N \cdot n)^2 + s^2]}{\frac{C_a}{A} M_r s^3 \left[ \sum_1^N \left\{ \frac{\frac{1}{N} K_1 (N \cdot n)^2}{(N \cdot n)^2 + s^2} \prod_1^N [(N \cdot n)^2 + s^2] \right\} \right] + \left( \frac{C_d}{A} + s \right) (1 + \tau_1 s) \prod_1^N [(N \cdot n)^2 + s^2]} \frac{F(s)}{M_R + M_F}$$

$$s^2 X(s) = \frac{\frac{C_a}{A} \tau_1 s^3 \left[ \sum_1^N \left\{ \frac{\frac{1}{N} K_1 (N \cdot n)^2}{(N \cdot n)^2 + s^2} \prod_1^N [(N \cdot n)^2 + s^2] \right\} \right] + \left( \frac{C_d}{A} + s \right) (1 + \tau_1 s) \prod_1^N [(N \cdot n)^2 + s^2]}{\frac{C_a}{A} M_r s^3 \left[ \sum_1^N \left\{ \frac{\frac{1}{N} K_1 (N \cdot n)^2}{(N \cdot n)^2 + s^2} \prod_1^N [(N \cdot n)^2 + s^2] \right\} \right] + \left( \frac{C_d}{A} + s \right) (1 + \tau_1 s) \prod_1^N [(N \cdot n)^2 + s^2]} \frac{F(s)}{M_R + M_F}$$

$$Z(s) = \frac{\frac{C_a}{A} \tau_1 s^3 \left[ \sum_1^N \left\{ \frac{\frac{1}{N} K_1 (N \cdot n)^2}{(N \cdot n)^2 + s^2} \prod_1^N [(N \cdot n)^2 + s^2] \right\} \right]}{\frac{C_a}{A} M_r s^3 \left[ \sum_1^N \left\{ \frac{\frac{1}{N} K_1 (N \cdot n)^2}{(N \cdot n)^2 + s^2} \prod_1^N [(N \cdot n)^2 + s^2] \right\} \right] + \left( \frac{C_d}{A} + s \right) (1 + \tau_1 s) \prod_1^N [(N \cdot n)^2 + s^2]} \frac{F(s)}{M_R + M_F}$$

where

- |  |  |
|--|--|
| $A$ = effective actuator area (in. <sup>2</sup> )                                    | $M_F$ = fuselage mass (lb-sec <sup>2</sup> /in.)   |
| $C_a$ = acceleration feedback gain (in. <sup>3</sup> -sec/<br>in.-sec <sup>2</sup> ) | $N$ = number of notches (1, 2, ... N)  |
| $C_d$ = displacement feedback gain (in. <sup>3</sup> -<br>sec/in.)                   | $s$ = Laplace operation (1/sec)  |
| $F(s)$ = Laplace transform of forcing function<br>(lb-sec)                           | $X(s)$ = Laplace transform of rotor absolute<br>displacement (in.-sec)                             |
| $K_1$ = relative notch gain (dimensionless)  | $Y(s)$ = Laplace transform of fuselage ab-<br>solute displacement (in.-sec)                        |
| $M_R$ = rotor mass (lb-sec <sup>2</sup> /in.)  | $Z(s)$ = Laplace transform of relative dis-<br>placement between rotor and fuse-<br>lage (in.-sec) |

$\tau_1$  = lead network time constant (sec)

$\omega_n$  = resonant frequency of notch filter (rad/sec).

Dynamic characteristics of components such as servo valve, hydraulic cylinder, and accelerometer are not included, since they do not affect the low-frequency response characteristics of the system. The dynamic characteristics of components were incorporated for system stability considerations as discussed in the next section.

## SYSTEM PERFORMANCE

An analog computer study was conducted to define the feasibility of applying the selected design to the isolation of rotor-induced vertical vibrations, based on rigid rotor and fuselage. Parameters and constraints for the study were as follows:

1. Gross weight range: 2000 to 80,000 lb.
2. Dynamic excitations: (a) vertical in-flight vibrations; (b) landing shock associated with sink speeds up to 10 ft/sec; (c) in-flight maneuver load of 3 g, with 0.6-sec rise time.
3. The relative deflection between rotor and fuselage was to be kept to a minimum. A maximum value of 1/2 in. for any of the dynamic excitations considered was a design goal.

Active isolation systems were designed to provide notches at  $b/\text{rev}$ ,  $2b/\text{rev}$  and  $3b/\text{rev}$  in all cases, based on a 4000-psi fluid pressure. The system is considered to incorporate automatic tracking of the rotor speed to insure that the notches occur at the right frequencies for changes in rotor rpm typically encountered in normal operations.

Feedback gains were selected both to yield stable systems and to minimize the relative deflections under landing shock and in-flight maneuvers. Satisfying these two requirements will generally require selection of different values of loop gain. The system transfer functions previously shown neglected the dynamic characteristics of the various components. For the parametric study, however, the system analog representation included component dynamics. For high values of  $b/\text{rev}$ , the first notch approaches frequencies where the dynamic response of components comes into play and the magnitude of gain which can be introduced in the loops must be reduced to maintain the desired system stability margin. However, low values of gain give rise to large relative deflections. Therefore, the response of each system to the various dynamic excitations was initially evaluated for different values of gains. In all cases, gain values were finally selected which gave rise to the smallest relative deflection between rotor and fuselage while maintaining at least a 25-db gain stability margin.

The frequency response shown in Fig. 5 is typical of the degree of isolation provided in

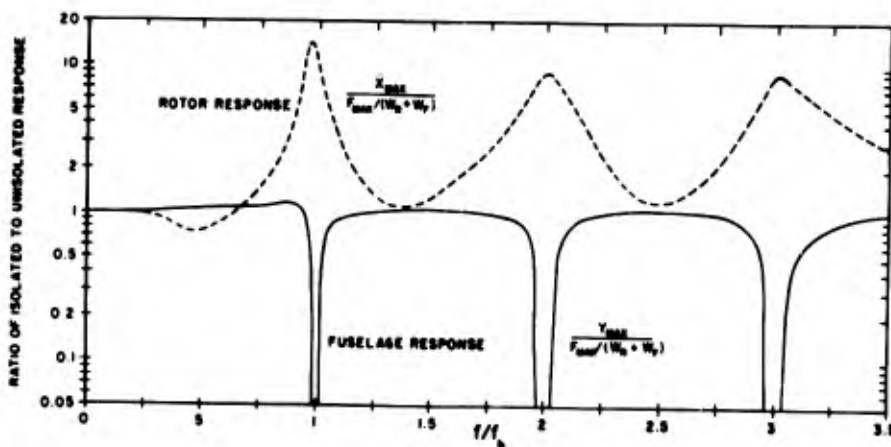


Fig. 5. Ratio of maximum isolated to unisolated rotor and fuselage acceleration for sinusoidal rotor-induced forces of amplitude  $F_{\max}$ , as a function of frequency ratio  $f/f_b$ , where  $f_b$  is the blade passage frequency (Hz), and  $W_R$  and  $W_F$  (lb), are the rotor and fuselage weights, respectively

all cases for in-flight vibrations. As indicated, 100 percent isolation of fuselage vibration is provided at  $b$  rev,  $2b$  rev, and  $3b$  rev. At each of the notch frequencies the acceleration of the isolated rotor is  $(M_F \cdot M_R) M_R$  times greater than the acceleration exhibited by the unisolated rotor. Normalized maximum relative deflections (expressed in in./g) under this condition are shown in Fig. 6 as a function of blade passage frequency. Review of actual flight test data indicates that the ratio  $F_{max} (W_R \cdot W_F)$  during severe transition can be as high as  $\pm 0.3$  g. Under these conditions,  $F_{max}$  ranges from  $\pm 3/16$  in. for  $b$  rev of 13.3 Hz to  $\pm 1/32$  in. for  $b$  rev of 26 Hz.

For the case of landing shock with 10-fps sink speed, the selected displacement feedback gains and acceleration compensation resulted in a maximum relative deflection of 1/2 in. for all gross weights. Typical response under landing shock is shown in Fig. 7. The landing gear in all cases was considered to provide a 3-Hz natural frequency based on the total helicopter weight. The fuselage acceleration  $\ddot{y}$  is primarily a function of the undercarriage stiffness characteristics. Maximum fuselage transmitted accelerations ranged from 5 to 6 g. The maximum rotor acceleration during landing  $\ddot{x}$  is an inverse function of the blade passage frequency, and ranged from 6 to 8 g.

Typical response for in-flight maneuvers is shown in Fig. 8 for a sustained 3-g load with a 0.6-sec rise time. For all fuselage weights

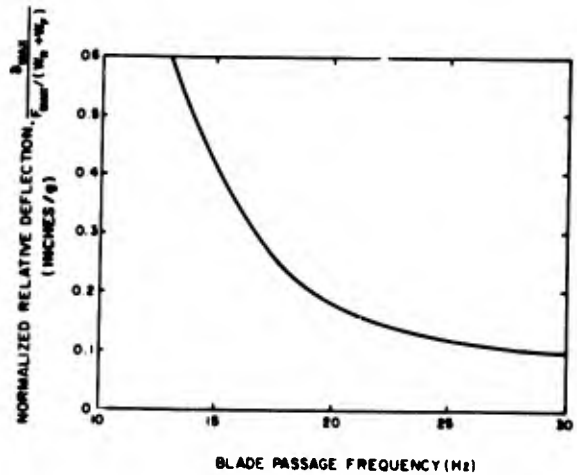


Fig. 6. Maximum relative deflection between isolated rotor and fuselage,  $F_{max}$  (in.), normalized with respect to acceleration of rigidly connected rotor,  $F_{max} (W_R \cdot W_F)$  (g), for sinusoidal rotor-induced forces of amplitude  $F_{max}$  (lb) as a function of blade passage frequency

considered, the peak rotor and fuselage acceleration overshoot from maneuver loads did not exceed 4 percent of the acceleration pulled during the maneuver. The maximum relative deflection between rotor and fuselage for this condition is also dependent on the blade passage frequency. The maximum relative deflections under the 3-g maneuver ranged from less

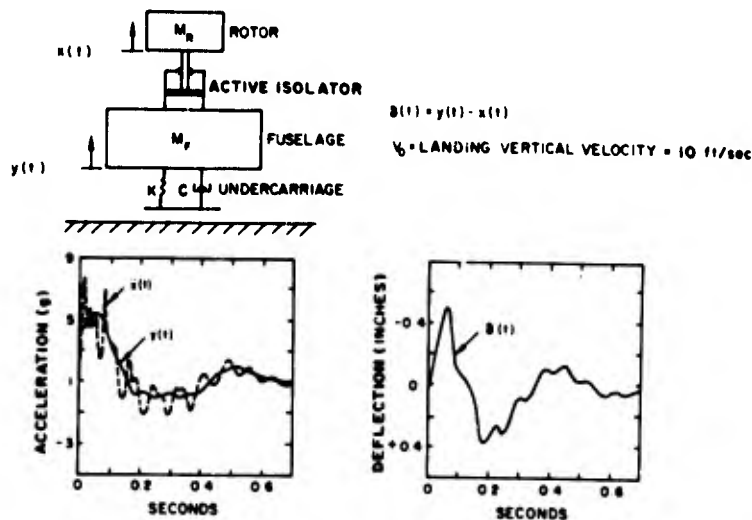


Fig. 7. Typical acceleration and relative displacement response of rotor and fuselage connected by electrohydraulic isolator for maximum expected value of sink speed  $V_0$  (ft/sec)

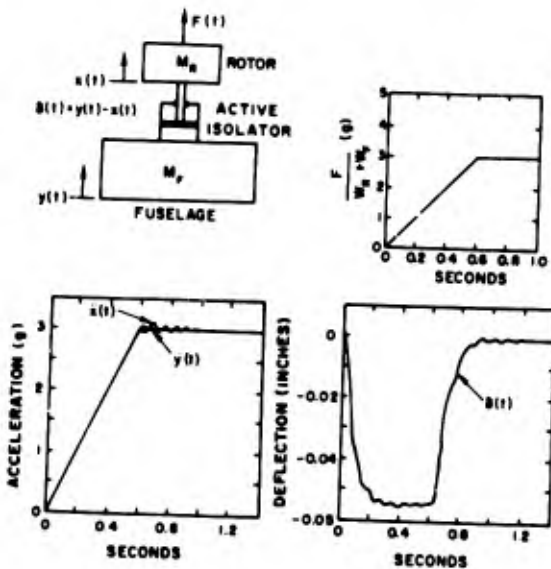


Fig. 8. Typical acceleration and relative displacement response of rotor and fuselage connected by electrohydraulic isolator for maximum expected values of maneuver loads  $F/(W_R + W_F)$  (g)

than 1/16 in. for a helicopter with blade passage frequency of 13.3 Hz (shown in Fig. 8) to 5/16 in. for blade passage frequency of 26 Hz.

## CONCLUSION

1. A stable active isolation system can be designed to provide 100 percent isolation from the helicopter rotor-induced vertical vibrations at the blade passage frequency and higher harmonics. Vibration isolation would also be provided during combined vibratory and transient excitations, such as can be expected during transition from one flight regime to another.

2. Relative deflections under maximum landing gear design capabilities of 10-fps sink speed would be less than 1/2 in. For lower

values of sink speeds, the relative deflections would be proportionately reduced.

3. During in-flight maneuvers, the maximum relative deflection between rotor and fuselage is a function of the number of g pulled, the weight of the helicopter, and the blade passage frequency. For maximum expected maneuver loads of 3 g relative deflection for all cases considered was less than 5/16 in. For maneuvers involving a lower number of g pulled, deflections would be less. For example, under a 1-g pull, the maximum deflection between rotor and fuselage for a 40,000-lb 6-blade helicopter is approximately 1/32 in.

4. Considering more typical operating conditions of 2- to 3-fps landing velocity and maneuver loads of 1.5 to 2 g, it is feasible to design an electrohydraulic multiple-notch isolator which provides isolation efficiency approaching 100 percent at the blade passage frequency and first two harmonics, with a maximum relative deflection of 1/8 in. for helicopters ranging in weight from 2000 to 80,000 lb.

The active isolation system described above can best be incorporated into new helicopter rotor configurations, since undoubtedly design problems would be encountered in adapting the approach to an existing rotor. Also, power requirements may become excessive, particularly for the heavier helicopters. Consideration must be given to in-plane rotor excitations, which though generally lower in magnitude than the vertical forces, are nevertheless present and would become the more significant ones, and perhaps even increase once the vertical vibration levels are reduced as shown. Nevertheless, the results of the analysis indicate that the vibration and displacement control provided by a multiple-notch electrohydraulic isolation system far surpasses those attained with any other types of system reported to date. Additional work is in process on experimental verification of system performance, effects of fuselage and rotor impedance on system response, incorporation of approach into practical hardware, and isolation of combined vertical and in-plane rotor-induced vibrations.

## REFERENCES

1. D. E. Brandt, "Vibration Control in Rotary-Winged Aircraft," Proc. AGARD Technical Meeting, Paris, AD805752, Jan. 1966
2. P. R. Payne, Helicopter Dynamics and Aerodynamics (Macmillan, New York), 1959
3. E. P. Schuett, "Helicopter Excitation Criteria," Kaman Aircraft Res. Note 67-3, Mar. 1967
4. C. E. Theobald, Jr., and R. Jones, "Isolation of Helicopter Rotor Vibratory Forces from the Fuselage," Air Force Rept. WADC TR 57-104, AD 130991, Sept. 1957

5. C. E. Crede, R. D. Cavanaugh, and H. N. Abramson, "Feasibility Study on Active Vibration Isolator for a Helicopter Rotor," Air Force Rept. WADC TR 58-103, Mar. 1958
6. L. E. Smollen, P. Marshal, and R. Gaisel, "A Servo Controlled Rotor Vibration Isolation System for the Reduction of Helicopter Vibration," IAS Paper 62-34
7. P. C. Calcaterra, "Performance Characteristics of Active Systems for Low Frequency Vibration Isolation," unpublished Master's thesis, MIT, May 1967
8. J. S. Pepi, "Vibration Isolation of Optical Aerial Reconnaissance Sensors," Air Force Rept. AFAL-TR-67-277, Oct. 1967
9. J. E. Ruzicka, "Passive and Active Shock Isolation," Proc. NASA Symposium on Transient Loads and Response of Space Vehicles, Hampton, Va., Nov. 1967, in press
10. P. C. Calcaterra, and D. W. Schubert, "Research on Active Vibration Isolation Techniques for Aircraft Pilot Protection," Air Force Rept. AMRL-TR-67-138, Oct. 1967

#### DISCUSSION

Mr. Salter (Ft. Halsted, England): I find an interesting contrast between your approach, in which you have a control accelerometer mounted on a rigid fuselage in a two-degree-of-freedom system, with the multi-degree-of-freedom systems which other speakers were discussing. To put my question rather unkindly perhaps, where on a practical fuselage would you envisage putting your control accelerometer?

Mr. Calcaterra: That was very kindly put. We are evaluating isolation systems. We have worked on conceptual designs and are looking at the base of the attachment point of the rotor to the fuselage structure at the end of the mass assembly.

Mr. Forkois (NRL): What was the maximum lift for which this helicopter system would work?

Mr. Calcaterra: We lifted up to 80,000 lb.

Mr. Forkois: Do you feel that it still represents a practical system?

Mr. Calcaterra: As I mentioned, for the heavy helicopters perhaps 40,000 to 50,000 lb would be a maximum from the point of view of the power requirements associated with such a system. For the lower weights, of course, we are talking about approximately 4-hp requirements for a 2000-lb helicopter.

\* \* \*

**BLANK PAGE**

# HYBRID VIBRATION-ISOLATION SYSTEM FOR HELICOPTERS\*

David Alan Bies and Thomas M. Yaug  
Bolt Beranek and Newman Inc.  
Los Angeles, California

A feasibility study of a vibration-isolation system which combines the functions of an active and a passive system was made. The isolator assembly was actively controlled at low frequencies and passively controlled at high frequencies. Two possible modes of operation were considered. Preliminary results of this investigation are reported.

## INTRODUCTION

Rotor-induced vibration in helicopters occurs primarily at the fundamental frequency of the rotor, at the blade passage frequency, and at higher harmonics. Since the fundamental frequency of the rotor may be as low as 3 Hz, effective vibration isolation is desirable down to this frequency. At the same time for helicopter control it is desirable that the isolation system be stiff in the frequency range from 0 to at least 0.5 Hz. These requirements are very difficult to meet with a purely passive vibration-isolation system. For example, a purely passive system may give very good vibration isolation in the frequency range well above resonance, but it will always amplify vibration levels below some minimum frequency determined by the system resonance and damping.

This report examines the feasibility of controlling a passive vibration-isolation system's low-frequency response with an active system. Such an arrangement might be called a hybrid vibration-isolation system. The analysis presented below is concerned only with the principles involved, not with particular applications. Some preliminary experimental results from tests with a small electromechanical model are presented.

## ANALYSIS OF HYBRID VIBRATION-ISOLATION SYSTEM

A prototype system which makes use of a hydraulic actuator for implementation of the

active element is shown schematically in Fig. 1. The system shown will have a low- and a high-frequency resonance. It is expected, however, that the active element will be quite stiff at high frequencies, so that the high-frequency resonance will occur above the frequency range of interest and only the low-frequency resonance will be of importance. Thus only the low-frequency resonance is discussed below.

The system shown in Fig. 1 functions as follows. The acceleration of the body to be isolated is measured in a specified frequency passband and integrated twice to obtain the absolute displacement in that frequency band. The signal is phase compensated and fed through a power amplifier to the mechanical power source and then to the active element. With respect to the isolated mass, the active element may be made to act like either a negative or a positive spring to ground by making it respond with a force either in phase with the absolute displacement of the isolated mass or opposite to it. Analysis of the system shown in Fig. 1 is given in the Appendix.

Figure 2 shows the results of calculations of transmissibility. Transmissibility (in decibels) =  $10 \log_{10} [(\text{mean square acceleration of isolated mass})/(\text{mean square acceleration of vibration source})]$ . Transmissibility is shown as a function of frequency for various active-element effective spring rates, which are normalized with respect to the spring rate of the passive support spring. For these calculations the assumption has been made that  $M_1 \ll M$  and  $k_1 \approx k$ .

\*This work is part of a continuing program sponsored by the Department of the Army, U.S. Army Aviation Materiel Laboratories, Fort Eustis, Virginia, under Contract DAAJ02-67-C-0082.



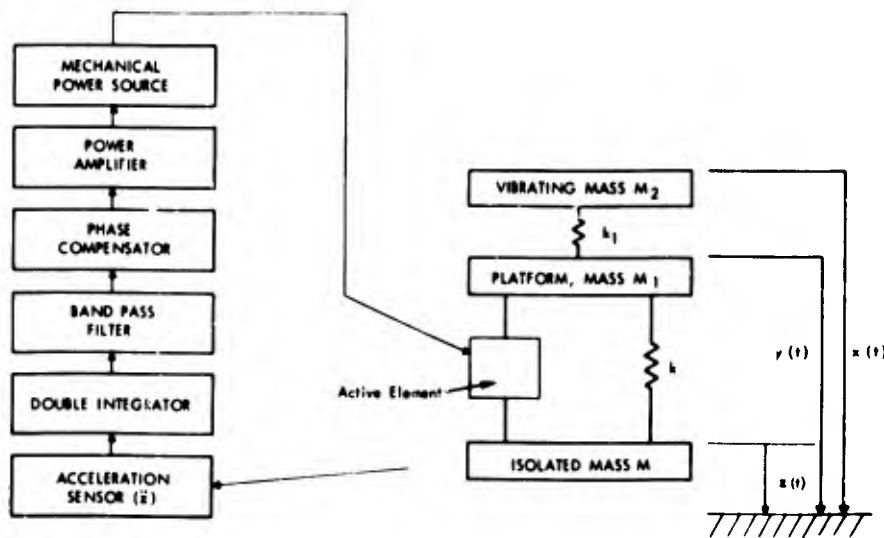


Fig. 1. Hybrid vibration-isolation system

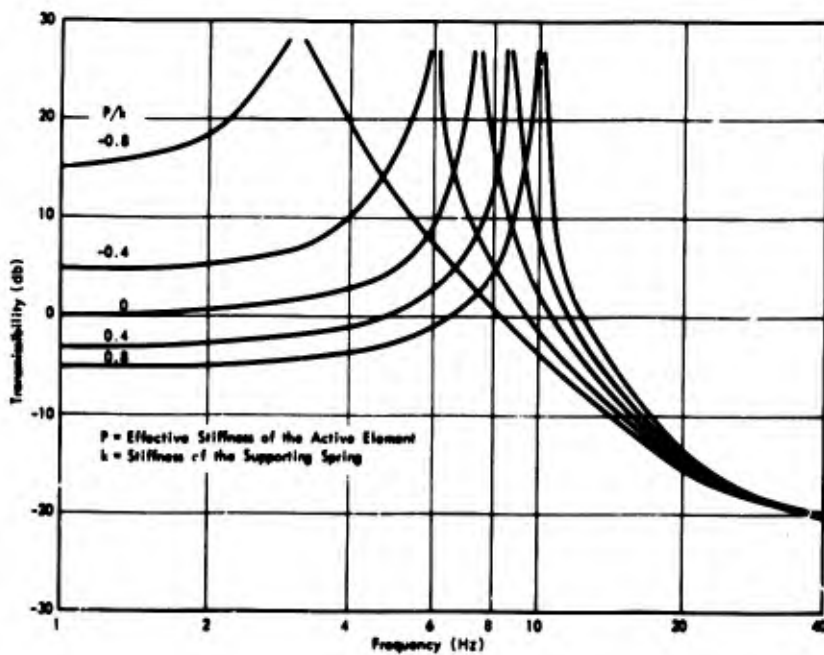


Fig. 2. Calculated transmissibility for various active-element spring rates  $P/k$

In Fig. 2, the natural resonant frequency of the isolation system was taken arbitrarily as 7.5 Hz. The family of curves shows the effect of changing the effective stiffness of the active element. The active element may produce a force in the direction of the displacement of the isolated mass, which is the case for  $P < 0$ , or a force opposite to the direction of the displacement, which is the case for  $P > 0$ .

A small electromechanical model vibration-isolation system has been constructed and some preliminary tests have been run with it. In this case the active element consisted of an electromagnetic shaker, which was used for ease in modeling. The high-frequency resonance was present but was ignored for the present purpose.

Some results of experimentation with the model of the prototype isolator are shown in Fig. 3. For this test the absolute displacement of the isolated mass was measured directly and fed through an amplifier into the active element. The system was driven sinusoidally at the frequencies shown by the data points. Care was taken to maintain the force either in phase with the displacement or opposite to it. The trends indicated by the data are as predicted by the curves in Fig. 2.

The results of Figs. 2 and 3 indicate that improved vibration isolation might be achieved either with (a) an active element which acts like a positive spring or with (b) an active element which acts like a negative spring where the active element responds to the absolute displacement of the mass to be isolated. For example, the displacement response would be passed through a passband filter which would reject frequencies above and below suitably chosen cutoff frequencies. The active element would then be driven as a negative spring in phase with the absolute displacement in this passband. Thus the response (Fig. 2) might follow a curve such as that given by  $P/k = -0.8$  up to, say, 6 Hz; then it would follow the  $P/k = 0.0$  curve.

As an alternative to driving the active element as a negative spring, the active element might be driven as a positive spring in a suitable

passband. In this case, the system response (Fig. 2) might follow the 0.8 curve above some low frequency which might be of the order of 1 Hz up to approximately 8 Hz. Above 8 Hz the system response would follow the 0.0, passive frequency response curve.

The transmissibility curve sometimes may be misleading. For example, the change in impedance of the load because of the isolation system may allow larger amplitude of motion at the source. The result would be that the actual motion of the isolated mass would be much larger than the motion implied by the transmissibility prediction based on a constant motion input. This matter has been investigated, and the results are indicated qualitatively in Figs. 4 and 5. The figures show the changes expected in vibration isolation with an active element where the driving force amplitude is assumed to be constant.

In Figs. 4 and 5 point A corresponds to the frequency of resonance of the system for the assumed value of effective stiffness  $P$  of the active element. Point B corresponds to the frequency of resonance of the system without the active element corresponding to  $P = 0$ . In Fig. 4 the active element is assumed to act like a negative spring, tending to drive the natural resonant frequency lower; thus point A is to the left of B. Figure 4 shows that isolation of the

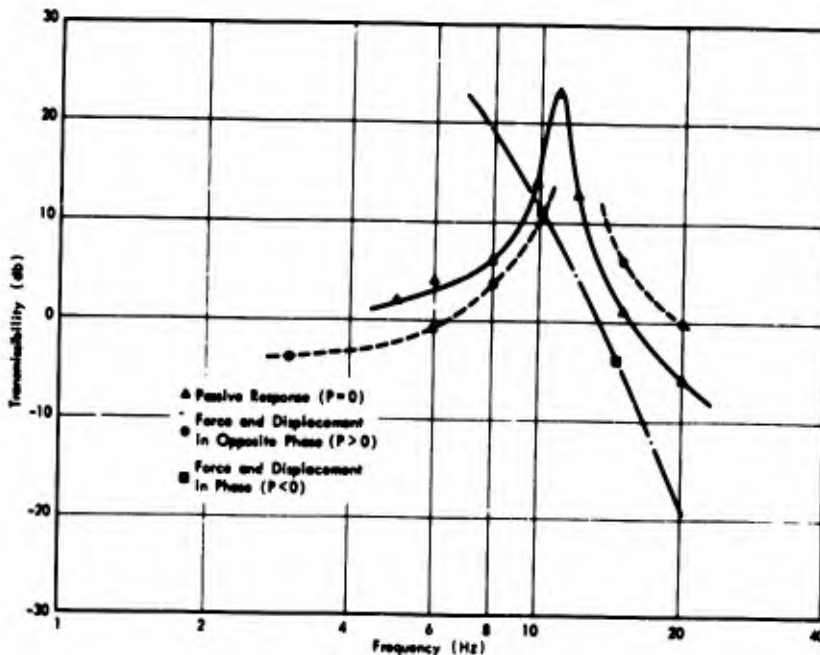


Fig. 3. Experimentally determined transmissibility of analog model, showing effect of phase between force and displacement of active element on system response

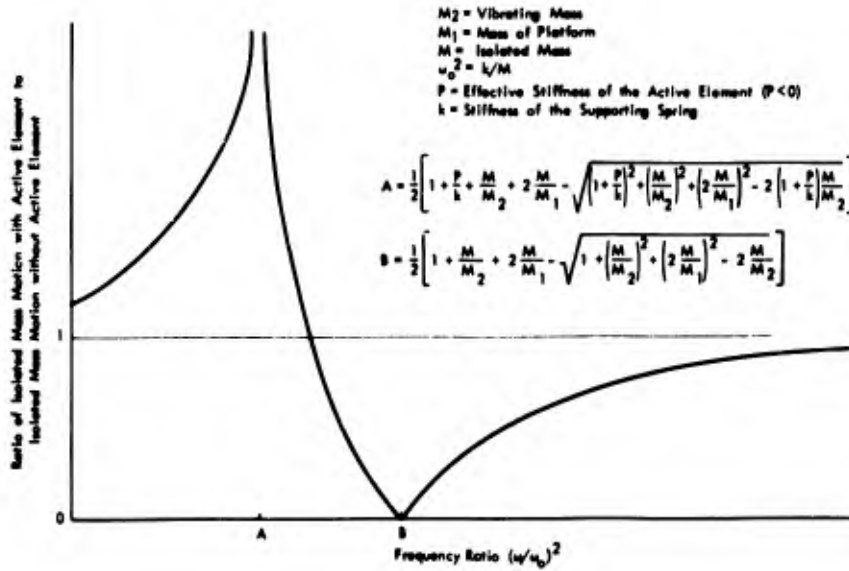


Fig. 4. Predicted change in vibration isolation with an active element which acts like a negative spring (those portions of the line below unity represent improvement in isolation, while those portions of the line above unity represent degradation of isolation)

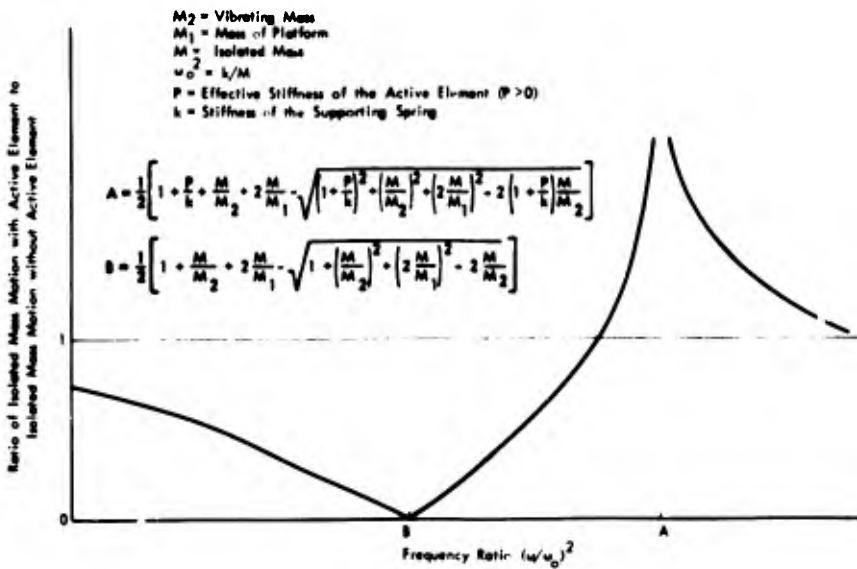


Fig. 5. Predicted change in vibration isolation with an active element which acts like a positive spring (those portions of the line below unity represent improvement in isolation, while those portions of the line above unity represent degradation of isolation)

isolated mass is improved above resonance (point A), but that at high frequencies the isolation is not significantly improved.

In Fig. 5 the active element is assumed to act like a positive spring, tending to drive the natural resonant frequency higher; thus point A is to the right of point B. Figure 5 shows that isolation is improved below resonance in this case.

### INVESTIGATION OF SIGNAL CONDITIONING CIRCUITS

The requirements for control of the undesirable resonance of a passive system are discussed above. Various modes of operation are conceivable, but in practice the choice is limited by the characteristics of feasible circuits. Possible signal conditioning circuits have been investigated by use of a digital computer. For each circuit considered, the transfer characteristics of the circuit have been mathematically formulated and the resulting expressions have been used in conjunction with the mathematical

model given in the Appendix to compute transmissibility as a function of frequency. In each formulation, key parameters have been varied step by step to see which choices might be made to give the best transmissibility results.

Figure 6 shows the results of one such calculation where the feedback circuit makes use of a simple bandpass filter whose lower cutoff frequency is 5.5 Hz. The frequency response of the filter is flat in the passband, and the gain of the feedback circuit is adjusted to give a value of  $P_k = -0.8$ . For these calculations, filter characteristics are based on measured phase shift and amplitude response of a suitable bandpass filter. The results are regarded as encouraging.

### CONCLUSION

In conclusion our preliminary investigation of the Hybrid Isolation System indicates that the system is feasible. The ultimate efficacy of the proposed system will be determined by work which is continuing.

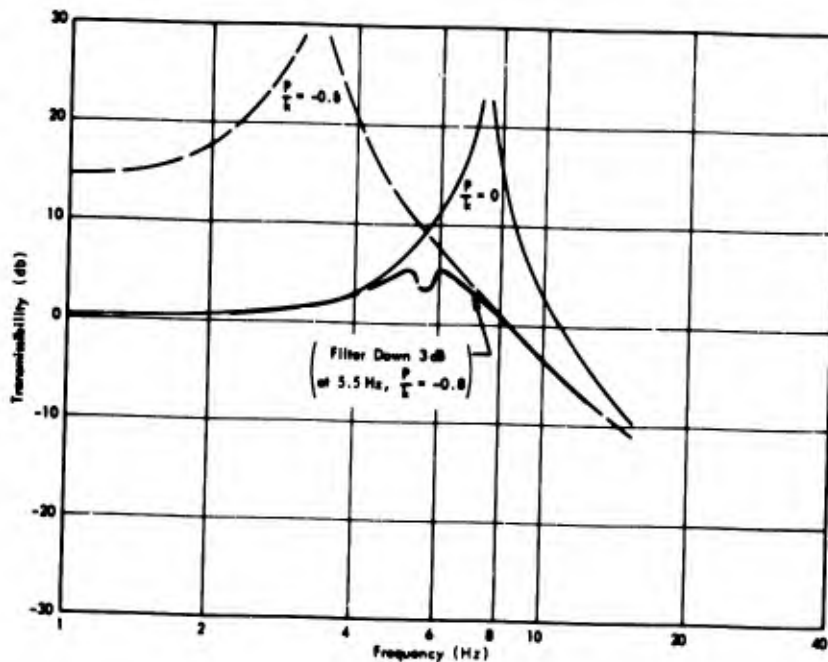


Fig. 6. Calculated transmissibility for an active system incorporating a realistic bandpass filter in the feedback circuit

## Appendix

### ANALYSIS OF PROTOTYPE HYBRID VIBRATION-ISOLATION SYSTEM (FIGURE 1)

#### SYMBOLS

$a_i$	Generalized coefficient in $n$ th order equation ( $i = 0, 1, \dots, n$ )
$\alpha$	Complex phase angle
$\beta$	Generalized variable in $n$ th order equation
$C$	Damping coefficient
$D$	Determinant of Eqs. (17)
$\Delta_i$	$i$ th determinant
$F_0$	Driving force acting on vibrating mass
$F_a$	Force generated by active element
$k$	Spring rate of spring from platform to isolated mass
$k_1$	Spring rate of spring from vibrating mass to platform
$M$	Mass of isolated mass
$M_1$	Mass of platform mass
$M_2$	Mass of vibrating mass
$P$	Effective stiffness of active element
$t$	Time
$\omega$	Angular frequency
$x$	Absolute displacement of vibrating mass
$x_0$	Amplitude of motion of vibrating mass
$y$	Absolute displacement of platform
$Y_0$	Amplitude of motion of platform
$z$	Absolute displacement of isolated mass
$Z_0$	Amplitude of motion of isolated mass
.	Dot above symbol indicates temporal differentiation

#### EQUATIONS OF MOTION

Let the force generated by the active element be proportional to the absolute displacement

of the isolated mass. The parameter  $P$  is then defined by

$$F_a = -Pz \quad (\text{A-1})$$

The equations of motion of the platform and the isolated mass may be written as follows using Eq. (A-1):

$$M_1 \ddot{y} + C(\dot{y} - \dot{z}) + k_1(y - x) + k(y - z) - Pz = 0,$$

and

$$M \ddot{z} + C(\dot{z} - \dot{y}) + k(z - y) + Pz = 0. \quad (\text{A-2})$$

Energy dissipation in the system has been accounted for by the introduction of the damping coefficient  $C$ .

#### CRITERIA FOR STABLE FREE VIBRATION

For free vibration,  $x(t) = 0$ . Solutions for Eqs. (A-2) are assumed of the form

$$y = Y_0 e^{\alpha t},$$

and

$$z = Z_0 e^{\alpha t}. \quad (\text{A-3})$$

By substituting Eqs. (A-3) into Eqs. (A-2), the following equations are obtained:

$$Y_0(M_1 \alpha^2 + C\alpha + k_1 + k) - Z_0(C\alpha + k + P) = 0,$$

and

$$-Y_0(C\alpha + k) + Z_0(M\alpha^2 + C\alpha + k + P) = 0. \quad (\text{A-4})$$

For nontrivial solutions of  $Y_0$  and  $Z_0$  in Eqs. (A-4), the determinant of their coefficients must be zero. This requirement leads to:

$$MM_1 \alpha^4 + C(M + M_1) \alpha^3 + \left[ M(k_1 + k) + M_1(k + P) \right] \alpha^2 + Ck_1 \alpha + k_1(k + P) = 0. \quad (\text{A-5})$$

In order that the system be stable, the solutions for  $y(t)$  and  $z(t)$  must decrease with time; thus the real part of  $\alpha$  is required to be negative. The Routh-Hurwitz criterion [1] states that the real parts of the roots  $\beta$  of the  $n$ th order equation

$$a_0 \beta^n + a_1 \beta^{n-1} + a_2 \beta^{n-2} + \dots + a_{n-1} \beta + a_n = 0$$

are negative provided that:

(a) all the coefficients  $a_0, a_1, \dots, a_n$  are positive, and

(b) all the determinants  $\Delta_i$  ( $i = 1, 2, \dots, n$ ) are also positive, where

$$\Delta_i = \begin{vmatrix} a_1 & a_0 & 0 & 0 & \dots \\ a_3 & a_2 & a_1 & a_0 & \dots \\ a_5 & a_4 & a_3 & a_2 & \dots \\ \dots & \dots & \dots & \dots & \dots \\ a_{2i-1} & a_{2i-2} & a_{2i-3} & a_{2i-4} & \dots & a_i \end{vmatrix}$$

If the subscript  $j$  of an element  $a_j$  in the determinant is greater than  $n$ , the element is set equal to zero. Note that  $\Delta_1 = a_1$  and  $\Delta_n = a_n \Delta_{n-1}$ ; hence,  $a_1 > 0$  and  $a_n > 0, \Delta_{n-1} > 0$  imply that  $\Delta_1 > 0$  and  $\Delta_n > 0$ , respectively. Thus  $\Delta_1$  and  $\Delta_n$  need not be actually evaluated.

Examination of Eq. (A-5) shows that  $a_0 > 0, a_1 > 0$ , and  $a_3 > 0$  are automatically satisfied. To satisfy  $a_4 > 0$  requires that

$$P > -k \quad (\text{A-6})$$

Equation (A-6) also makes  $a_2 > 0$ . However,  $a_2 > 0$  provides another restriction on  $P$ , namely

$$P > - \left[ \frac{M}{M_1} (k_1 + k) + k \right] \quad (\text{A-7})$$

To completely satisfy criterion 2,  $\Delta_2$  and  $\Delta_3$  must be positive. The requirement that  $\Delta_2 > 0$  is equivalent to

$$P > - \frac{M}{M_1} \left[ \frac{M(k_1 + k) + M_1 k_1}{M + M_1} \right] - k \quad (\text{A-8})$$

Similarly, the requirement that  $\Delta_3 > 0$  leads to

$$P < \frac{Mk_1}{M + M_1} \quad (\text{A-9})$$

With the assumptions that  $M_1 \ll M$ , and  $k_1 \approx k$ , Eqs. (A-6) through (A-9) restrict the allowable values of  $P$  for stable-free vibration to the range

$$-k < P < \frac{Mk_1}{M + M_1} \quad (\text{A-10})$$

Note that the range of  $P$  is independent of the damping coefficient  $C$ , as long as  $C$  is positive.

## TRANSMISSIBILITY OF SYSTEM WITH ACTIVE ELEMENT

Let  $x(t)$  in Eqs. (A-2) be the excitation source of the system, and let  $x(t)$  assume the form

$$x(t) = X_0 e^{i\omega t} \quad (\text{A-11})$$

The forced responses  $y(t)$  and  $z(t)$  now take the form

$$y(t) = Y_0 e^{i\omega t}$$

and

$$z(t) = Z_0 e^{i\omega t} \quad (\text{A-12})$$

Substitution of Eqs. (A-11) and (A-12) into Eqs. (A-2) yields (with the assumption that  $C$  is positive but small, so that for convenience,  $C$  may be neglected in the following calculation):

$$Y_0(-M_1\omega^2 + k_1 + k) + Z_0(-P - k) = k_1 X_0$$

and

$$(\text{A-13})$$

$$Y_0(-k_2) + Z_0(-M\omega^2 + k + P) = 0$$

Equations (A-13) may be solved for the ratio of  $Z_0/X_0$ , and gives

$$\frac{Z_0}{X_0} = \frac{k_1 k}{MM_1\omega^4 - [M(k_1 + k) + M_1(P + k)]\omega^2 + k_1(k + P)} \quad (\text{A-14})$$

for each value of  $P$  in the range

$$- \frac{Mk_1}{M + M_1} < P < k$$

there is a corresponding exciting frequency  $\omega$  such that the denominator on the right hand side of Eq. (A-14) becomes zero. This is the resonance frequency of the system with the particular value of  $P$ . The transmissibility of the system with an active element for several values of  $P$  is shown in Fig. 2, where the effects of isolation or amplification of the motion of the isolated mass are easily seen.

## COMPARISON OF SYSTEM BEHAVIOR WITH AND WITHOUT ACTIVE ELEMENT

With the same force acting on the vibrating mass, the presence of an active element may increase or decrease the amplitude of motion of the vibration source. Therefore, results in Fig. 2 may be misleading, since a small transmissibility does not necessarily mean a small

amplitude of motion of the isolated mass. A better judgment of the actual gain by using an active element is obtained by comparing the amplitudes of motion of the isolated mass with and without the active element. The force acting on the vibrating mass is assumed to be the same for both cases.

Under the assumption that a force  $F_0 e^{i \cdot t}$  acts on the vibrating mass, the equations of motion of the system shown in Fig. 1 become:

$$\begin{aligned} M_2 \ddot{x} + k_1(x - y) &= F_0 e^{i \cdot t} \\ M_1 \ddot{y} + k(y - z) + k_1(-x) - Pz &= 0 \end{aligned} \quad (\text{A-15})$$

and

$$M \ddot{z} + k(z - y) + Pz = 0$$

The motions of the masses can be assumed to be

$$\begin{aligned} x(t) &= X_0 e^{i \cdot t} \\ y(t) &= Y_0 e^{i \cdot t} \end{aligned} \quad (\text{A-16})$$

and

$$z(t) = Z_0 e^{i \cdot t}$$

Substitution of Eqs. (A-16) into Eqs. (A-15) gives the following:

$$X_0(-M_2 \omega^2 + k_1) + Y_0(-k_1) = F_0$$

$$X_0(-k_1) + Y_0(-M_1 \omega^2 + k + k_1) - Z_0(P + k) = 0 \quad (\text{A-17})$$

and

$$-Y_0 k + Z_0(-M \omega^2 + k + P) = 0$$

Equations (A-17) can be solved for  $Z_0$  in terms of  $F_0$  and the physical constants  $M, M_1, M_2, k_1$  and  $k$ . Then, letting  $P = 0$  in Eqs. (A-17), the amplitude of  $Z_0$  without the active element can be obtained in a similar way. The final result is the ratio of the above two amplitudes which, after some algebra, becomes:

$$\frac{(Z_0|_P)}{(Z_0|_{P=0})} = \frac{D|_{P=0}}{D|_P} \quad (\text{A-18})$$

In the above expression  $D|_P$  is the determinant of coefficients of  $X_0, Y_0,$  and  $Z_0$  in Eqs. (A-17) and  $D|_{P=0}$  is obtained by letting  $P = 0$  in  $D|_P$ . The ratio  $|(Z_0|_P)/(Z_0|_{P=0})|$  is plotted for the frequency range of interest (around the lower resonance of the system), and is presented qualitatively in Figs. 4 and 5 for  $P < 0$  and  $P > 0$ , respectively. Those values smaller than 1 indicate improvement in vibration isolation with an active element.

#### REFERENCE

1. Chihiro Hayashi, Nonlinear Oscillations in Physical Systems (McGraw-Hill, New York), 1964, pp. 71-73

#### DISCUSSION

**Mr. Verga, Hazeltine Corp.:** Your system consisted of an isolated mass plus two additional items, an active element and an inactive element. The active element was a black box. Now, the inactive element I gather consists of something like a shock or vibration absorber. Could you please say a few words as to exactly what the inactive elements of your vibration system contains?

**Mr. Bies:** The passive system essentially was just a spring. As I mentioned to begin with, this is a very preliminary report. We were thinking originally in terms of isolating the rotor vibration from the fuselage, but there are many difficulties with that. We have since thought in terms of part of the passenger compartment with respect to the fuselage, or some other combination. If you want to think of the rotor as being isolated from the fuselage then you might think of that first mass spring as some kind of a

spring between the fuselage and the rotor. That platform is a stiff member which has to have some mass, but is an attachment between the spring and another spring with the active elements. The isolated mass then is whatever it is you want to isolate.

**Voice:** This active system in no way preserved a statically fixed relation between the supporting structure and your isolated mass. This simply provides damping for a resonance peak, but does not maintain static relation. Do I understand that correctly?

**Mr. Bies:** The idea was that the system would become stiff at very low frequencies. Presumably the low frequency range would cover the range of control of the helicopter, so that the deflection you would get would be that part which is inherent in the passive part of this system which is supposed to work in the

higher frequency range. Effectively, what we are trying to do is to make the second part look like a lumped mass on a spring over most of the frequency range, say above 15 or 20 Hz. Below that the active system compensates for the inherent resonance that you would have with a lumped mass-spring system.

Voice: The thing that puzzles me about it is that your active element is reacting against a small mass. At very low frequencies this could have no ability to resist extension of your main spring.

Mr. Bies: Well, at very low frequencies our main spring is supposed to be stiff.

Mr. Dudley, Aerospace Corp.: Did you do any systems analysis as far as the alternative of mounting your passive element on the equipment to be protected as opposed to mounting it on the mounting plate?

Mr. Bies: We have not done that yet. As I mentioned, this is really very preliminary work that I am reporting. We have only been engaged in this for a few months.

\* \* \*



**BLANK PAGE**

# RECENT ADVANCES IN THE STUDY OF SYNCHRONOUS VIBRATION ABSORBERS\*

A. V. Srinivasan  
Kaman Corporation  
Bloomfield, Connecticut

Theoretical and experimental results of a study of two gyroscopic configurations as synchronous vibration absorbers are discussed.

The null frequencies in a gyroscopic system are a function of the speed of the gyrowheel. Therefore, gyroscopic configurations as vibration absorbers possess the unique feature that they can be synchronized so that an antiresonance can always be obtained no matter what the driving frequency is. The absorber can thus be made effective over any desired bandwidth of frequencies by synchronizing the speed of the gyrowheel. This is in direct contrast with conventional Frahm absorbers, which are effective only at the frequency to which they are tuned.

One configuration discussed, the "Perissogyro" vibration absorber, consists of a gyrodisk at one end of a shaft, the other end of which is connected to a cross pivot. The disk, drive system, and cross pivots rotate in unison. The analysis and the experiments provide for two degrees of rotational freedom about the cross pivot and two degrees of translational freedom. The two translational degrees of freedom are (a) along X, the direction of excitation, and (b) along Y, perpendicular to X. The theoretical and experimental analyses provide for a spring rate along Y. Two distinct nulls are predicted by theory. During experimentation it was found that the higher nulls could not be detected easily, although a tendency toward reaching a higher null was noticeable.

It is shown that while a null can always be obtained in the direction of excitation, oscillations will always occur in an orthogonal direction. A modification of the Perissogyro is studied to obtain nulls in both directions.

In the second configuration, which is essentially a top, the gyro disk rotates in relation to the shaft on which it is mounted. The shaft itself is mounted on a cross pivot so that the device may oscillate in two directions perpendicular to each other.

## INTRODUCTION

Conventional dynamic vibration absorbers invented by Frahm in 1909 are still quite widely used because of their simplicity. In general, Frahm absorbers are considered as a "fix" to a vibration problem rather than a solution in the original design of a structure, because their effectiveness is restricted to a small range of excitation frequency. Also, conventional absorbers are a definite weight penalty except in cases where a useful piece of equipment can be used as a sprung mass. To be effective, vibration absorbers used in aircraft such as compound aircraft, rotary wing spacecraft decelerators, and certain VTOL aircraft should

necessarily possess a broad bandwidth of null frequency. Previous research (Ref. 1 and 2) has shown that gyroscopic vibration absorbers can be successfully synchronized to provide the needed bandwidth in situations where the exciting frequency varies over a considerable range. The general response of a structure with such a synchronous vibration absorber is shown in Fig. 1.

Synchronous vibration absorbers hold promise as useful devices which may be incorporated into the original design of a structure to minimize vibration levels. By proper analysis of a structure, the effective masses at various stations may be determined so that the ideal

\*Research was performed under National Aeronautics and Space Administration Contract NASW-1394, Harvey Brown, director.

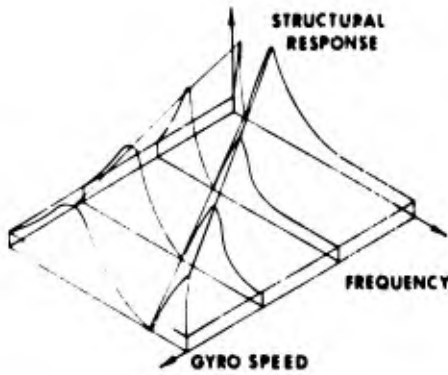


Fig. 1. General response of a structure with a synchronous vibration absorber

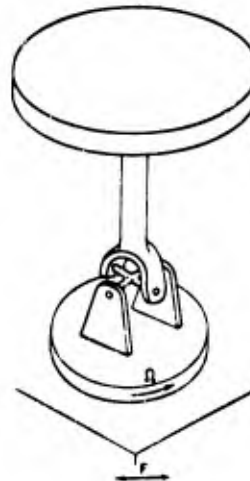


Fig. 2. Perissogyro vibration absorber

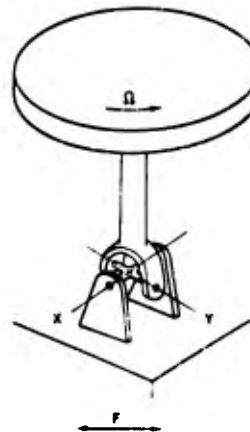


Fig. 3. Alternate configuration of the perissogyro vibration absorber

position to locate the synchronous absorbers may be determined in the early design stages. Thus, the engineer can define the most efficient structure for strength and weight and reduce vibration problems to a desired minimum.

Two gyroscopic configurations shown in Figs. 2 and 3 are examined in some detail to determine their feasibility as synchronous vibration absorbers. The configuration shown in Fig. 2, designated here as Perissogyro vibration absorber, consists of a disk constrained to rotate about a fixed axis but having angular degrees of freedom about the rotating axes. Figure 3 describes a similar arrangement with only one difference, in that the spin axis is fixed to the disk. It is shown later that the configuration of Fig. 3 is merely a special case of that of Fig. 2.

Emphasis is placed on discussion of results obtained from theory and experiment. Details of analysis are omitted. Numerical results are presented in graphical form and show considerable agreement between theory and experiment.

## ANALYSIS

The analysis is based on the following considerations:

1. The synchronous vibration absorbers have two degrees of translational freedom and two degrees of rotational freedom about the cross pivot.

2. The spin velocity of the disk is considered as a constant (i.e.,  $\dot{\alpha} = \omega$ ).

3. The potential energy in the system resulting from gravitational forces is negligible.

4. Angular oscillations of the absorbers are small.

Based on these considerations, the equations of motion for the Perissogyro may be shown to be:

$$I_x \ddot{\theta} + \Omega I_z \dot{\theta} + Mh \ddot{X}_0 = 0 \quad (1)$$

$$I_x \ddot{\theta} - \Omega I_z \dot{\theta} + Mh \ddot{Y}_0 = 0 \quad (2)$$

$$Mh \ddot{\eta} + \bar{M} \ddot{X}_0 = f_x, \quad (3)$$

$$Mh \ddot{\zeta} + \bar{M} \ddot{Y}_0 + k_y Y_0 = 0, \quad (4)$$

where

$$\eta = \theta \cos \psi + \phi \sin \psi, \quad (5)$$

$$\zeta = \theta \sin \psi - \phi \cos \psi, \quad (6)$$

and

$m$  = mass of disk,

$\bar{M}$  = total mass that is oscillating (includes the effective mass of the vibrating structure),

$h$  = height of centroid of gyro disk from the cross pivots,

$I_x, I_z$  = inertias about  $x$  and  $z$  axes, respectively,

$k_y$  = lateral spring rate.

Other symbols are shown in Fig. 4.

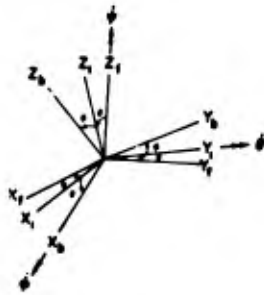


Fig. 4. Coordinate transformation

Assuming steady-state oscillations, the null equation obtained by equating the expression for the coordinate  $X_0$  to zero reduces to

$$\left( \frac{M_1}{I_x} - \frac{M}{M_1} \right) \omega^2 \left( 1 - \frac{I_x^2}{I_x^2} \frac{M}{M_1} + \frac{k_y}{M_1} \right) - \frac{k_y}{M_1} \omega^2 \frac{I_x^2}{I_x^2} = 0, \quad (7)$$

where  $\omega$  is the frequency of excitation.

Numerical results obtained from solving Eq. (7) have been compared with those obtained from experiment. These are shown in Fig. 5. A discussion of these results appears in a later section of this paper.

An examination of Fig. 4 indicates that the generalized coordinates  $\eta, \zeta$  for the Perissogyro are written in terms of the angular oscillations  $\theta, \phi$  in the rotating system of coordinates. Since the pivots in the configuration shown in Fig. 3 do not rotate,  $\theta$  and  $\phi$  themselves serve as generalized coordinates in this case. Thus the equations of motion are very similar to Eq. (1) through (4) and the null equation coincides with Eq. (7). By virtue of the transformation equations (Eqs. 5 and 6), the angular oscillatory responses in the two devices will, however, be different. In terms of the null characteristics, the configuration shown in Fig. 3 is identical to that of Fig. 2. Therefore, further discussion will be confined to the Perissogyro vibration absorber only.

From Eqs. (1) through (4), the response in the lateral direction can be computed as

$$\frac{DY_0}{f_x} = \frac{I_x}{I_x} M_1 \omega^5, \quad (8)$$

where  $D$  is the determinant of the coefficient matrix formed from Eqs. 1-4.

It is evident from Eq. (8) that lateral oscillations will always occur no matter what the excitation frequency is. Therefore, even though a null is attained along the  $X$  direction, the system will have oscillations in the orthogonal direction. This apparently imposes a serious limitation on the use of the Perissogyro vibration absorber. However, it is clear from Eq. (6) that the displacement  $Y_0$  is linearly related to the speed,  $\omega$ , of the gyrowheel. Therefore it is possible to obtain a null along the lateral direction also by combining two Perissogyro absorbers in such a way that the direction of rotation of one of the gyrowheels is opposite to that of the other. Such a device is designated here as Double Perissogyro vibration absorber. While the feasibility of attaining nulls simultaneously in two orthogonal directions is determined in theory, detailed experimentation will be necessary to provide support to the theoretical development.

Details of analysis for the Double Perissogyro vibration absorber are omitted. Only the null equation is included here to aid discussion and comparison. Thus, for the Double Perissogyro the null equation is

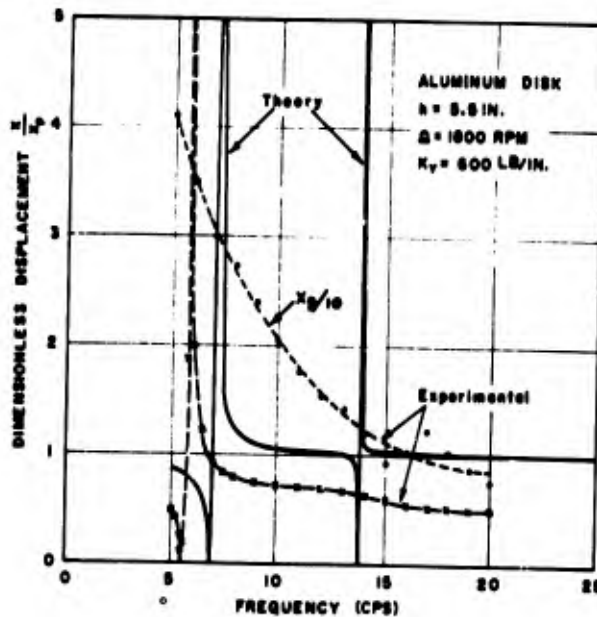


Fig. 5. Theoretical and experimental response curves

$$\omega = \Omega \sqrt{I_z/I_x} \quad (9)$$

which coincides with the expression for  $\omega$  obtained from equation (7) when  $k_y \rightarrow \infty$ .

## EXPERIMENTATION

The overall purpose of the experimentation was to obtain reasonable confirmation of the theoretical development of the Perissogyro vibration absorber. To accomplish this, an absorber was designed using a Hooke's joint, one end of which is connected to a synchronous motor and the other to a circular aluminum plate at one end of a steel rod. The schematic and a photograph of the setup are shown in Fig. 6 and 7. The speed and the direction of rotation of the motor could be controlled at either 1800 or 3600 rpm. The entire absorber was then mounted on two shafts which rotate in opposite directions to remove the effect of friction forces along the direction of oscillation. Plunger springs were mounted laterally to provide lateral spring rate.

A 50-lb shaker was used to excite the system. Two MB velocity pickups were mounted on the base of the Perissogyro in the direction of excitation and perpendicular to it. The outputs of the pickups were fed to an oscilloscope from which the results were recorded manually. On some tests, actual traces of the output were obtained to facilitate discussion of results.

To compare the theoretical results with the experimental results, it was necessary to determine the actual spring rate in the lateral direction. This was measured in a simple experiment, the results of which are shown in Fig. 8. This load-displacement curve being slightly nonlinear, the spring rate was approximated to be around 600 lb/in.

In order to determine experimentally the variation of antiresonant frequency with the speed of the gyrowheel, the excitation frequency was set at a particular value and the motor running at 3600 rpm was turned off. As the motor continued to decelerate, the actual instantaneous speed of rotation was read on an electronic counter when the null was located on the oscilloscope. This procedure was repeated for various values of the excitation frequency. A comparison of the null-speed characteristics predicted by theory (with  $k_y$  as parameter) with those obtained from experiment is presented in Fig. 9.

One of the problems encountered during experimentation pertains to self-excited oscillations of the Perissogyro. These oscillations were at times quite violent, and repeated trials were necessary before reasonably satisfactory conditions were obtained. The linear theory does not suggest possibilities of any such apparently unstable conditions. Further detailed experimental and theoretical investigations

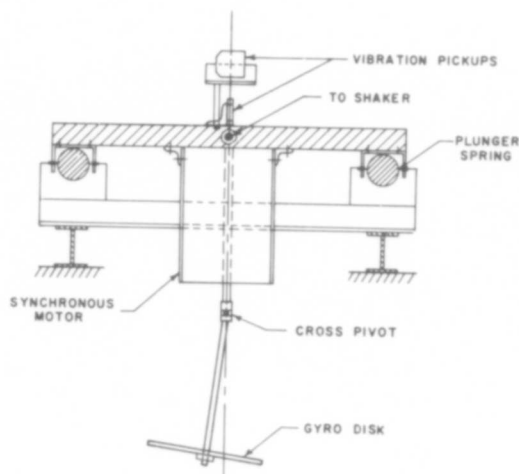


Fig. 6. Schematic of the experimental setup

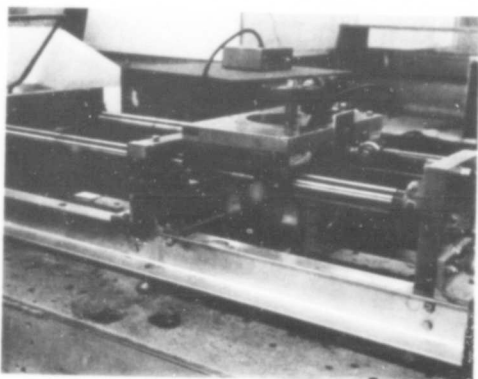


Fig. 7. Experimental setup

would be necessary to obtain a fully satisfactory explanation of this problem.

#### RESULTS AND DISCUSSION

Figure 5 shows the principal features of the Perissogyro vibration absorber as obtained from theory and experiment. Dimensionless values of amplitudes are obtained by dividing the measured output by corresponding values obtained by shaking the Perissogyro absorber with the motor turned off. The latter data are

termed  $X_p$  and indicate the response of the absorber as a pendulum.

An examination of Fig. 9 indicates that the theoretical null-speed curves have two branches, one corresponding to a lower null and the other corresponding to a higher null. The lower branch in each case (i.e., for each  $k_y$ ) approaches asymptotically a value close to the lowest value of the corresponding higher branch. As  $k_y \rightarrow \infty$ , the higher branches tend to a horizontal line at a null frequency also at  $\infty$ . The lower branches tend to the corresponding curve for the Double Perissogyro vibration absorber. This is appropriate in view of the fact that the Double Perissogyro always has a null in the lateral direction, a condition which corresponds to having an infinite spring rate in that direction. The null-speed plot obtained by experiment appears to approximate the corresponding curve obtained by theory for a  $k_y = 600$  lb/in. This confirms the observation made earlier that the experimental setup responds approximately at a 600-lb/in. lateral spring rate.

The experiments show distinctly the presence of only the lower nulls, although a tendency to reach the higher nulls was observed. Such a tendency can be seen by examining the output trace shown in Fig. 10.

For the Single Perissogyro vibration absorber the null-speed curves are nearly straight only for certain speeds of the gyrowheel. Thus, linear synchronization of the null frequencies with the gyrospeeds is possible over a limited

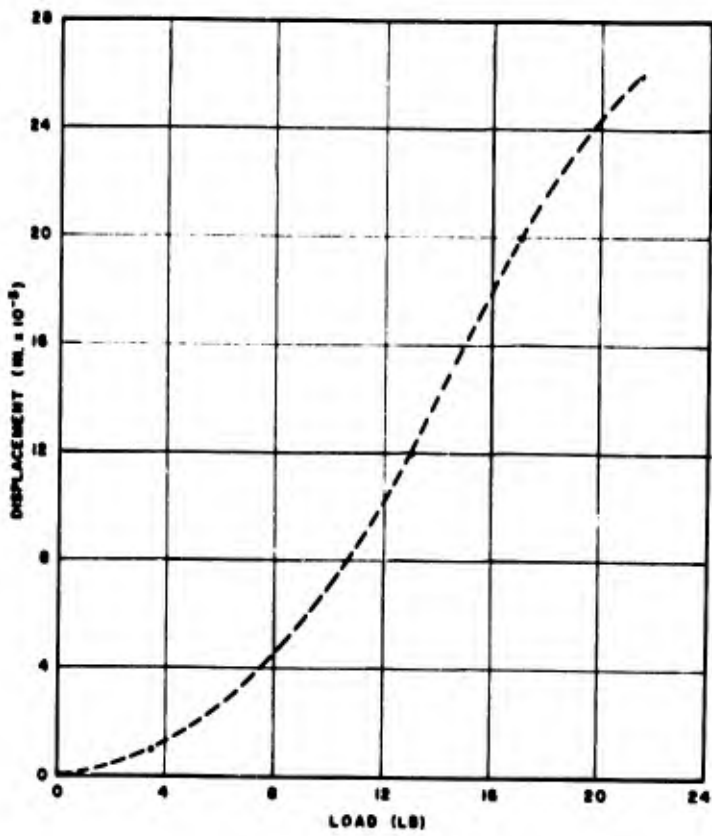


Fig. 8. Experimental determination of lateral spring rate

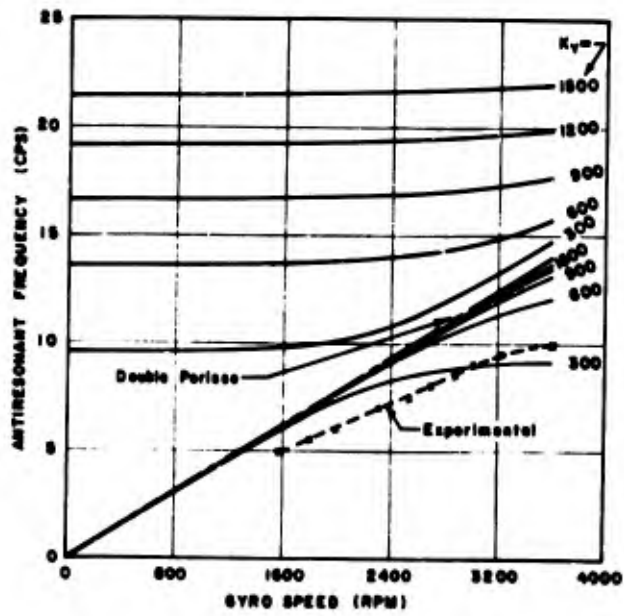


Fig. 9. Variation of antiresonant frequency with gyrospeed

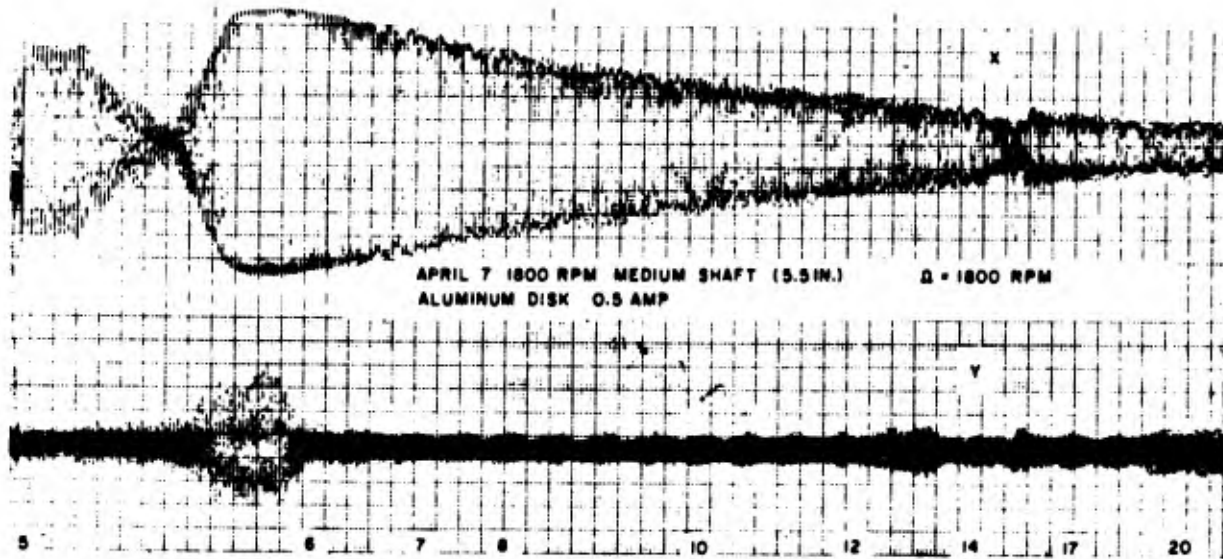


Fig. 10. Traces of response curves obtained experimentally

range of gyrospeeds. This range is dependent on the physical parameters of the absorber. However, for the Double Perissogyro vibration absorber the null-speed characteristic is a straight line. Thus linear synchronization is possible for any range of gyrospeeds. Experimental investigation of the Double Perissogyro vibration absorber is currently in progress.

#### ACKNOWLEDGMENTS

Grateful acknowledgments are due to Robert Jones and William G. Flannelly, Chief and Assistant Chief of Vibrations at Kaman, for their helpful criticism and discussion during the preparation of this paper.

#### REFERENCES

1. W. G. Flannelly and J. C. Wilson, "Analytical Research on a Synchronous Vibration Absorber," NASA CR 338, Dec. 1965
2. R. Jones, "The Gyroscopic Vibration Absorber," paper presented at the ASME Vibrations Conference, Boston, Mass., Mar. 1967

#### DISCUSSION

Mr. Roach: I would like to take the privilege of asking the first question. What happens, in the case of helicopters in very heavy maneuvering conditions, such as we are running on the XH51, where we are actually able to loop the helicopter in 2, 2-1/2 g maneuver loads. Some of these isolation systems seem to be wonderful in a quasi-static condition of operation,

but what happens when heavy maneuver loads are imposed?

Mr. Srinivasan: The type of input to which you refer is more impulsive than the simple steady state conditions which we have assumed. What we have done is really very preliminary work. Applications of the type that you are talking about are still very far off.

\* \* \*



**BLANK PAGE**

# OPTIMIZING THE DYNAMIC ABSORBER TO INCREASE SYSTEM DAMPING

Gary K. Jones  
NASA Goddard Space Flight Center  
Greenbelt, Maryland

Technical problems encountered in the operation of the Orbiting Geophysical Observatory (OGO) III spacecraft called for an investigation of the dynamic characteristics of the dynamic absorber. When properly tuned and damped, the dynamic absorber, which consists of a damped spring-mass system, has the effect of reducing the transmissibility and increasing the modal damping of the system to which it is attached.

Several references in the technical literature deal with the influence of the dynamic absorber on transmissibility, but yield very little information on modal damping which can have a significant effect on system stability. Thus, the main purpose of this investigation was to define analytically the effect on system damping produced by the dynamic absorber. A mathematical model which consisted of a damped dynamic absorber attached to the mass of a simple spring-mass system was used. The differential equations of motion for the system were derived. The characteristic equation was formed and solved for various values of system parameters with a digital computer program. For a given set of parameters, two values of modal damping were determined. The lower value (minimum modal damping) was of primary interest since it represented a lower bound on modal damping.

The results of the investigation indicated that the value of absorber damping which optimizes modal damping is 163 percent of that which optimizes transmissibility. The results also indicated that the optimum value of absorber tuning is the same with respect to transmissibility and modal damping. Both tuning and damping errors were found to produce significant changes in modal damping.

## INTRODUCTION

Motivated by technical problems encountered in the operation of the OGO III spacecraft, an investigation of the dynamic characteristics of dynamic absorbers was initiated. When properly tuned and damped, the dynamic absorber, which consists of a damped spring-mass system, has the effect of reducing the dynamic response and increasing the modal damping of the system to which it is attached. A search of the technical literature revealed several references [1-9] dealing with the dynamic absorber but yielding very little useful design information. In particular, modal damping, which can have a significant influence on system stability, was not discussed. Also, very few data were available on the effects of nonoptimal tuning or damping on the performance of the dynamic absorber. Thus, the main purpose of this investigation was analytically to generate dynamic absorber design information.

## SYMBOLS

- C Dynamic absorber viscous damping constant
- e Natural logarithm base (2.718...)
- F<sub>0</sub> Peak oscillatory exciting force
- |H(ω)| Dynamic response function
- I<sub>1</sub> Imaginary part of root pair  $\bar{\lambda}_1$
- K<sub>1</sub> Primary system spring constant
- K<sub>2</sub> Dynamic absorber spring constant
- M<sub>1</sub> Primary system mass
- M<sub>2</sub> Dynamic absorber mass
- R<sub>1</sub> Real part of root pair  $\bar{\lambda}_1$

- $x_1$  Motion of  $M_1$ ,  $= X_1 \sin \omega t$
- $x_2$  Motion of  $M_2$ ,  $= X_2 \sin \omega t$
- $X_1$  Peak dynamic displacement of  $M_1$
- $X_2$  Peak dynamic displacement of  $M_2$
- $X_0$  Peak oscillatory exciting displacement
- $\alpha$  Tuning ratio,  $= \omega/\omega_1$
- $\alpha_0$  Optimum value of tuning ratio,  $= 1/(1+\mu)$
- $\delta_1$  Modal logarithmic decrement,  $= 2\pi R_1/I_1$
- $\zeta_a$  Dynamic absorber damping parameter,  $= C/2M_2\omega_1$
- $\zeta_{a0}$  Value of  $\zeta_a$  required to optimize  $|H(\omega)|$ ,

$$= \sqrt{\frac{3\mu}{8(1+\mu)^3}}$$

- $\delta_1$  Modal damping,  $= \delta_1/2\pi$
- Forcing frequency ratio,  $= \omega/\omega_1$
- $\omega_j$   $j$ th root of characteristic equation
- $\omega_{j1}$   $j$ th conjugate root pair,  $= -R_1 \pm iI_1$
- $\mu$  Mass ratio,  $= M_2/M_1$
- $\tau_1$  Period of oscillation,  $= 2\pi/\omega_{D1}$
- Frequency of excitation
- Primary system frequency,  $= \sqrt{K_1/M_1}$

- $\omega_2$  Dynamic absorber frequency,  $= \sqrt{K_2/M_2}$
- $\omega_{D1}$  Coupled damped frequency of  $i$ th mode

### ANALYTIC TECHNIQUE

The system analyzed was a damped dynamic absorber attached to the mass of a simple spring-mass system (Fig. 1). Note that the dynamic characteristics of this system have been extensively investigated from the standpoint of forced vibration, and the values of absorber tuning  $\alpha$  and damping  $\zeta_a$  necessary to minimize the dynamic response (transmissibility) were defined, in Ref. [1]:

$$\alpha_0 = \frac{1}{1+\mu}$$

and

$$\zeta_{a0} = \sqrt{\frac{3\mu}{8(1+\mu)^3}}$$

This investigation, however, was concerned with optimizing the modal damping  $\zeta_1$  rather than the dynamic response; this required an investigation of the free vibration characteristics of the system shown in Fig. 1. Starting with the differential equations of motion:

$$M_1 \ddot{x}_1 + K_1 x_1 + K_2(x_1 - x_2) + C(\dot{x}_1 - \dot{x}_2) = 0,$$

and

$$M_2 \ddot{x}_2 + K_2(x_2 - x_1) + C(\dot{x}_2 - \dot{x}_1) = 0.$$

The characteristic equation was derived:

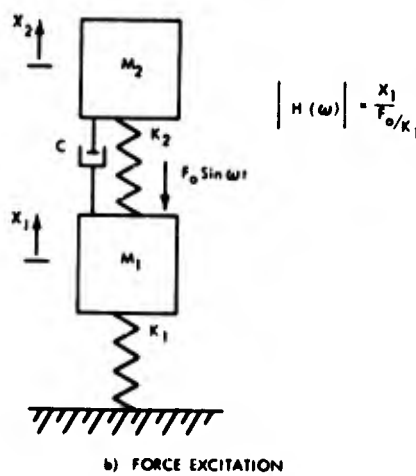
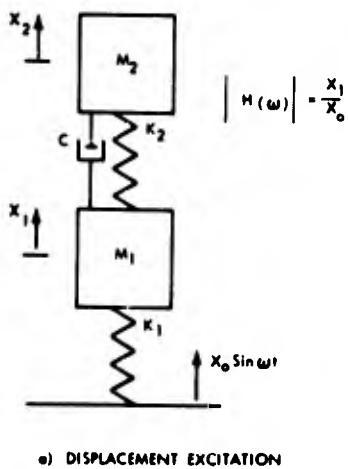


Fig. 1. Analytical models

$$\left(\frac{\lambda}{\omega_1}\right)^4 + 2\zeta_n(1+\mu)\left(\frac{\lambda}{\omega_1}\right)^3 + [a^2(1+\mu) + 1]\left(\frac{\lambda}{\omega_1}\right)^2 + 2\zeta_n\left(\frac{\lambda}{\omega_1}\right) + a^2 = 0,$$

where

$$X_1 = a_1 e^{\lambda_1 t} + b_1 e^{\lambda_2 t} + c_1 e^{\lambda_3 t} + d_1 e^{\lambda_4 t},$$

and

$$X_2 = a_2 e^{\lambda_1 t} + b_2 e^{\lambda_2 t} + c_2 e^{\lambda_3 t} + d_2 e^{\lambda_4 t}.$$

The four complex roots ( $\lambda_j$ ) of the characteristic equation were determined with a digital computer program for various values of  $\mu$ ,  $a$ , and  $\zeta_n$ :

$$0.01 \leq \mu \leq 0.20,$$

$$0.8a_0 \leq a \leq 1.2a_0,$$

$$0.8\zeta_{n0} \leq \zeta_n \leq 1.8\zeta_{n0}.$$

The complex roots occur in conjugate pairs; thus two conjugate pairs ( $\bar{\lambda}_i$ ) were obtained from the four roots:

$$\bar{\lambda}_i = -R_i \pm iI_i; \quad i = 1, 2.$$

The displacements  $X_1$  and  $X_2$  were of the form

$$X_1 = a_1 e^{-R_1 t} e^{iI_1 t} + \dots$$

Since the imaginary part of the roots  $I_i$  was the modal frequency and that the real part of the root  $R_i$  was the decay constant, the logarithmic decrement was expressed as

$$\delta_i = \zeta_n \frac{c}{R_i(t+\tau_i)} = -R_i t + R_i t + R_i \tau_i = R_i \tau_i.$$

But

$$\tau_i = \frac{2\pi}{I_i}.$$

Thus

$$\delta_i = \frac{R_i 2\pi}{I_i}.$$

The modal damping expression  $\zeta_i$  was defined as

$$\zeta_i = \frac{\delta_i}{2\pi} = \frac{R_i}{I_i}.$$

This relation makes use of the expression [8] serving to define approximately the relation of  $\delta$  to  $C/C_c$  in a single-degree-of-freedom system. Thus the parameter  $\zeta_i$  can be thought of as either logarithmic decrement divided by  $2\pi$  or as approximating the modal damping ratio  $(C/C_c)_i$ . For a given set of system parameters, two values of modal damping  $\zeta_i$  were determined, with the lower value (minimum modal damping) being of primary interest since it represented a lower bound on modal damping.

For the purposes of comparison, the effect of system parameter variation on the dynamic response function (transmissibility) was determined. The dynamic response function  $|H(\omega)|$  was defined to correspond to the ratio of the dynamic displacement to either static displacement for force excitation or base amplitude for base displacement excitation [1]:

$$|H(\omega)| = X_1/X_0 \text{ displacement excitation (Fig. 1a);}$$

$$|H(\omega)| = \frac{X_1}{F_0/K_1} \text{ force excitation (Fig. 1b);}$$

$$|H(\omega)| =$$

$$\left\{ \frac{(a^2 - \omega^2)^2 + 4\zeta_n^2 \omega^2}{4\zeta_n^2 \omega^2 [-1 + (1+\mu)\omega^2]^2 + [\mu a^2 \omega^2 - (\omega^2 - 1)(\omega^2 - a^2)]^2} \right\}^{1/2}$$

The expression for  $|H(\omega)|$  was programmed on a digital computer and solved for various values of system parameters. The dynamic response function was then plotted as a function of the forcing frequency ratio  $\omega$ , and the peak dynamic response for various combinations of  $\mu$ ,  $a$ , and  $\zeta_n$  were determined.

## RESULTS

Evaluation of the results indicated that the optimum values of tuning and damping with respect to minimum modal damping were  $\omega_0$  and  $1.63\zeta_{n0}$ . Note that this value of absorber damping differs from that which optimizes the dynamic response. Thus if the main objective of the designer is to maximize modal damping, the value of absorber damping should not correspond to the "optimum damping" as defined from the standpoint of transmissibility in Refs. 1 through 9. The results indicated that the lower damped mode could be primarily associated with the main mass motion, at least at the upper and lower limits of the range of tuning

ratios investigated in the analyses. The basis for this conclusion is that the frequency of the lower damped mode at the lower limit of tuning ratio approached the main mass frequency  $\omega_1$  and at the upper limit of tuning ratio approached the frequency of a system having  $M_2$  rigidly attached to  $M_1$ :

$$\sqrt{\frac{K_1}{M_1 + M_2}}$$

The values of minimum modal damping  $\zeta_1$  (Fig. 2) for the optimum tuned and damped conditions,  $\alpha = \alpha_0$  and  $\zeta_a = 1.63 \zeta_{a0}$ , were found to range from 0.05 at a mass ratio of 0.01 to 0.229 at a mass ratio of 0.20.

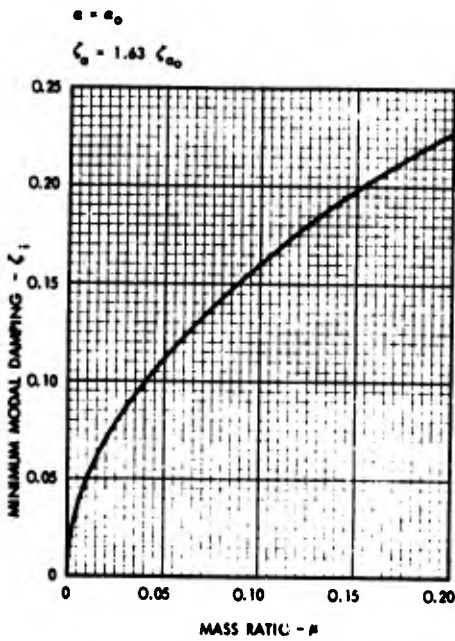


Fig. 2. Optimum dynamic absorber performance

Both tuning and damping errors were found to produce significant changes (Figs. 3 and 4) in modal damping. To illustrate, at a mass ratio of 0.10, an error of +10 percent in tuning reduced the minimum modal damping by 54 percent, and the same percentage error in damping decreased the minimum modal damping by 37 percent.

In contrast, the results (Fig. 5) indicate that the effectiveness of the dynamic absorber in lowering peak dynamic response is significantly reduced by small variations in tuning from the optimal value and is only slightly

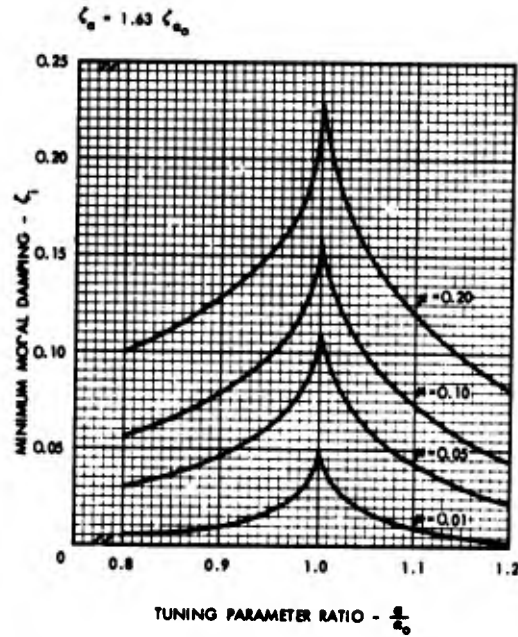


Fig. 3. Dynamic absorber performance: optimum absorber damping, variation in tuning

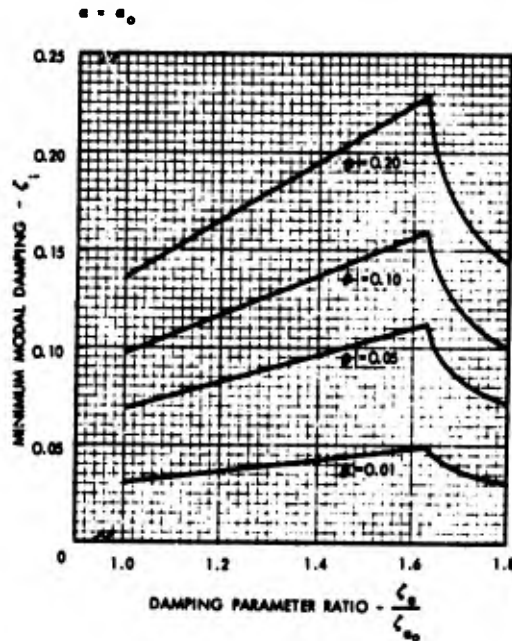


Fig. 4. Dynamic absorber performance: optimum tuning, variation in absorber damping

reduced by an equivalent variation in damping from the optimal value. For example, at a mass ratio of 0.10, a +10 percent error in

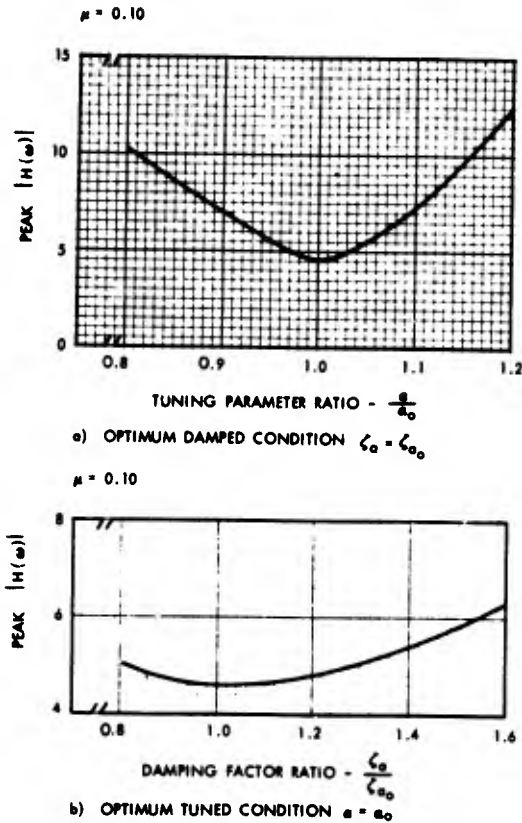


Fig. 5. Peak dynamic response --  $|H(\omega)|$

tuning increases the peak dynamic response by 61 percent, while the same percentage error in damping increases peak dynamic response by only 1 percent.

From the previous discussion of optimum tuning and damping, one problem encountered by the designer becomes apparent: selecting the value of absorber damping. Obviously if he is interested only in reducing dynamic response (transmissibility), the value of absorber damping should be  $\zeta_{a0}$ ; or if his only concern is maximizing the damping in the lower damped mode, the value of absorber damping should be  $1.63\zeta_{a0}$ . For situations where both transmissibility and modal damping are of equal importance, the value of absorber damping that yields the same percentage deviation for both of the parameters from their optimal values was found to be closer ( $\approx 1.4\zeta_{a0}$ ) to the value that optimizes modal damping ( $1.63\zeta_{a0}$ ) rather than the transmissibility optimum ( $1.0\zeta_{a0}$ ).

The effect of combinations of absorber tuning and damping errors on the modal damping

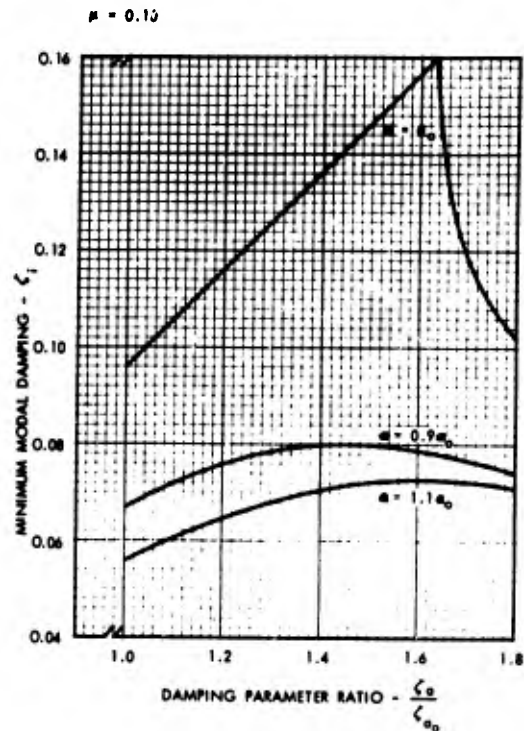


Fig. 6. Dynamic absorber performance: variation in absorber damping and tuning

parameter  $\zeta_1$  was investigated. It was concluded from the results that simple superposing of the individual effects would not yield valid results for systems having errors in both tuning and damping. For example (Fig. 6), at mass ratio of 0.10 a +10 percent error in both absorber damping and tuning had the effect of reducing the minimum modal damping by 55 percent, while superposing the individual effects yields a reduction of 71 percent.

## CONCLUSIONS

1. The value of absorber damping required to optimize minimum modal damping is 163 percent of that which optimizes the dynamic response function. In contrast, the optimum value of absorber tuning is the same with respect to both the dynamic response function and minimum modal damping.

2. If both dynamic response and minimum modal damping are of equal importance to the designer, then the value of absorber damping should be closer to the value that optimizes minimum modal damping rather than the transmissibility optimum.

3. Relatively small errors in either absorber damping or tuning significantly reduce minimum modal damping.

4. Superposing the individual effects of errors in absorber tuning and damping on minimum modal damping will not yield valid results for systems having both these errors.

#### REFERENCES

1. J. P. Den Hartog, Mechanical Vibrations (McGraw-Hill, New York), 1956
2. D. I. G. Jones, A. D. Nashif, and R. L. Adkins, "Effect of Tuned Dampers on the Vibrations of Simple Structures," AIAA J., 5(2):310 (1967)
3. V. H. Neubert, "Dynamic Absorbers Applied to a Bar That Has Solid Damping," J. Acoust. Soc. Amer., 36:873 (1964)
4. J. C. Snowdon, "Vibration of Cantilever Beams to Which Dynamic Absorbers are Attached," J. Acoust. Soc. Amer., 39:878 (1966)
5. J. C. Snowdon, "Steady State Behavior of the Dynamic Absorber," J. Acoust. Soc. Amer., 31:1096 (1959)
6. H. R. Spence and J. H. Winter, "Application of the Vibration Absorber Principle for the Protection of Airborne Electronic Equipment," Shock, Vibration and Associated Environments, Bulletin 28, Part IV, pp. 57-64, 1960
7. K. N. Tong, Theory of Mechanical Vibration (Wiley, New York), 1960
8. W. T. Thomson, Mechanical Vibrations (Prentice-Hall, Englewood Cliffs, N.J.) 1953
9. D. Young, "Theory of Dynamic Vibration Absorbers For Beams," Proc. 1st U. S. Nat. Congr. Appl. Mech., pp. 91-96, 1952

\* \* \*

# APPLICATION OF THE DYNAMIC ANTIRESONANT VIBRATION ISOLATOR TO HELICOPTER VIBRATION CONTROL\*

Robert Jones and William G. Flannelly  
Kaman Aircraft  
Bloomfield, Connecticut

Because helicopters characteristically exhibit large-amplitude vibration at low frequencies and are subject to transient accelerations of long duration in maneuvers, conventional vibration isolation techniques have been largely unsuccessful in protecting components and crew. Under the sponsorship of the U.S. Army Aviation Materiel Laboratories (AVLABS), at the Army's Aviation Research Center, Fort Eustis, Virginia, the vibrations research staff of Kaman Aircraft conducted experimental and analytical investigations of the dynamic antiresonant vibration isolator (DAVI), an inertially coupled isolation device which permits a high degree of isolation at discrete low frequencies without sacrifice of elastic stiffness.

The principles upon which the DAVI is based and laboratory experimentation on a DAVI isolated helicopter pilot's seat are described. The effects of shock inputs and damping on DAVI performance are shown through analysis and experiment. The need for two-dimensional DAVI action in multidirectional excitation environment is demonstrated by the results of helicopter flight testing of a unidirectional DAVI platform.

Laboratory test results are presented to show the independence of DAVI isolation from the weight of the isolated item, clearly violating the "static deflection rule" of conventional isolators. The principles of the family of series-damped DAVI's are outlined, and experimental confirmation of the capability of the series-damped DAVI's for passively producing a damped resonance and a completely undamped antiresonance is presented.

A summary of work now underway, under AVLABS sponsorship, on the application of DAVI to helicopter rotor isolation reveals unique possibilities for the alleviation of rotor-induced vibration in helicopters.

## INTRODUCTION

Great advancement has been made in the state of the art in helicopter analysis and design. However, even with this advancement, major vibration problems still exist in the present-day helicopter. With the coming of faster helicopters, and compound and composite aircraft, these vibration problems will in all probability increase.

The major source of these vibrations are the rotor-induced shears, both vertical and in-plane. The predominate frequency of excitation is the "nth" harmonic of the n-bladed helicopter; i.e., for a two-bladed helicopter, the predominate frequency is two per revolution; for a three-bladed helicopter, three per revolution, etc. In present-day helicopters, this predominate frequency ranges approximately

between 8.5 and 24 cps. Thus, very-low-frequency, high-amplitude vibrations are encountered. Conventional isolation has been used with limited success on some components. However, to insure pilot and passenger comfort, seat isolation would be an ideal solution, with the possible ultimate goal of isolating the fuselage from the rotor-induced vibration. For these applications, conventional isolators are not practical. The natural frequency is a function of the isolated mass. A passenger or pilot seat system, for example, which is isolated when fully loaded, could magnify the vibration when lightly loaded or empty. For vertical isolation of the fuselage from the rotor system, a relatively soft system having large static deflections is required. For maneuvers, excessive deflections are obtained. To avoid these drawbacks, there is a need for an isolator which provides a given amount of isolation at a given

\*This paper was not presented at the Symposium.



frequency, independent of the magnitude of the isolated mass.

### NOMENCLATURE

- C Damping coefficient of the DAVI, lb-sec/in.
- C<sub>c</sub> Damping coefficient of the series element, lb-sec/in.
- K Spring rate of the DAVI, lb/in.
- K<sub>c</sub> Spring rate of the series element, lb/in.
- I Mass moment of inertia of bar about its own center of gravity, lb-in.-sec<sup>2</sup>
- m<sub>1</sub> Isolated mass, lb-sec<sup>2</sup>/in.
- m<sub>2</sub> DAVI bar mass, lb-sec<sup>2</sup>/in.
- m<sub>3</sub> Intermediate mass of series DAVI, lb-sec<sup>2</sup>/in.
- m<sub>R</sub> Mass of rotor, engine, and transmission of helicopter, lb-sec<sup>2</sup>/in.
- m<sub>f</sub> Mass of fuselage of helicopter, lb-sec<sup>2</sup>/in.
- R Distance from isolated pivot to center of gravity of bar, in.
- r Distance between pivots, in.
- T<sub>D</sub> Transmissibility
- t Time
- ρ Radius of gyration of bar about its own center of gravity, in.
- ω Frequency

### DAVI THEORY

The dynamic antiresonant vibration isolator (DAVI) is a passive vibration isolation device which can provide a high degree of isolation at low frequency with very low static deflection. At a predetermined antiresonant frequency, the nearly zero transmissibility across a DAVI is independent of the mass of the isolated item. The feasibility of the DAVI conception has been shown through experimental and analytical work supported by the U.S. Army Aviation Materiel Laboratories (AVLABS).

As shown in Fig. 1, the DAVI consists of a bar of mass m<sub>2</sub> pivoted to the base and elsewhere

pivoted to the isolated mass m<sub>1</sub>. The distance from the upper (isolated) pivot to the center of gravity of the bar (R) is measured positively in the direction of the input pivot. The isolated mass m<sub>1</sub> is connected to the base by a spring of rate K and a damper of rate C. Considering a sinusoidal displacement excitation, y<sub>3</sub> on the base, the energy equations of the system are:

$$T = \frac{1}{2} m_1 \dot{y}_1^2 + \frac{1}{2} m_2 \left[ \dot{y}_1^2 \left(1 - \frac{R}{r}\right)^2 + 2\dot{y}_1 \dot{y}_3 \frac{R}{r} \left(1 - \frac{R}{r}\right) + \left(\frac{R}{r}\right)^2 \dot{y}_3^2 \right] + \frac{1}{2} \frac{I}{r^2} (\dot{y}_1^2 - 2\dot{y}_1 \dot{y}_3 + \dot{y}_3^2) \quad (1)$$

$$V = \frac{1}{2} K (y_1 - y_3)^2 \quad (2)$$

$$D = \frac{1}{2} C (\dot{y}_1 - \dot{y}_3)^2 \quad (3)$$

and the equation of motion is

$$m_1 \ddot{y}_1 + m_2 \left[ \ddot{y}_1 \left(1 - \frac{R}{r}\right)^2 + \frac{R}{r} \left(1 - \frac{R}{r}\right) \ddot{y}_3 \right] + \frac{I}{r^2} (\ddot{y}_1 - \ddot{y}_3) + C(\dot{y}_1 - \dot{y}_3) + K(y_1 - y_3) = 0 \quad (4)$$

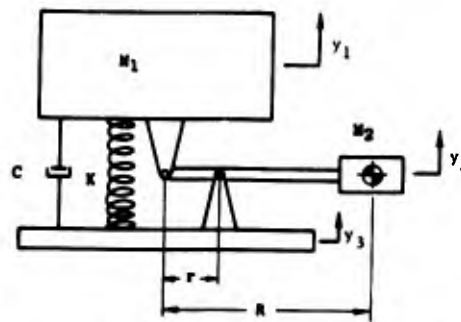


Fig. 1. Diagram of DAVI Alpha

Assuming a sinusoidal solution and solving for y<sub>1</sub>/y<sub>3</sub>, the undamped transmissibility is:

$$T_D = \frac{K - \omega^2 \left[ \frac{I}{r^2} + m_2 \frac{R}{r} \left( \frac{R}{r} - 1 \right) \right]}{K - \omega^2 \left[ m_1 + m_2 \left( \frac{R}{r} - 1 \right)^2 + \frac{I}{r^2} \right]} \quad (5)$$

It is seen from the numerator that when the inertia forces equal the spring forces, the

transmissibility is zero. This antiresonant frequency is given by:

$$\omega_A^2 = \frac{K}{\frac{I}{r^2} + m_2 \frac{R}{r} \left( \frac{R}{r} - 1 \right)} \quad (6)$$

The isolated mass  $m_1$  does not appear in the above equations. Therefore, the magnitude of the isolated mass  $m_1$  does not affect the transmissibility at this frequency.

The natural frequency of the DAVI is obtained by setting the denominator of Eq. (5) to zero or

$$\omega_{12}^2 = \frac{K}{m_1 + m_2 \left( \frac{R}{r} - 1 \right)^2 + \frac{I}{r^2}} \quad (7)$$

The additional effective mass terms in Eq. (7) relating to  $m_2$  and  $I$  cause the DAVI to have a lower natural frequency than a conventional isolator with the same spring rate. Therefore, when the DAVI and conventional isolator have the same natural frequency, the static deflection of the DAVI will be much less.

At very high frequencies, the spring terms in Eq. (5) are negligible compared with the inertial terms. Therefore, the high-frequency DAVI transmissibility is:

$$T_{DVHF} = \frac{\frac{I}{r^2} + m_2 \frac{R}{r} \left( \frac{R}{r} - 1 \right)}{\frac{I}{r^2} + m_2 \left( \frac{R}{r} - 1 \right)^2 + m_1} \quad (8)$$

The high-frequency isolation of the DAVI asymptotically approaches a finite value rather than zero as in a conventional system.

The transmissibility of the DAVI, as seen from Eq. (5), has six controllable parameters: the spring rate, the isolated mass, the bar mass, the bar inertia, the pivot distance ( $r$ ), and the bar center of gravity ( $R$ ). Controlling six parameters, rather than just the isolated mass and spring rate of the undamped conventional system, entails significantly more work, but it gives the engineer much greater freedom in designing an isolation system than he has with a conventional isolator.

The absolute transmissibility of the damped DAVI is given by

$$|T|^2 = \frac{\left\{ K - \omega^2 \left[ \frac{I}{r^2} + m_2 \frac{R}{r} \left( \frac{R}{r} - 1 \right) \right] \right\}^2 + \omega^2 C^2}{\left\{ K - \omega^2 \left[ m_1 + m_2 \left( \frac{R}{r} - 1 \right)^2 + \frac{I}{r^2} \right] \right\}^2 + \omega^2 C^2} \quad (9)$$

and it is noted that at the antiresonant frequency, zero transmissibility is not obtained with damping. Although zero transmissibility is not possible in this case, very high antiresonant isolation and limited resonance transmissibilities are achievable.

Figure 2 is a typical damped DAVI transmissibility curve. Note that damping narrows rather than broadens the bandwidth and that it causes the resonant frequency to decrease and the antiresonant frequency to increase. At very high frequency, the DAVI transmissibility equation is dominated by the mass terms and damping has negligible effect.

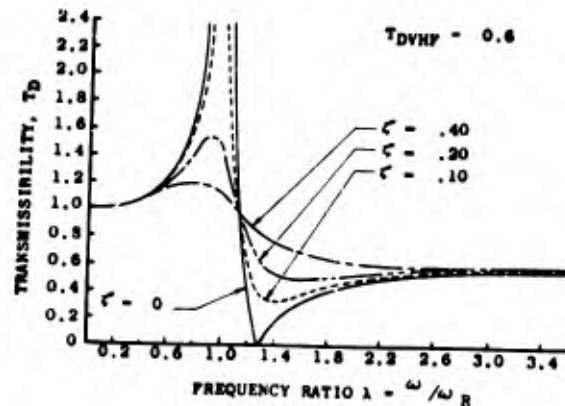


Fig. 2. Damped DAVI transmissibility

## DAVI EXPERIMENTATION

To confirm the theoretical finding, laboratory testing was done. Figure 3 is a photograph of the unidirectional DAVI tested. This prototype model was designed to have a variable  $r$  (distance between pivots) from 0.75 to 2.0 in. Without changing any of the physical hardware, such as springs, an antiresonant frequency can be obtained from 4 to 30 cps. Eighteen tests were done for six different  $R/r$  values ranging from -6.1 to 4.8, and for three different isolated weights of 11, 27, and 42 lb. Figures 4 and 5 show typical results obtained from this series

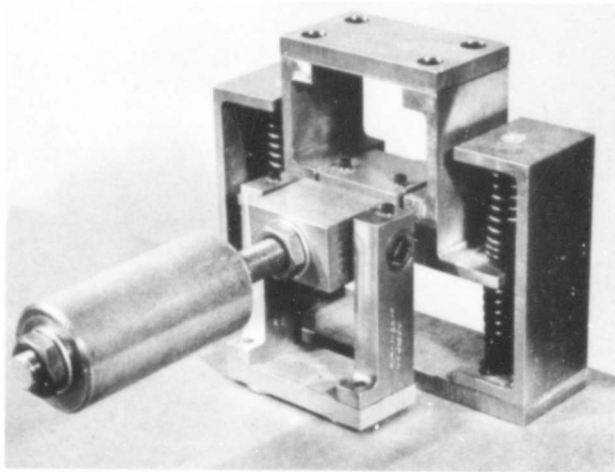


Fig. 3. DAVI prototype model

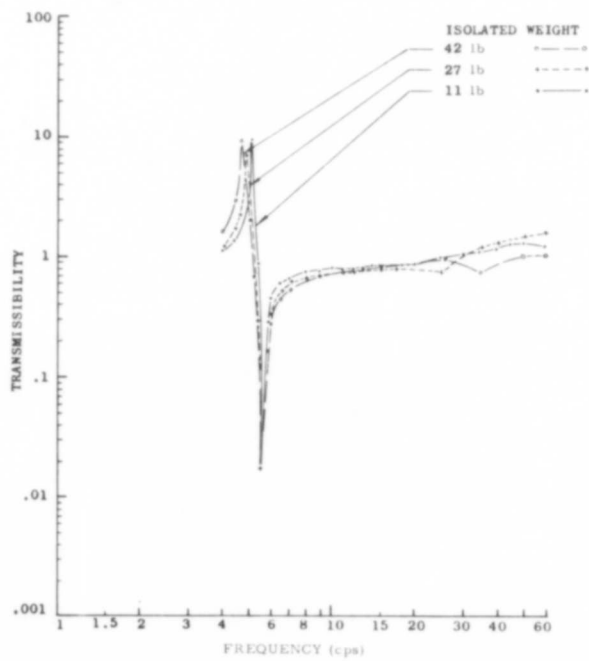


Fig. 4. Experimental response of DAVI for  $R/r = -6.131$

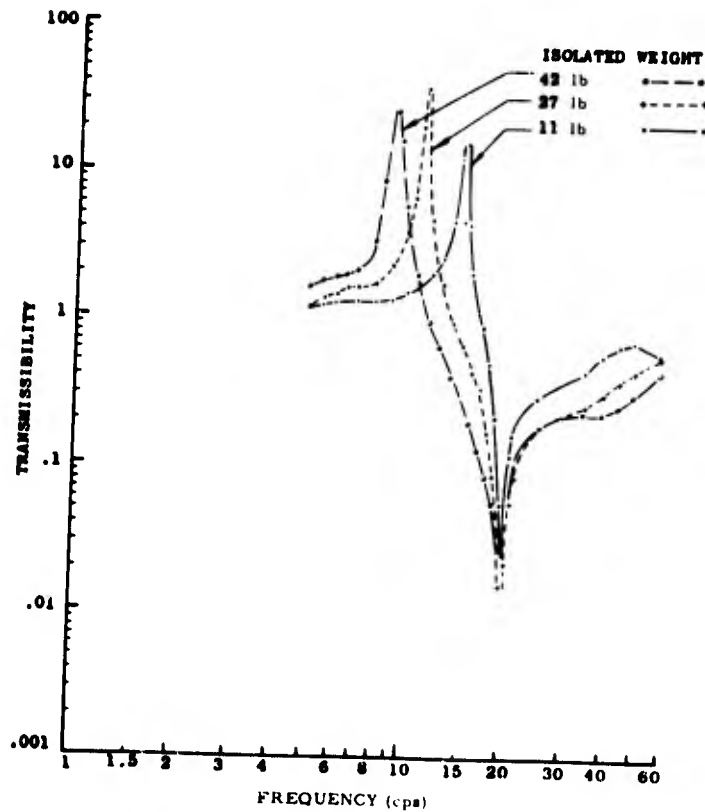


Fig. 5. Experimental response of DAVI for  $R_r = 2.26$

of tests. It is seen from Fig. 4 that the antiresonance is at approximately 5.6 cps and was not affected by the magnitude of the isolated mass. It is also seen that the natural frequency of the DAVI was reduced by an increase in the isolated weight. Figure 5 shows similar results, except that the antiresonant frequency is approximately 20 cps. The change in results was obtained by changing the  $R_r$  value from -6.13 to 2.26

A comparison was made between the tests and analytical results. A comparison was also made between a conventional and DAVI Alpha isolation system having the same spring rate. Figures 6 and 7 show the results of this comparison. It is seen that the predicted and test results of the DAVI compare very well. In Fig. 6, it is seen that the antiresonant frequency is well below the natural frequency of the conventional isolator, and isolation is obtained at a

frequency much lower than that of the conventional system with the same spring rate.

To determine the shock characteristics of the DAVI, drop tests were done on a VP-400 Varipulse machine. The DAVI was subjected to half-sine, sawtooth, and square-wave inputs. A comparison was made with a conventional system of equivalent spring rate by removing the inertia bar of the DAVI. Figure 8 shows the installation of the platform in the drop test machine. Figure 9 shows the drop test results of a 41-lb DAVI isolated platform, and Fig. 10 shows the results of an equivalent conventional system with the same spring rate. In Fig. 9 it is seen that the DAVI has an initial peak and then oscillates at its natural frequency. This initial peak has been predicted by theory and is a function of the high-frequency isolation of the DAVI. In Fig. 10, when comparing with Fig. 9, it is seen that higher g levels have been transmitted to the conventionally isolated platform.

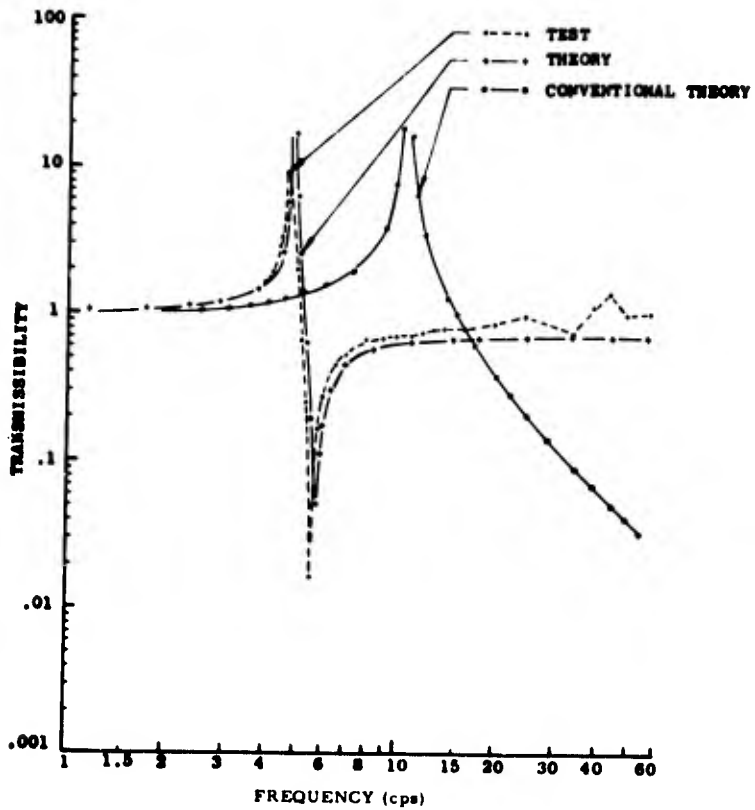


Fig. 6. Analytical and experimental response for an isolated weight of 11 lb and  $R/r = -6.131$

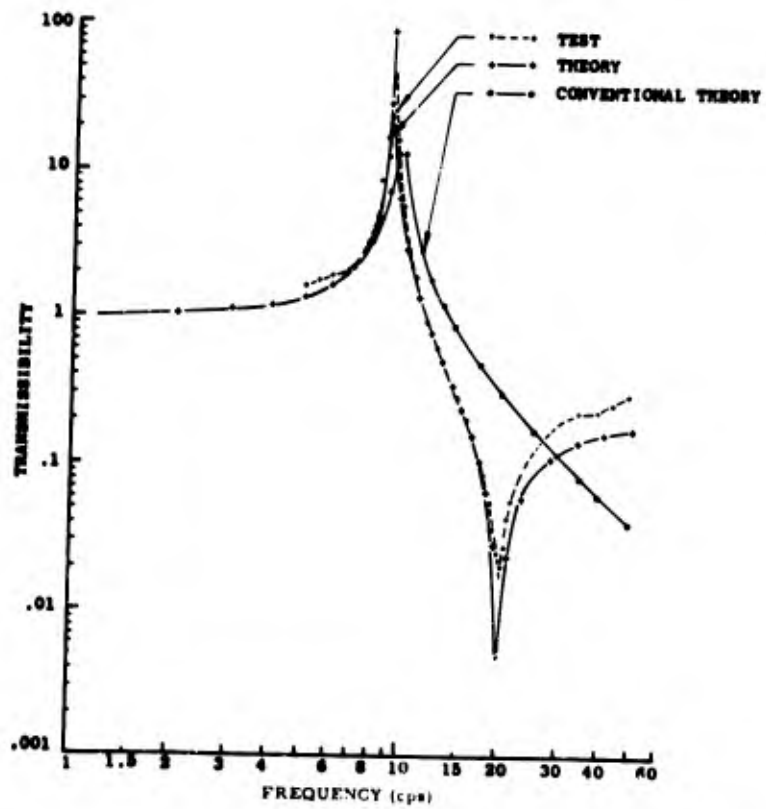


Fig. 7. Analytical and experimental response for an isolated weight of 42 lb and  $R/r = 2.26$

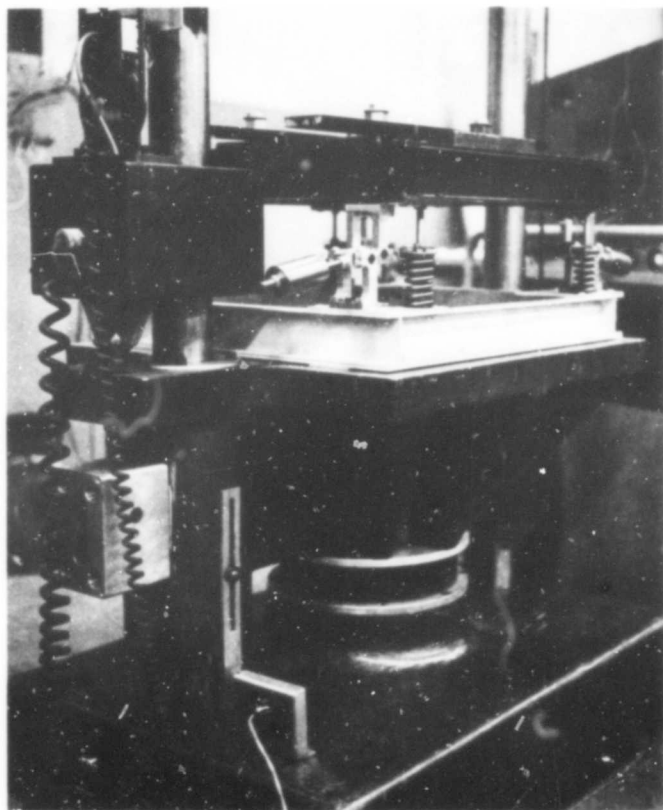


Fig. 8. Installation of DAVI platform in the VP-400 varipulse machine

Fig. 9. Shock response of DAVI platform for sawtooth type input

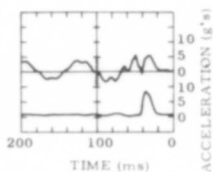
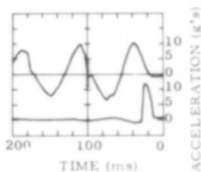


Fig. 10. Shock response of conventionally isolated platform for sawtooth type of input



#### APPLICATION TO HELICOPTER VIBRATION CONTROL

Because helicopters characteristically exhibit large-amplitude vibration at low frequencies and are subject to transient accelerations, the DAVI is ideally suited to isolate these inherent vibration characteristics. Isolating the instrument panel, thus eliminating

blurred instruments, is one means of increasing pilot safety by reducing pilot fatigue. Figure 11 illustrates this in that an instrument was attached to the input side of the DAVI platform and compared to an instrument attached to the output side. Note the ease of reading the upper instrument as compared to the lower instruments.

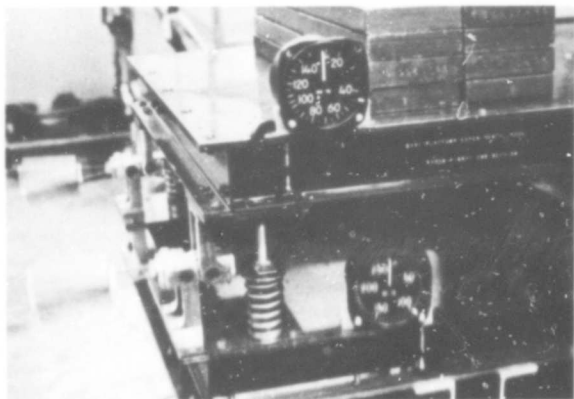


Fig. 11. DAVI platform installation

Another means of reducing pilot fatigue is the isolation of the seat itself. This, of course, could be extended to passenger seats to insure passenger comfort. In Fig. 12, a member of the Kaman vibrations research staff, seated in a regulation military helicopter pilot's seat, is shown isolated from an input of approximately 1.0 g at 10.5 cps. The isolation is approximately 98 percent effective. Comparable isolation from a conventional isolator at this

frequency would require a minimum static deflection of 5.0 in. or 35.0 times as much as the DAVI. Various individuals ranging from a 105-lb secretary to a 220-lb test pilot were tested in this seat with no effect on the antiresonant frequency and negligible effect on the amount of antiresonant isolation.

The ultimate goal is the isolation of the fuselage from the rotor-induced vibration.

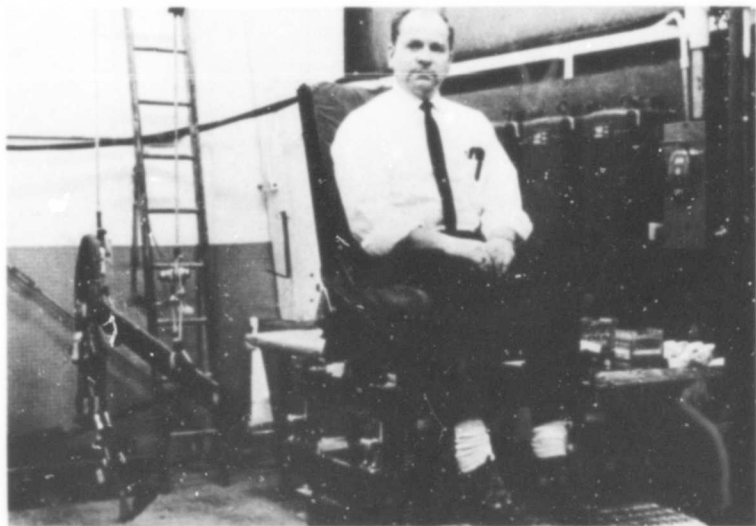


Fig. 12. Experimental seat isolation

Kaman is presently studying, under AVLABS sponsorship, the application of the DAVI to helicopter rotor isolation. Conventional isolation has been used to isolate against the in-plane forces resulting from rotor blade shears. For vertical isolation, however, a relatively soft system having large static deflections is required; for maneuvers, excessive deflections are required.

In the contract now being conducted at Kaman on rotor isolation, the six rigid-body degrees of freedom of the upper body (rotor) and the lower body (fuselage) are considered. However, to indicate the feasibility of DAVI isolation, only vertical isolation is considered here.

The response of the DAVI isolated helicopter as compared to a nonisolated helicopter is:

$$\frac{y_{FD}}{y_{FNM}} = \frac{\frac{R}{\delta_{ST}} - \omega^2 \frac{m_2}{m_f} \left[ \frac{\rho^2}{r^2} + \frac{R}{r} \left( \frac{R}{r} - 1 \right) \right]}{\frac{R}{\delta_{ST}} - \omega^2 \left\{ \mu_R + \frac{m_2}{m_f} \left[ \frac{\rho^2}{r^2} + \left( \frac{R}{r} \right)^2 - \mu_R \left( 2 \frac{R}{r} - 1 \right) \right] \right\}} \quad (10)$$

where

$$\delta_{ST} = \frac{m_f g}{K}$$

$$\mu_R = \frac{m_R}{n_1 m_f + m_f}$$

It is seen from the above equation that when the numerator is zero, 100 percent isolation is obtained; the antiresonant frequency is

$$\omega_A^2 = \frac{\frac{R}{\delta_{ST}}}{\frac{m_2}{m_f} \left[ \frac{\rho^2}{r^2} + \left( \frac{R}{r} \right) \left( \frac{R}{r} - 1 \right) \right]} \quad (11)$$

The antiresonant frequency should be tuned to the  $n/\text{rev}$  of the helicopter. Figure 13 shows a typical curve of the vertical response ratio vs frequency normalized on  $n/\text{rev}$ . It is seen from this curve that the antiresonance is tuned to the  $n/\text{rev}$ . The natural frequency is designed to be between the  $1/\text{rev}$  and  $n/\text{rev}$  of the helicopter such that  $1/\text{rev}$  is never amplified more than 10 percent. The response ratio of the higher harmonics greater than  $n/\text{rev}$  approaches a finite value less than 1.0 and depends upon the ratio of  $\omega_R^2/\omega_A^2$ .

Feasibility studies are being done for helicopters weighing between 2000 and 100,000 lb and having from two to seven blades. Although

there are many design criteria that must be considered in such a study, the two most important are minimum weight and minimum static deflection. Table 1 shows the static deflection obtained and percentage of DAVI weight to total weight required to isolate the fuselage from the rotor-engine-transmission system of four different gross weight helicopters.

TABLE 1  
Static Deflection and Percentage  
of DAVI Weight

Gross Weight (lb)	Number of Blades	Static Deflection (in.)	DAVI Weight/GW (%)
2,200	4	0.05	0.16
6,600	2	0.15	0.42
10,000	3	0.10	0.37
39,000	6	0.075	0.28

Figure 14 shows the results of the response as normalized to the predominant  $n$ th harmonic acceleration. It is seen that excellent isolation is obtained in the higher harmonics and  $1/\text{rev}$  amplification is a minimum.

In the design of an isolation system in a helicopter, consideration must be given to the transient response. The system should be designed to give a minimum of deflection for the transient load and also a minimum of overshoot. The buildup of load on the rotor may result from a gust, a transient maneuver, or steady-state maneuver.

For the transient response considered to be a one-half  $(1 - \cos \Omega t)$  input, the deflection in the springs of the isolation system is

$$\Delta y = \frac{n_x \left[ 1 + \frac{m_2}{m_f} \left( 1 - \frac{R}{r} \right) \right] \delta_{ST}}{2 \left( 1 - \frac{\Omega^2}{\omega_R^2} \right)} \times \left\{ \left[ \left( 1 - \frac{\Omega^2}{\omega_R^2} \right) + \frac{\Omega^2}{\omega_R^2} \cos \omega_R t - \cos \Omega t \right]_0^t + \left[ \left( 1 - \frac{\Omega^2}{\omega_R^2} \right) + \frac{\Omega^2}{\omega_R^2} \cos \omega_R (t - t_1) - \cos \Omega (t - t_1) \right]_{t_1}^t \right\} \quad (12)$$



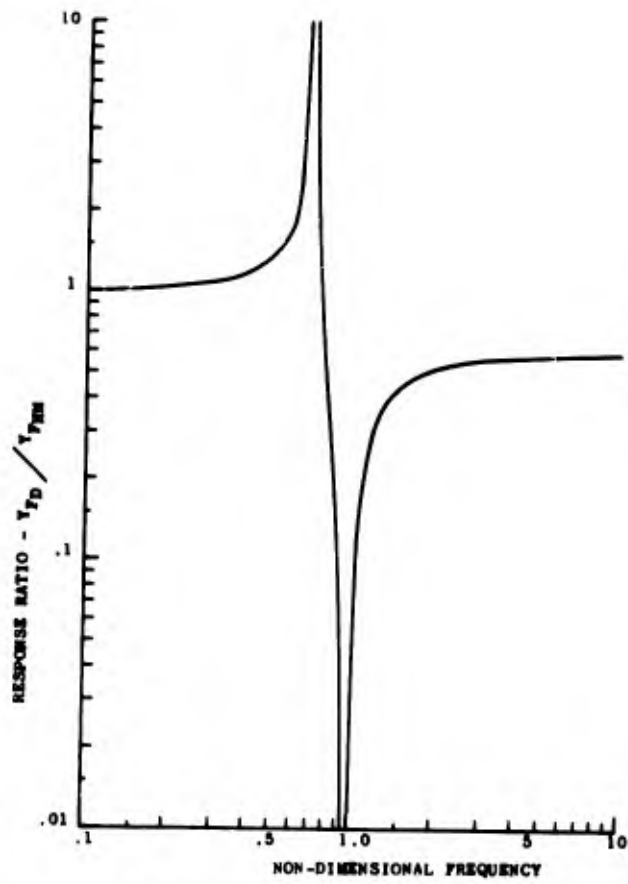


Fig. 13. Vertical response ratio of an isolated helicopter

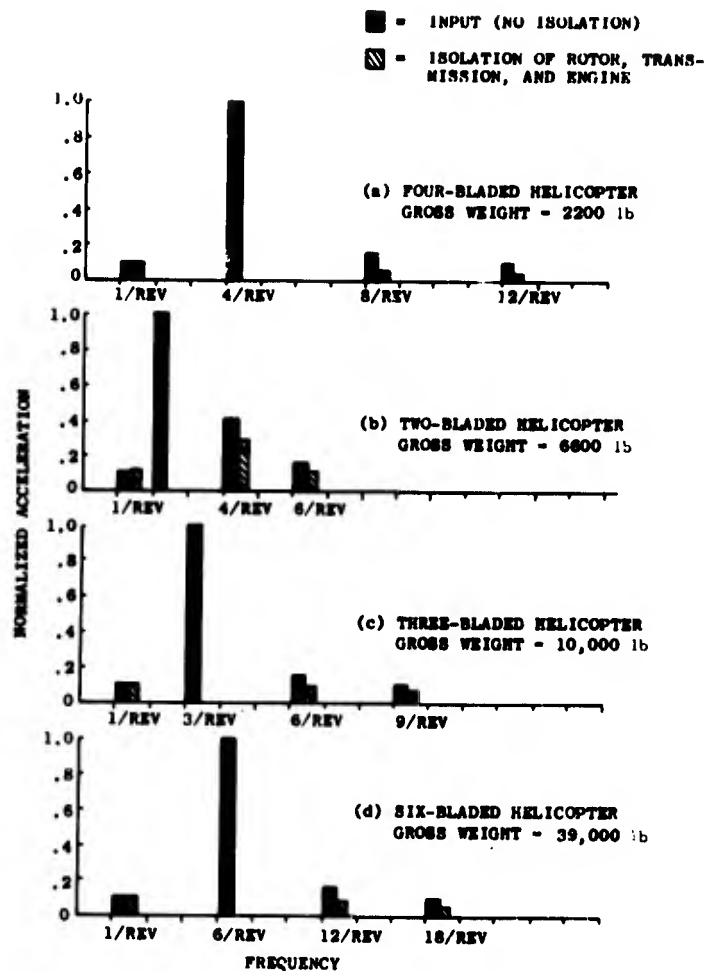


Fig. 14. Response with the DAVI rotor isolation system for various helicopter configurations

It is seen from the above equation that the magnitude of the deflections depends upon the static deflection and can be solved as a ratio of the period of input over the period of the natural frequency. This is shown in Fig. 15. For example, the 10,000-lb, 3-bladed helicopter has a static deflection of 0.075 in. and a natural frequency of 85.5 rad/sec or a period of 0.0735 sec. An input that has a period of only 0.2 sec, which is a rapid buildup of load on a rotor, gives a  $t_1/t_2$  ratio of 2.72. From this figure it is seen that the maximum deflection in the spring is  $1.02n_g \delta_{ST}$ . Therefore, for a 3-g load factor, deflection in the spring of the DAVI isolation system including the overshoot is only 0.2295 in.

### FLIGHT TEST OF DAVI ISOLATED PLATFORM

To determine the characteristics of the DAVI isolation system under actual vibration environment, a unidirectional DAVI platform was flight tested in a Kaman UH-2 helicopter. The platform was installed in the cargo area of the helicopter, and eight accelerometers were used to determine the accelerations of the vertical outputs and inputs at the four locations of the unidirectional DAVI isolators. Two accelerometers were used to determine the longitudinal and lateral inputs to the DAVI isolated platform.

The unidirectional DAVI's, which were designed for vertical isolation only, were tuned to 18.3 cps, which is the predominant excitation frequency of the UH-2 helicopter. Platforms weighing 50, 150, and 200 lb were flown.

Figure 16 shows the results of the test of the 50-lb platform in which the output at each DAVI is divided by the input to give the transmissibility. The results are shown only for a frequency of four/rev. The change in frequency results from an rpm sweep from 92 to 102 percent rotor rpm. A comparison is made with the theoretical transmissibility for a pure vertical input. Also shown is the theoretical transmissibility of a conventionally isolated 50-lb platform having the same spring rate.

It is seen from Fig. 16 that the test results were much higher than the results predicted by the DAVI theory. One reason for this is that the vertical output resulted not just from the vertical input, but also from the longitudinal and lateral inputs causing pitching and rolling of the platform, thus affecting the vertical accelerations on the platform. Because of this complex input to the unidirectional DAVI's, only fair isolation was obtained at the antiresonant frequency of 18.3 cps. However, the conventional isolator, as shown by theory, would have amplified the input throughout this frequency range.

The results indicate the need of a two-dimensional DAVI that gives isolation in a plane perpendicular to the axis of the bar. Figure 17 shows a two-dimensional DAVI which uses flexural pivots in a Hooke's joint arrangement. Tests of this model show isotropic DAVI performance in a plane perpendicular to the axis of the bar. Over 99 percent antiresonant isolation was obtained in all directions in the vibrating plane of the bar.

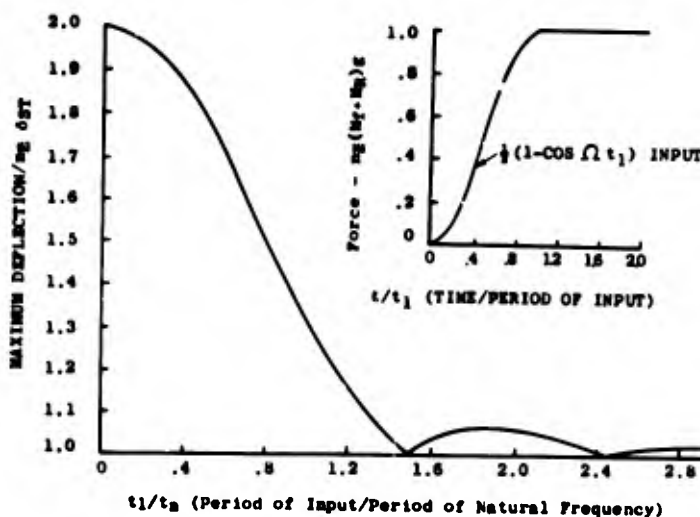


Fig. 15. Maximum deflection from transient input

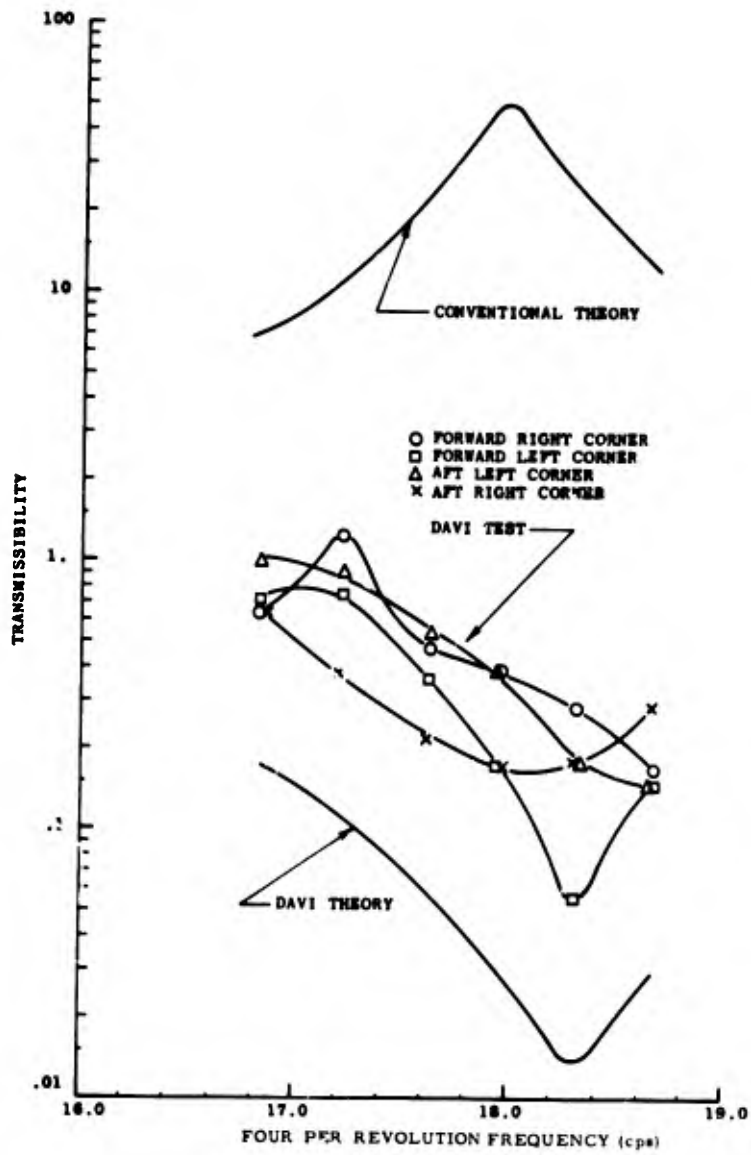


Fig. 16. Flight test results of a 50-lb unidirectional DAVI isolated platform

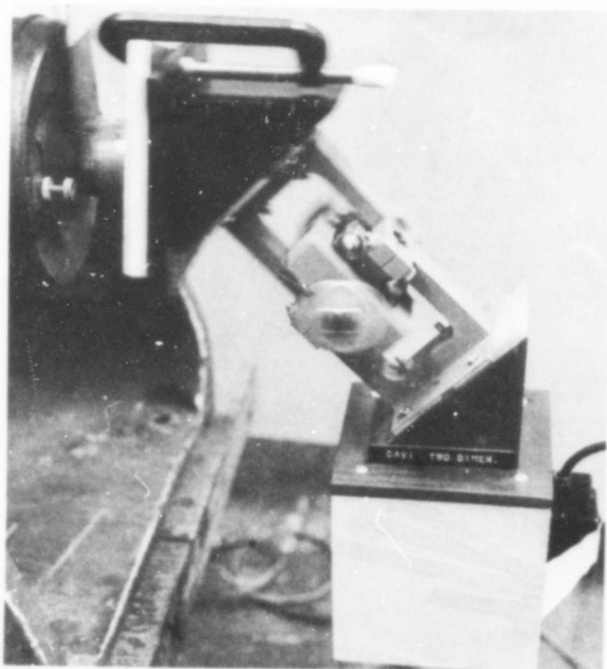


Fig. 17. Experimental model of a two-dimensional DAVI

#### SERIES-TYPE DAVI

The analysis and tests on the unidirectional and two-dimensional DAVI's have shown the capability of low-frequency isolation in obtaining an antiresonant frequency that is not affected by the weight of the isolated item. However, this system approaches a finite value of isolation at high frequency, which may be a disadvantage for some applications. To obtain high-frequency isolation approaching zero and retain the advantages of the simple DAVI, a series system

can be designed. Figure 18 shows such series systems. (For this paper, discussion is restricted to the DAVI Gamma. However, results of the DAVI Beta are similar.)

The DAVI Gamma is an incorporation of the simple DAVI and conventional isolation systems. The mass to be isolated is supported by the conventional system, which in turn, is supported by the DAVI connected to the base. From Fig. 19, a schematic of the DAVI Gamma, the energy equations can be derived:

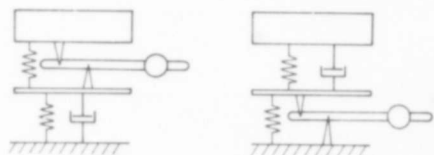


Fig. 18. Diagram of series-damped DAVI's (left, Beta; right, Gamma)

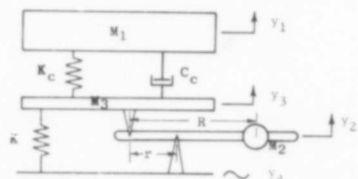


Fig. 19. Diagram of DAVI Gamma

$$T = \frac{1}{2} m_1 \dot{y}_1^2 + \frac{1}{2} m_2 \left[ \frac{R}{r} \dot{y}_4 - \left( \frac{R}{r} - 1 \right) \dot{y}_3 \right]^2 + \frac{1}{2} m_3 \dot{y}_3^2 + \frac{1}{2} \frac{I}{r^2} (\dot{y}_3 - \dot{y}_4)^2 \quad (13)$$

$$V = \frac{1}{2} K (y_3 - y_4)^2 + \frac{1}{2} K_c (y_1 - y_3)^2 \quad (14)$$

$$D = \frac{1}{2} C_c (\dot{y}_1 - \dot{y}_3)^2 \quad (15)$$

Applying Lagrange's equation, the equations of motion are

$$m_1 \ddot{y}_1 + C_c \dot{y}_1 + K_c y_1 - C_c \dot{y}_3 - K_c y_3 = 0 \quad (16)$$

$$\left[ m_3 + m_2 \left( \frac{R}{r} - 1 \right)^2 + \frac{I}{r^2} \right] \ddot{y}_3 + C_c \dot{y}_3 + (K_c + K) y_3 - C_c \dot{y}_1 - K_c y_1 + \left[ m_2 \frac{R}{r} \left( \frac{R}{r} - 1 \right) + \frac{I}{r^2} \right] \ddot{y}_4 + K y_4 = 0 \quad (17)$$

Assuming a sinusoidal solution and solving for the transmissibility, the transmissibility is

$$T_{D_y} = \frac{\left\{ K - \left[ m_2 \frac{R}{r} \left( \frac{R}{r} - 1 \right) + \frac{I}{r^2} \right]^2 \right\} (K_c + i C_c)}{\dots} \quad (18)$$

where

$$\Delta = m_1 \left[ m_3 + m_2 \left( \frac{R}{r} - 1 \right)^2 + \frac{I}{r^2} \right]^2 - \left\{ \left[ m_3 + m_2 \left( \frac{R}{r} - 1 \right)^2 + \frac{I}{r^2} \right] K_c + m_1 K_c + m_1 K \right\}^2 + K K_c + i \left\{ \left[ m_3 + m_2 \left( \frac{R}{r} - 1 \right)^2 + \frac{I}{r^2} \right] C_c \right\}^2 - m_3 C_c^2 + C_c K$$

It is seen from this transmissibility equation that the amplitude at resonance can be controlled by the damping in the series system, but that 100 percent isolation can be obtained at the antiresonant frequency of the DAVI. Also, when  $\omega$  approaches infinity, the transmissibility approaches zero. Thus, the DAVI Gamma can be designed to give approximately 100 percent

isolation at a discrete frequency, to have controlled resonant amplitudes, and to give high-frequency isolation.

To confirm the analytical findings, laboratory model tests were done. The model used in these tests is identical to that shown in Fig. 3 in which the series element was the spring rates of another DAVI unit with the inertia bar and pivots removed. Thus, the spring rates  $K$  and  $K_c$  were equal. To control the amount of damping across the series element, a rotary damper was used.

In all 12 tests done, four configurations were tested, each having three different values of damping across the series element. The antiresonance of the DAVI element was changed by changing the inertia bar parameters; 27 lb was the isolated weight. Figures 20 through 25 show the results obtained. Figures 20, 21, and 22 show the results of the DAVI Gamma which has the antiresonance between the two natural frequencies. It is seen that the increased damping reduced the amplitude at resonance without affecting the antiresonance. Although there is a resonance at approximately 25 cps, isolation is obtained. The damping increases this isolation from approximately 40 percent to 80 percent. The isolation obtained at the antiresonant frequency is over 98 percent. It is also seen that the test results compare favorably with the analytical results.

Figures 23, 24, and 25 show the results of the DAVI Gamma with the antiresonance above the two natural frequencies. Even the lightly damped system shows good isolation at the second natural frequency. The increased damping essentially eliminated the higher natural frequency. Again comparisons of test results and analytical results are excellent. A test was also done with the DAVI element removed, the results of which are shown in Fig. 25. It is seen that better isolation is obtained with the DAVI at the higher frequencies than with the equivalent conventional system.

The test and analytical results show that a series-type DAVI can produce an antiresonant frequency, damped resonances, and high-frequency isolation. The series DAVI can be designed to give better high-frequency isolation than a conventional isolator with the same spring rate.

The series-type DAVI could be used for components requiring isolation from transmission and engine high-frequency excitation. It possibly could be used for gun mounts on armed helicopters.

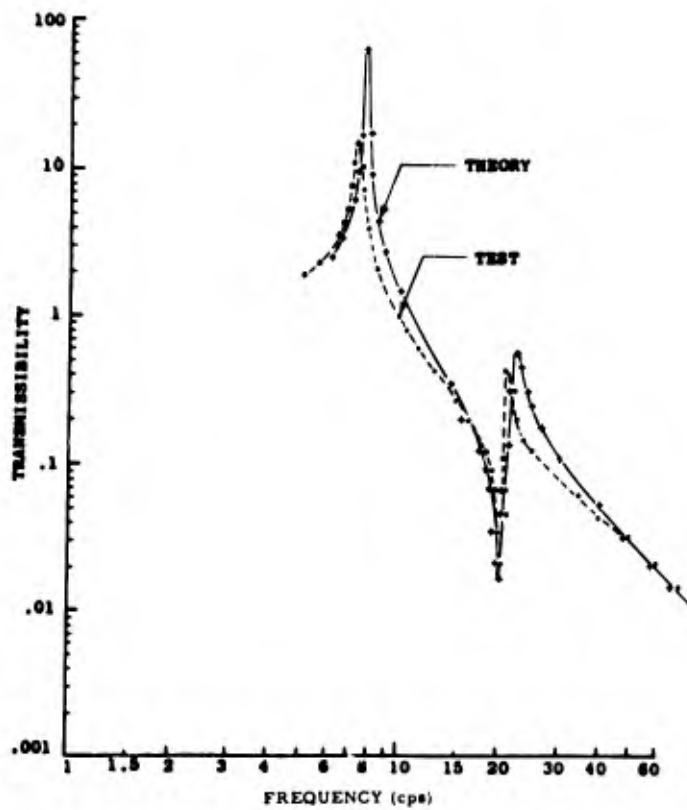


Fig. 20. Analytical and experimental response of the DAVI Gamma with a damping ratio = 0.016 and  $R/r = -1.135$

Fig. 21. Analytical and experimental response of DAVI Gamma with a damping ratio = 0.05 and  $R/r = -1.135$

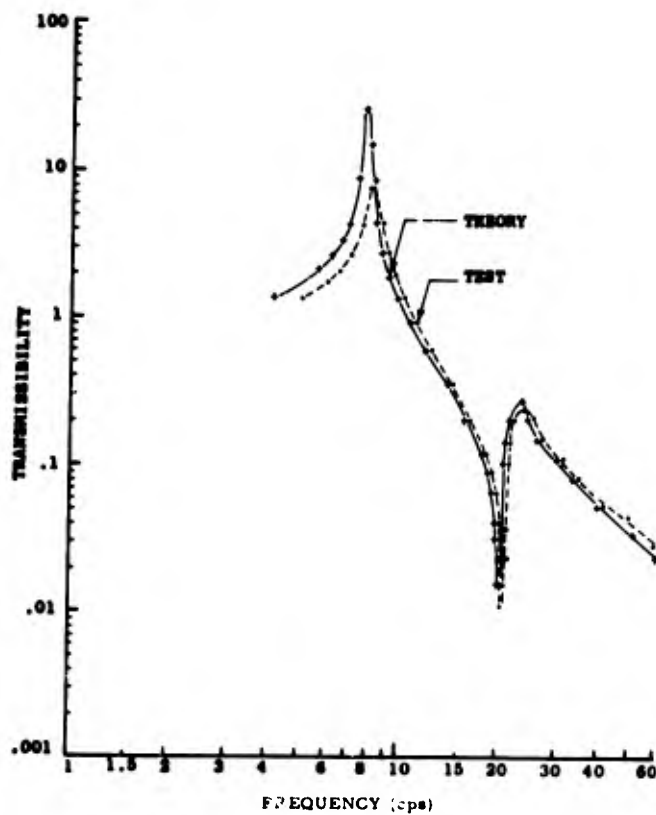


Fig. 22 Analytical and experimental response of DAVI Gamma with a damping ratio = 0.117 and  $R/r = -1.135$

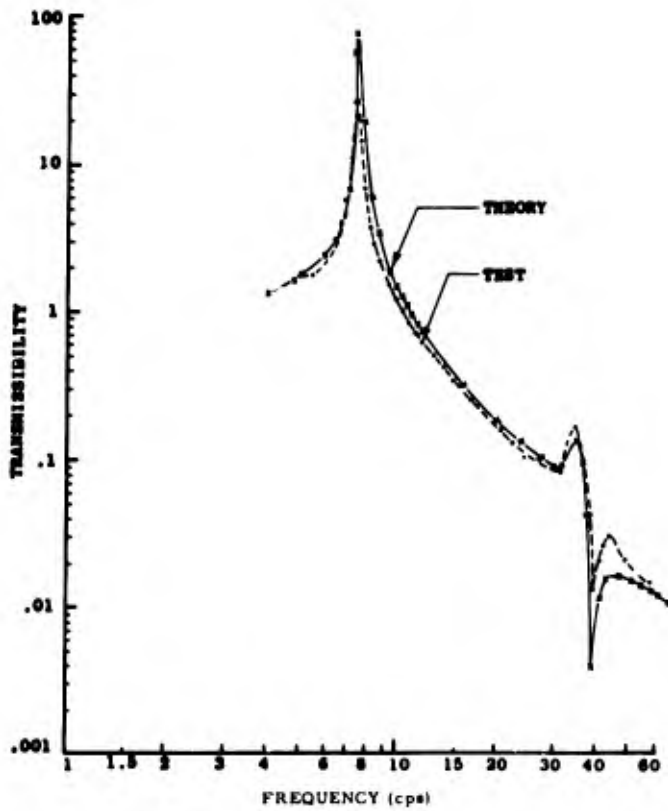
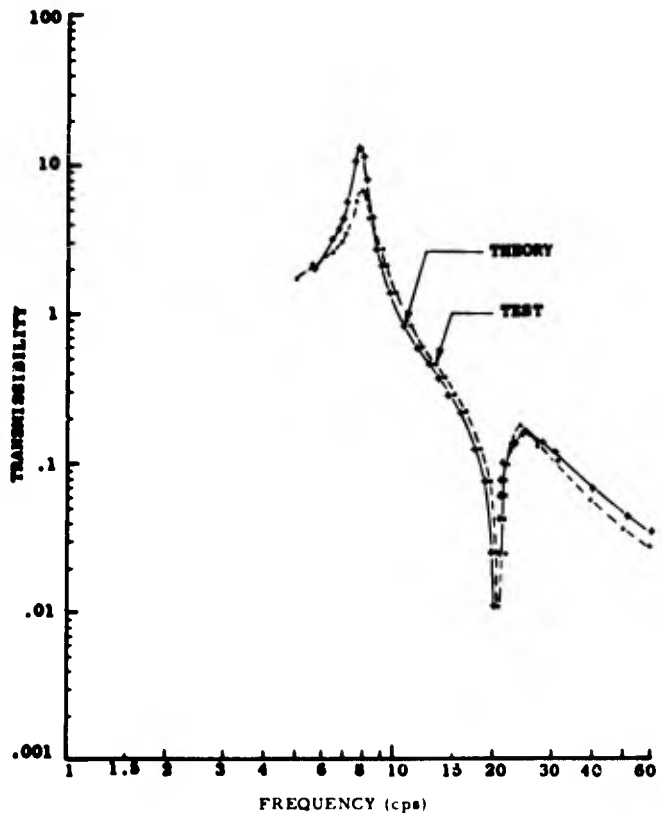


Fig. 23. Analytical and experimental response of DAVI Gamma with a damping ratio = 0.016 and  $R/r = -0.5$



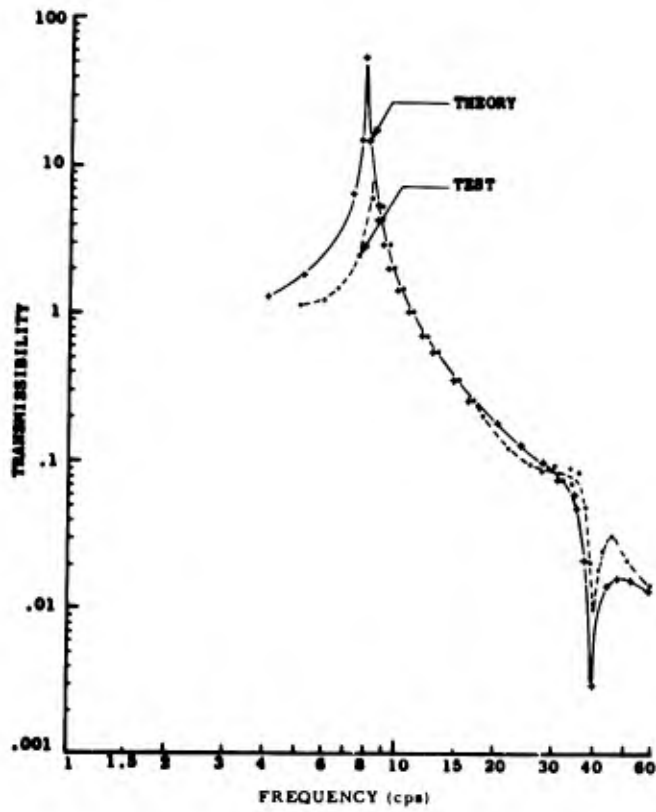
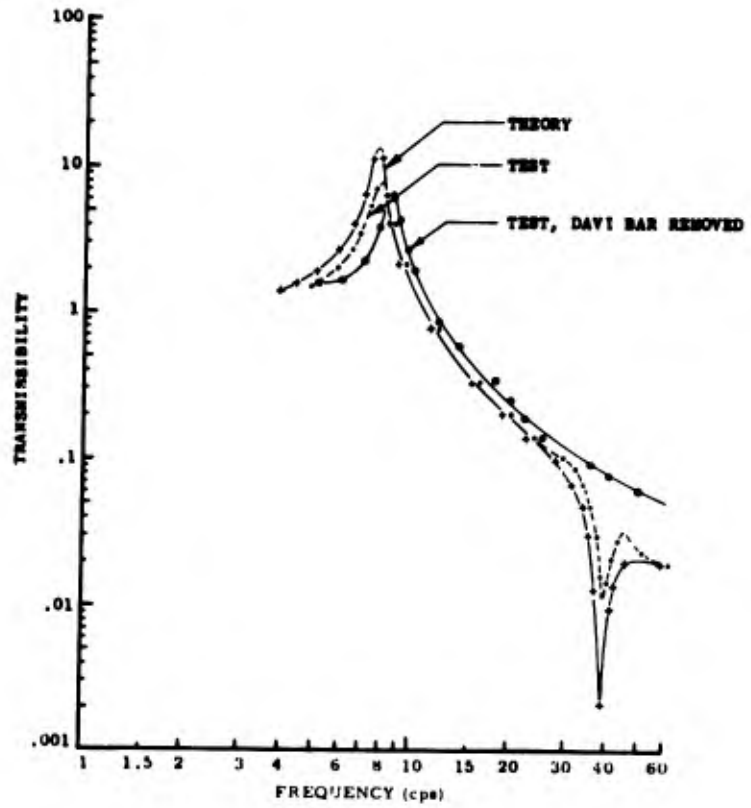


Fig. 24. Analytical and experimental response of DAVI Gamma with a damping ratio = 0.05 and  $R/r = -0.5$

Fig. 25. Analytical and experimental response of DAVI Gamma with a damping ratio = 0.117 and  $R/r = -0.5$ , and experimental response with DAVI element removed



## CONCLUSIONS

1. Analytical and empirical work completed have established the feasibility of antiresonance isolation, independent of the isolated mass, at low frequencies and with high static stiffness.

2. Flight test results indicate a need for two-dimensional DAVI isolation in any direction in a plane perpendicular to its axis.

3. Test results show the feasibility of helicopter pilot and passenger seat isolation, and analytical results show the feasibility of helicopter rotor isolation.

4. Analytical and test results show the feasibility of a series-type DAVI that can simultaneously produce an essentially undamped antiresonance and a damped resonance, and obtain high-frequency isolation. It can be designed to give better isolation than a conventional isolator of the same stiffness.

## BIBLIOGRAPHY

R. C. Anderson, and M. F. Smith, "A Study of the Kaman Dynamic Antiresonant Vibration Isolator," USAAVLABS Tech. Rept. 65-75, Jan. 1966

C. E. Crede, Vibration and Shock Isolation (Wiley, New York), 1951

J. P. Den Hartog, Mechanical Vibrations (4th ed.) (McGraw-Hill, New York), 1956

W. G. Flannelly, "Dynamic Antiresonant Vibration Isolator," Kaman Aircraft Rept. RN 63-1, Nov. 1963

W. G. Flannelly, "The Dynamic Antiresonant Vibration Isolator," Proc. Ann. Forum Amer. Helicopter Soc. (1966)

\* \* \*